Modelling the mesoscale variability in the greater Agulhas Current System using a Hybrid Coordinate Ocean Model

Björn-Christoph Backeberg

Thesis Presented for the Degree of

DOCTOR OF PHILOSOPHY

August 2009

Department of Oceanography

University of Cape Town

South Africa

Modelling the mesoscale variability in the greater Agulhas Current System using a Hybrid Coordinate Ocean Model

Björn-Christoph Backeberg

Ph.D. Thesis in Physical Oceanography

August 2009

Department of Oceanography

University of Cape Town

South Africa

Abstract

The ocean circulation dynamics in the greater Agulhas Current system are dominated by mesoscale variability, which is highly non-linear, and therefore difficult to measure and simulate accurately. Moreover, the shedding of Agulhas rings from the retroflection south of Africa, which is the dominant mechanism by which warm and saline water flows from the Indian into the Atlantic Ocean, is thought to be a crucial component of the thermohaline circulation. With the goal of providing an accurate simulation of the greater Agulhas Current system, and in particular its mesoscale variability, a high resolution Hybrid Coordinate Ocean Model is set up in a nested configuration. In two 11 year simulation experiments, the effect of a higher order momentum advection scheme on the simulated ocean dynamics is tested and evaluated against available satellite observations and *in-situ* measurements. Quantitative analyses and model validation methods are developed to objectively evaluate the simulation experiments. The resultant skewness analyses and spatial variograms are objective measures for assessing the model simulation and additionally provide new insights on the mesoscale dynamics of the greater Agulhas Current system. A 4^{th} order momentum advection scheme is shown to significantly improve the simulation of the region, in particular the dynamics of the southern Agulhas Current and the retroflection are greatly improved. From the analyses of the two model simulations in conjunction with satellite observations and *in-situ* measurements, it is found that the Indo-Atlantic inter-ocean exchange, and the shedding of Agulhas rings from the retroflection, is sensitive to the strength of the Agulhas Current, which in turn is influenced by the flow dynamics in the Mozambique Channel and south of Madagascar. Mesoscale eddies drifting from these source regions to the Agulhas Current play an important role, and the connection between the Agulhas Current and the respective source regions provides a link to large-scale variability in the Indian Ocean, which in turn is related to interannual modes of variability such as the Indian Ocean Dipole and El Niño Southern Oscillation.

Supervisors

Prof. Chris J. C. Reason

Department of Oceanography, University of Cape Town, South Africa

Prof. Johnny A. Johannessen

Mohn-Sverdrup Center for Global Ocean Studies and Operational Oceanography

Nansen Environmental and Remote Sensing Center

Geophysical Institute, University of Bergen, Norway

Dr. Laurent Bertino

Mohn-Sverdrup Center for Global Ocean Studies and Operational Oceanography

Nansen Environmental and Remote Sensing Center

Acknowledgments

The list of people I want to thank for their guidance and input is endless. Be it in casual discussions during tea (or over a beer), during a surf or a climb, or in meetings specifically geared to keep me on track, your collective and individual contributions have made finishing this Ph.D. seem almost easy! And for that I thank you.

Foremost, I would like to thank my supervisors, Chris Reason, Johnny Johannessen, and Laurent Bertino for their continued support and guidance, and for making it possible for me to continue working with the team at the Nansen Center in Bergen (Norway), based from Cape Town. Throughout my Ph.D. I have been lucky to have had the opportunity to frequently visit Bergen, for extended periods. During these visits Johnny and Laurent in particular, have spent many hours critically revising and discussing my work with me, for which I am very grateful.

I feel privileged to have worked with such a dynamic team of scientists over the last few years, and I want to thank both my co-students and colleagues at UCT as well as the team at the Mohn-Sverdrup and Nansen Center in Bergen for their enthusiasm, their eagerness to help and their capacity for problem solving. Especially, Francois, Knut-Arild, Cecilie, and Intissar (depending on who was at their desk at the time), have spent many a minute responding to questions often sent in panic via Internet messenger. In Cape Town, discussions (individually or in a group) usually with Seb, Neil, Ross, Natalie and my office co-habitant Jenny have often led to new insights and approaches.

Last, but definitely not least I want to thank my family and friends for their support. Especially my better half Christiane, for putting up with me and my seemingly endless soliloquies about work. Thank you for always finding my marbles!

Preface

This thesis is submitted for the degree of Doctor of Philosophy (Ph.D.) in Physical Oceanography at the University of Cape Town, South Africa. This work has resulted from a collaborative effort between the Department of Oceanography, University of Cape Town in South Africa, and the Mohn-Sverdrup Center for Global Ocean Studies and Operational Oceanography at the Nansen Environmental and Remote Sensing Center, in Bergen, Norway. The support from the Mohn-Sverdrup Center for Global Ocean Studies and Operational Oceanography, through a private donation from Trond Mohn C/O Frank Mohn AS, Bergen, Norway, as well as a grant for CPU time from the Norwegian Super-computing (NOTUR) project, and financial assistance from the National Research Foundation of South Africa are gratefully acknowledged.

The thesis focuses on the development and evaluation of a high-resolution ocean circulation model of the greater Agulhas Current system, for the purpose of advancing our understanding of the complicated ocean currents in the region. The work consists of three parts. First, the introduction outlines the motivation of the thesis followed by a detailed description of the model system used to simulate the region. Secondly, four chapters are presented, which discuss the implementation, development and improvements of the model system together the scientific contribution gained from the work. Lastly, these four chapters are discussed and in conclusion the main findings are presented and suggestions for future work are considered.

The four major chapters are based on published and submitted material (including the relevant literature review) as indicated below:

Chapter 3 *Based on the work published as:*

The greater Agulhas Current system: An integrated study of its mesoscale variability. **Backeberg, B. C., J. A. Johannessen, L. Bertino, and C. J. C. Reason**, *Journal of Operational Oceanography*, 1(1):29-44, 2008.

Chapter 4 *Based on the work published as:*

Evaluating two numerical advection schemes in HYCOM for eddy-resolving modelling of the Agulhas Current. **Backeberg, B. C., L. Bertino, and J. A. Johannessen**, *Ocean Science*, 5:173-190, 2009.

Chapter 5 *Based on the work published as:*

A connection between the South Equatorial Current north of Madagascar and Mozambique

Channel Eddies. **Backeberg, B. C. and C. J. C. Reason**, *Geophysical Research Letters*, 37 (L04604), doi:10.1029/2009GL041950, 2010.

Chapter 6 *Based on the work submitted as:*

Mesoscale transport variability in the Agulhas system and its connection to leakage into the South Atlantic Ocean. **Backeberg, B. C., J. A. Johannessen and C. J. C. Reason**, *Journal of Geophysical Research*, submitted.

Declaration

I declare that the published and submitted material is my own unaided work, which includes all analyses of the data, creating of the figures, and writing the discussions of the results. I hereby certify that unless stated, all work contained within this thesis is my own to the best of my knowledge.

Additional co-authors are included on the published and submitted material due to their contribution in an advisory and editorial capacity toward the final publication.

Björn C. Backeberg

October 5^{th}, 2009

Contents

Abstract i

Supervisors ii

Acknowledgements iii

Preface iv

Declaration vi

1 Introduction **1**

1.1 Motivation 1

1.2 Objectives 2

2 The Hybrid Coordinate Ocean Model **5**

2.1 Vertical coordinate scheme 5

2.2 Mixing processes 7

2.3 Model setup 8

2.4 Model spin-up, forcing procedures and heat flux parameterisation 10

2.5 Nesting procedures 11

2.6 Simulation experiments 11

2.6.1 Details of the momentum advection schemes 12

3 Analysis of the Agulhas system using the Hybrid Coordinate Ocean Model 16

3.1 Introduction . . . 17

3.2 Data Description . . . 18

3.2.1 Satellite data . . . 18

3.2.2 Surface drifter data . . . 19

3.2.3 HYCOM . . . 19

3.3 Observation-model intercomparison . . . 20

3.3.1 Passive microwaves . . . 20

3.3.2 Altimetry . . . 22

3.3.3 Surface drifter data . . . 25

3.4 Space-time analysis . . . 28

3.4.1 Hovmöller analyses . . . 29

3.4.2 Frequency analysis . . . 32

3.4.3 Feature tracking and drift estimates . . . 36

3.5 Summary and conclusion . . . 39

4 Assessing the impact of a higher order numerical advection scheme on the circulation 41

4.1 Introduction . . . 42

4.2 Description of observations and model . . . 44

4.2.1 Satellite altimetry . . . 44

4.2.2 Sea surface temperatures (SSTs) . . . 44

4.2.3 HYCOM . . . 45

4.3 Assessment of the simulation results . . . 46

4.3.1 Vorticity analysis . . . 47

4.3.2 Mean SST distribution . . . 48

4.3.3 The vertical structure of the northern Agulhas Current . . . 50

4.3.4 Transport in the northern Agulhas Current . . . 53
4.4 Analyses of the mesoscale variability . . . 56
4.4.1 Sea surface height variations . . . 56
4.4.2 Sea level skewness . . . 59
4.4.2.1 Assessment from altimetry measurements . . . 60
4.4.2.2 Comparison to HYCOM simulations . . . 63
4.4.3 Variogram analysis . . . 64
4.4.3.1 Comparison to a spatial Fourier analysis . . . 66
4.4.3.2 Quantifying spatial scales of mesoscale variability . . . 69
4.5 Conclusions . . . 71

5 On the formation of Mozambique Channel Eddies 73

5.1 Introduction . . . 74
5.2 Data and methods . . . 75
5.3 Results and discussion . . . 79

6 Mesoscale transport variability in the greater Agulhas Current system 84

6.1 Introduction . . . 85
6.2 HYCOM . . . 87
6.3 Mean transports in the greater Agulhas Current system . . . 87
6.4 Mesoscale transport variability . . . 89
6.5 Surface drifter observations . . . 98
6.6 Correlation to vorticity . . . 102
6.7 Downstream effect of strong transports in the Agulhas Current . . . 107
6.8 Summary and conclusion . . . 113

7 Discussion and conclusion **115**

7.1 Summary 115

7.2 Major findings 118

7.3 Future work 120

Bibliography **122**

Chapter 1

Introduction

1.1 Motivation

The ocean circulation around southern Africa is dominated by a very strong western boundary current, known as the Agulhas Current, which flows poleward along the eastern coast of southern Africa. South of Africa, the current separates from the continental margin and turns back upon itself in what is known as the Agulhas retroflection. Following this loop, most of the current flows back toward the South Indian Ocean, but periodically large anti-clockwise rotating pools of warm water, called Agulhas rings, are detached from the retroflection loop and drift into the South Atlantic Ocean (Lutjeharms, 2006). The process of Agulhas ring shedding from the retroflection is considered to be an important source of warm and salty water for the Atlantic Ocean (Biastoch et al., 2008a), and the Agulhas leakage is thought to play a crucial role in maintaining the Atlantic Ocean meridional overturning circulation, which has implications for climate change scenarios (Peeters et al., 2004).

The ocean dynamics involved in the Agulhas leakage are very complex, and quantifying the magnitude of the Indo-Atlantic inter-ocean exchange of volume, heat and salt is a formidable challenge. It is very difficult to measure the mean circulation patterns and inter-ocean fluxes, and providing realistic simulations is complicated by the highly non-linear nature of the mesoscale variability governing the retroflection regime (Biastoch et al., 2008b). Furthermore, the link between the Agulhas leakage and mesoscale perturbations further upstream is poorly understood (van Leeuwen et al., 2000). Due to a scarcity of *in-situ* observations, modelling activities play a crucial role in furthering the understanding of the link to the Indian Ocean as well as the ocean dynamics of the Agulhas Current and the retroflection region.

Over the past few years, high performance computing has advanced to a stage where it has become possible to integrate models for relatively long periods that resolve high resolution temporal and spatial scales important for understanding the mesoscale variability of the ocean. Furthermore, increased technological capacity and availability of data from space borne sensors monitoring the ocean surface, such as satellite altimeters, as well as *in-situ* observation programs provide the means to rigorously test and validate the ocean models. The need to improve the numerics of the modelling systems has arisen from these model validation efforts and simulation inter-comparisons.

The Hybrid Coordinate Ocean Model (HYCOM; Bleck, 2002) combines the optimal features from isopycnic-coordinate ocean models used in climate studies with those using Cartesian vertical coordinates. HYCOM is able to dynamically change its vertical layer distribution between isopycnic (ρ), z-level and bathymetry following σ-coordinates, regularly adjusting to an optimal vertical structure most suitable for a specific region of the ocean. In this way, HYCOM avoids problems inherent in isopycnal coordinate ocean models, when simulating unstratified waters and efficiently resolves regions of vertical density gradients, such as the thermocline and surface fronts.

The greater Agulhas Current system presents a unique environment in which to test the capability of ocean models. The intense mesoscale oceanic signals and gradients are well captured in satellite remote sensing observations (e.g. Lutjeharms, 1981) providing an important data set with which to validate the model. While the long term goal of this work is to assess the ability of HYCOM to simulate the greater Agulhas Current region for the purpose of implementing the model as one component in an operational monitoring and forecasting system, applying and validating model improvements provides a better quantitative understanding of the role and influence of mesoscale variability and dynamics in the Agulhas Current and the retroflection region. In turn, advancing the knowledge of this mesoscale variability and dynamics will facilitate model validation, which is essential in order to gradually progress towards establishing and implementing an operational system for the greater Agulhas Current regime. Confidence in the accuracy of the model simulation in free-running mode is also an important requirement prior to implementing data assimilation in the model.

1.2 Objectives

The main objective of this work is to **implement the Hybrid Coordinate Ocean Model for the greater Agulhas Current region** and test its capability to simulate this intense western boundary

current and associated mesoscale variability. The need to focus on improving model numerics rather than increasing the model grid resolution as a means to improve model simulations has been highlighted (Barnier et al., 2006), and in a recent study the advantages of implementing a higher order momentum advection scheme in HYCOM have been documented (Winther et al., 2007). Thus, a further objective of this study is to **assess the impact on the circulation dynamics of applying a higher order momentum advection scheme in HYCOM of the Agulhas system**. In achieving these two objectives this study aims to contribute toward advancing the **understanding of the mesoscale dynamics and eddy evolving processes** in the region by analysing the model output in conjunction with satellite observations and *in-situ* measurements. In particular, the **link between the Agulhas leakage and the mesoscale perturbations further upstream** is addressed. Eddies originating from the source regions of the Agulhas Current, namely the Mozambique Channel and south of Madagascar, are thought to play an important role in generating disturbances in the Agulhas Current core that ultimately affect the Agulhas leakage by triggering the shedding of Agulhas rings from the retroflection (e.g. van Leeuwen et al., 2000; Schouten et al., 2002; Penven et al., 2006b). However, the mechanism through which Mozambique Channel Eddies are formed remains poorly understood, and estimates of the contribution of mesoscale eddies toward the volume flux in the Agulhas Current system remain to be quantified adequately.

This thesis is seperated into six chapters. Chapter 2 provides a detailed description of the Hybrid Coordinate Ocean Model set up to simulate the region. In Chapter 3, the first simulation experiment of HYCOM for the greater Agulhas Current system is validated against available satellite remote sensing observations as well as *in-situ* measurements. The capabilities of the model as well as its limitations are discussed, and the oceanographic findings presented. The second simulation experiment is discussed in Chapter 4, where a 4^{th} order momentum advection scheme is implemented as a means to improve the model simulation. The results are compared to the first simulation experiment, and statistical validation methods are explored. While Chapters 3 and 4 focus on the implementation and validation of the model and numerical advancements, Chapters 5 and 6 focus on oceanographic application. Specifically, the eddy formation mechanism in the Mozambique Channel has, to date, not been very well explored, and in Chapter 5 output from the second simulation experiment is used in combination with geostrophic current observations derived from satellite altimeter measurements to propose a mechanism that connects the formation of mesoscale eddies in the Mozambique Channel to the South Equatorial Current north of Madagascar. Finally, in Chapter 6 the transport variability in the Agulhas system and the contribution from mesoscale eddies is investigated using the second simulation experiment, and the connection of the upstream variations to the leakage into

the South Atlantic Ocean is explored. The main findings of this work are summarised and discussed in Chapter 7, concluding with suggestions for future work.

The relevant literature is reviewed and discussed in the introduction to each of the four major chapters of this thesis.

Chapter 2

The Hybrid Coordinate Ocean Model

The Hybrid Coordinate Ocean Model (HYCOM) is a primitive equation model, that combines the optimal features of isopycnic-coordinate and fixed-grid ocean circulation models within one framework (Bleck, 2002)[1]. When simulating oceanic circulation, isopycnic vertical coordinates in ocean models have the advantage of retaining water mass properties over long time integrations, however, these models were not designed to represent unstratified or convectively unstable water columns. HYCOM is able to avoid problems which might occur in simulating such water columns by smoothly interchanging its vertical coordinates between isopycnic (ρ), z-level and sigma (σ) coordinates (Figure 2.1).

At each time-step, HYCOM determines an optimal hybrid layer distribution, interchanging between isopycnic vertical coordinates when simulating the stratified open ocean, z-level coordinates when resolving upper-ocean mixed layer dynamic processes and σ-coordinates in the shallow coastal regions. During these vertical coordinate interchanges, emphasis is placed on restoring the grid to isopycnic coordinates.

2.1 Vertical coordinate scheme

Simulating the vertical movement of water masses in ocean models can be divided into two forms of representation: Lagrangian and Eulerian motion. Representation as Lagrangian motion, in isopycnic models, allows the coordinate surface to move with the respective water masses in the vertical. Allowing the layer thickness to vary in time is achieved by casting the continuity equation as a prognostic layer thickness tendency equation (Equation 2.1), which enables isopycnic coordinate models to retain water

[1]The HYCOM user manual and additional documentation can be found on the HYCOM Consortium webpages: `www.hycom.org`

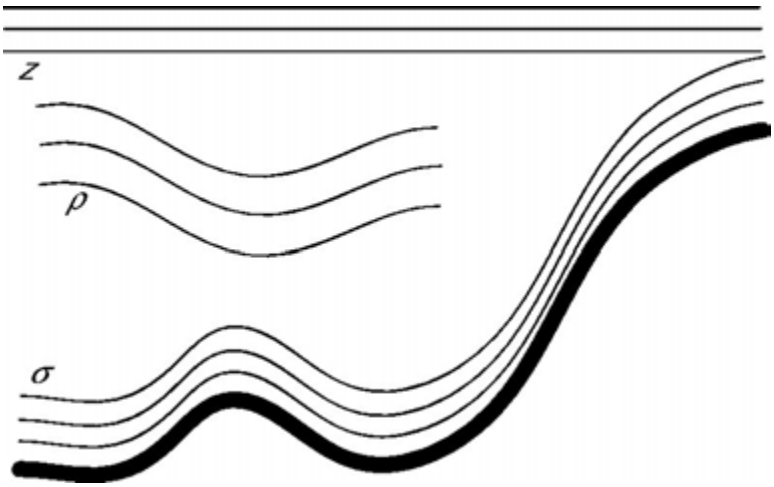

Figure 2.1: Illustration of the three different vertical coordinate schemes utilised in HYCOM.

mass characteristics over long time integrations. The Eulerian approach, used in z-level and σ-coordinate models, utilises a fixed vertical coordinate system, where water is allowed to pass through a coordinate surface, and are thus prone to artificial diffusion.

The principal difference of HYCOM from other numerical models is that it uses both methods of representation, this can be best described in the models representation of the equation of continuity:

$$\frac{\delta}{\delta t_s}(\frac{\delta p}{\delta s}) + \bigtriangledown_s \cdot (\mathrm{v}\frac{\delta \mathrm{p}}{\delta \mathrm{s}}) + \frac{\delta}{\delta s}(\dot{s}\frac{\delta p}{\delta s}) = 0 \tag{2.1}$$

where v = (u, v) is the horizontal velocity vector, p the pressure and s is a vertical coordinate, which is held constant during partial differentiation. The vertical mass flux through a surface (s) is described by the term $\dot{s}\delta p/\delta s$, which is fundamental in hybrid coordinate modelling. It determines the spacing and movement of the layer interfaces, termed the "grid generator".

The grid generator utilised the fact that all layers have an assigned target density and a minimum layer thickness, which is defined for all layers except for the deep layers intersecting the ocean topography. These assigned densities allow the vertical coordinate layers to maintain a finite thickness, by switching from isopycnic coordinates to z-level coordinates when the upper isopycnic layer approaches this minimum thickness. The resulting z-level coordinate is placed at a depth according to a predefined rule, which controls the z-level spacing given by Equation 2.2:

$$\delta_n(k) = min(\delta_p^{max},\, \delta_p^{min} f_p^{k-1}) \tag{2.2}$$

where δ_p^{max} is the maximum z-level thickness, δ_p^{min} the minimum z-level thickness, and f_p the stretching factor. The result is a top layer thickness of δ_p^{min} and a minimum allowed thickness bounded by δ_p^{max} for each layer k.

A characteristic of the hybrid coordinate scheme in HYCOM results in an additional vertical coordinate transition, namely to σ-coordinates in shallow regions. This transition is determined by specifying the number of σ-coordinate layers (N_σ) and the minimum thickness allowed (δ_p^{min}), which gives rise to an additional expression for the minimum layer thickness allowed for each layer:

$$\delta_n'(k) = max[\delta_s^{min},\, min(\delta_n, \frac{D}{N_\sigma})] \tag{2.3}$$

where D is the water depth. Therefore transition to σ-coordinate levels occurs only where the water depth becomes sufficiently shallow to allow $D/N_\sigma < \delta_n$.

2.2 Mixing processes

The horizontal advection and mixing of layer thickness, tracers and momentum is achieved in HYCOM by using a two-dimensional calculation acting on individual layers. This is similar to the Miami Isopycnal Coordinate Model (MICOM; Bleck and Smith, 1990). The horizontal advection of layer thickness results in a vertical movement of the layer interfaces, and horizontal diffusion of temperature and salinity in the isopycnic layers may lead to a deviation from the reference density. In such a situation two water masses, of the same density but different temperatures or salinities, may form a new water mass with a different density. To avoid this, the grid generator is required to restore the coordinate surface to their reference densities at each time step.

The vertical mixing is represented as a combination of cabbeling, restoration processes and explicitly prescribed physical mixing. The vertical mixing scheme employed in the version of HYCOM used at the Nansen Environmental and Remote Sensing Center (NERSC) is the K-Profile Parameterisation (KPP; Large et al., 1994). KPP matches the mixing parameterisation of the ocean interior to that of the surface boundary layer, and takes into account mixing processes resulting from wind and mixed layer turbulence.

Additional mixing parameterisation for internal wave breaking, vertical current shear, salt fingering and double diffusion processes are defined, and a background vertical mixing coefficient ensures diapycnal diffusion in the deep ocean.

An examination of HYCOM simulations in the shelf sea region of the North Sea (Winther and Evensen, 2006) suggested the use of an enhanced KPP mixing scheme to reduce erroneous mixing on shallow continental shelves. Additionally it was shown that the KPP mixing scheme is sensitive to the presence of freshwater, which implies that a good representation of freshwater input is required.

2.3 Model setup

The HYCOM system set up to simulate the Agulhas Current system involves two models: a coarse resolution, basin-scale model of the Indian and Southern Oceans (INDIA), which provides boundary conditions for a regional nested high-resolution model of the Agulhas Current system (AGULHAS; Figure 2.2).

The model grids were created using the conformal mapping tool developed by Bentsen et al. (1999), and realistic ocean bathymetry data, from the 1' resolution General Bathymetric Chart of the Oceans (GEBCO; `www.ngdc.noaa.gov/mgg/gebco`) was interpolated to each of the model grids.

INDIA HYCOM

The INDIA model has a geographical extent which includes the Indian and Southern Ocean (see Figure 2.2). Its horizontal resolution ranges from 14 km in the north, near India, to 42 km in the south, near Antarctica. The vertical discretisation in the model uses 30 vertical hybrid layers with target densities referenced to σ_0 (= 1000 kg.m^{-3}), ranging from 21.0 to 28.3 kg.m^{-3}.

At the open boundaries, the temperatures and salinities are relaxed toward monthly mean climatologies produced by the Generalized Digital Environmental Model (GDEM; Teague et al., 1990). Two in / outflow ports have been defined: (1) a 10 Sv westward inflow through the Indonesian Throughflow and (2) a 10 Sv outward flux in the South Pacific Ocean. The model is also coupled to an Elastic-Viscous-Plastic sea ice model (EVP; *Lisæter et al., 2003*), to simulate ice drift in the Antarctic Ocean.

Following the 8 year spin-up, a simulation experiment beginning in 1996 was run until the end of 2006. Continental run-off from rivers as well as tidal amplitudes were excluded from the simulation.

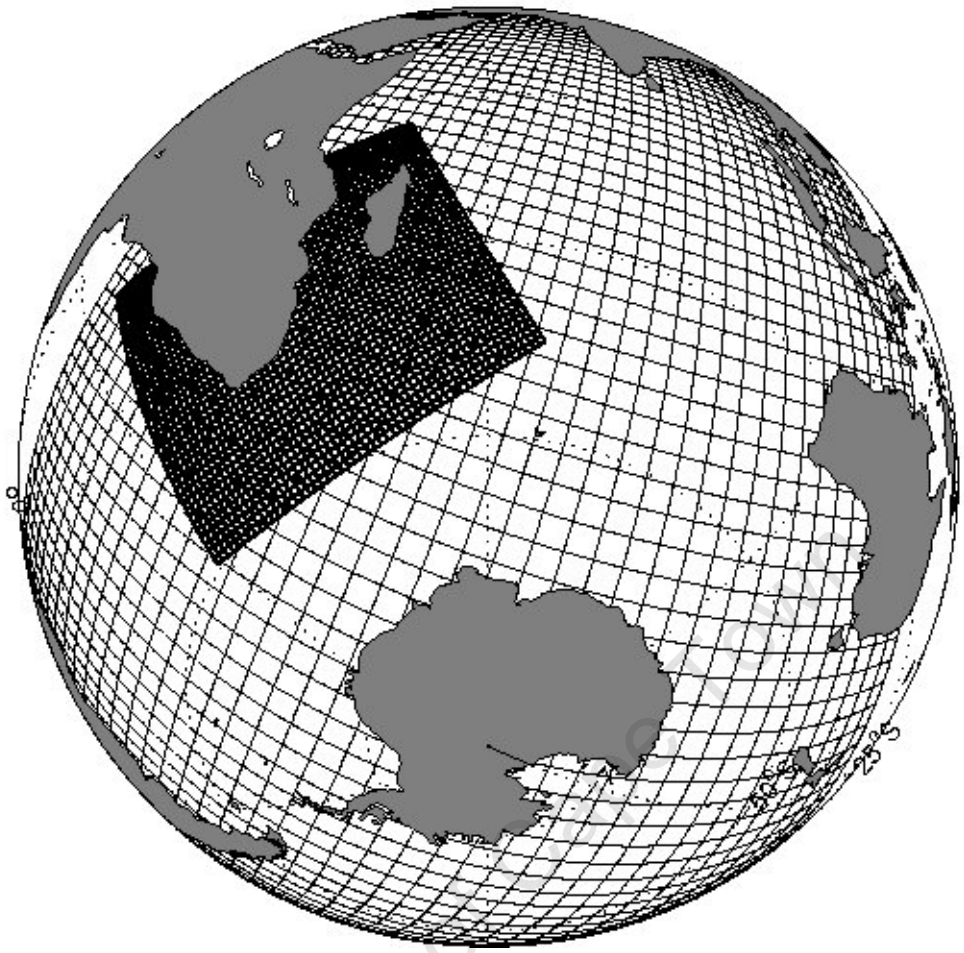

Figure 2.2: Illustration of the HYCOM model system: coarse resolution basin-scale (INDIA) model grid, provides boundary conditions for a high-resolution nested regional (AGULHAS) model grid. Every tenth grid point was plotted to produce the respective mesh grids, therefore each box consists of 10x10 grid cells.

AGULHAS HYCOM

A $1/10^{th}$ of a degree model of the Agulhas Current system is nested within the INDIA model (Section 2.3). It receives boundary conditions determined by output from the INDIA model at the its boundary grid coordinates. The geographical domain extends from $0° - 60°$E and from $10° - 50°$S, to include the major features of the Agulhas Current system, namely the source regions, the Mozambique Channel and the East Madagascar Current, the Agulhas Current core, the Agulhas retroflection, the ring shedding corridor and the Agulhas return current.

The vertical discretisation in the AGULHAS model mimics that of the INDIA model: 30 hybrid layers with target densities ranging from 21.0 to 28.3, referenced to σ_0.

The AGULHAS model was initialised from a balanced INDIA model field interpolated onto the high resolution grid, and a simulation experiment was run concurrently with the INDIA model from the beginning

of 1996 to the end of 2006. Neither river fluxes nor tidal amplitudes were included in the regional model simulation.

The hydrography of the regional HYCOM of the Agulhas has been compared to available WOCE sections in Backeberg (2006), and the vertical structure in the greater Agulhas Current system has been found to be reasonably well represented in the model.

2.4 Model spin-up, forcing procedures and heat flux parameterisation

The INDIA model was initialised from Generalized Digital Environmental Model (GDEM; Teague et al., 1990) data, and a spin-up period of 8 years using monthly mean climatological forcing was run to allow it to reach a balanced state prior to beginning the simulation experiments. The forcing data used during the spin-up period is based on the ERA40 re-analysis (Uppala et al., 2005), with a correction applied to dampen the strong precipitation bias of the ERA40 re-analysis in the tropical oceans (Troccoli and Kållberg, 2004).

Rather than running a spin-up simulation, the AGULHAS model was initialised from a balanced INDIA model field, which was interpolated to the high resolution model grid.

During the simulation experiments, the models are forced at 6-hourly intervals using interannual synoptic atmospheric forcing fields from ERA40, before 2002 and the operational analyses from ECMWF are applied after July 2003. Cloud cover data from the Comprehensive Ocean-Atmosphere Data Set (COADS; Slutz et al., 1985) and precipitation data from Legates and Willmott (1990) are also applied.

Surface fluxes of heat and mass, except for the shortwave thermal radiation are absorbed in the surface mixed layer of the model. The shortwave radiation may penetrate to deeper layers depending on the clarity of the water, using the exponential decay model of Jerlov (1976). In HYCOM, there are two choices for the bulk parameterisation of the surface fluxes, the first is the standard constant bulk coefficients, and the second uses the sophisticated parameterisation scheme of Kara et al. (2000), which include the effects of dynamic stability derived from a statistical analysis of global monthly climatologies. The user also has the option of relaxing the near-surface temperature or salinity to climatology.

2.5 Nesting procedures

The NERSC-version of HYCOM utilises a one way nesting scheme, where boundary conditions for the AGULHAS model are relaxed towards output provided by the INDIA model. For the slow varying variables such as baroclinic velocity, temperature, salinity and layer interfaces, the boundary condition calculations are based on the flow relaxation scheme (FRS; Davies, 1983). The faster moving barotropic variables are treated in a hyperbolic wave equation for pressure and vertically integrated velocities (Browning and Kreiss, 1982, 1986), these must be treated carefully to avoid reflection of waves at the open boundaries. Numerical instabilities do occur at the boundary, and it is important that these do not affect the region of study.

The INDIA model provides values for the AGULHAS model boundaries every 6 hours that are interpolated to the (usually) higher resolution grid. The AGULHAS model then reads the boundary conditions every 6 hours, and interpolates in time for the individual time steps.

2.6 Simulation experiments

Two simulation experiments of the nested high resolution model are discussed in this thesis. Both simulations start in January 1996 and end in December 2006.

The first experiment, following the implementation of HYCOM for the Agulhas system, uses the standard 2^{nd} (O2) order momentum advection scheme, which is the standard scheme used in HYCOM. In the second simulation experiment, a 4^{th} order (O4) momentum advection scheme based on the quadratic upstream interpolation for convective kinematics scheme (QUICK; Leonard, 1979) was implemented. The

Parameter	O2	O4	Explanation
slip	-1	-1	$+1$ for free-slip,-1 for non-slip boundary conditions
visco2	0.10	0.07	deformation-dependent Laplacian viscosity factor (m^2/s)
visco4	0.00	0.00	deformation-dependent bi-harmonic viscosity factor (m^2/s)
veldf2	0.03	0.00	diffusion velocity (m/s) for Laplacian momentum dissipation
veldf4	0.01	0.00	diffusion velocity (m/s) for bi-harmonic momentum dissipation
thkdf2	0.00	0.00	diffusion velocity (m/s) for Laplacian thickness diffusion
thkdf4	0.01	0.00	diffusion velocity (m/s) for bi-harmonic thickness diffusion
temdf2	0.015	0.005	diffusion velocity (m/s) for Laplacian temperature/salinity diffusion

Table 2.1: Values and explanations of parameters chosen for the two simulation experiments. The values of the parameters chosen for the two simulation experiments were carefully adjusted at the lowermost acceptable values for both simulation experiments.

bi-harmonic viscosity built into the 4^{th} order scheme was modified to minimise the viscosity coefficient as in Winther et al. (2007).

Table 2.1 indicates the values of the parameters chosen for the two simulation experiments. The viscosity parameters have been carefully adjusted to the lowermost acceptable value. Lower viscosities in the 4^{th} order scheme allow for numerical instabilities that eventually cause the model to crash, by violation of the Courant-Friedrichs-Lewy (CFL) conditions, and in the 2^{nd} order scheme, they exhibit unphysical numerical noise.

Both simulations use the same nesting conditions from INDIA, and in each case the same horizontal forcing fields, as described above, were applied.

2.6.1 Details of the momentum advection schemes

There are numerous ways in which a model simulation may be improved. Usually the model grid resolution is increased in order to reduce the truncation error. Another option is to implement higher-order finite difference approximations as a means to reduce the truncation error, which has a significantly lower computational cost compared to increasing the model grid resolution. In Chapter 4, the impact of applying a higher order momentum advection scheme for simulating the Agulhas Current is discussed. The description of the momentum advection schemes here focuses on the spatial discretisation. The temporal discretisation in the experiments presented in this thesis are based on leapfrog schemes with sufficiently small time steps to assume that errors are principally associated with the spatial discretisation.

From the discussions in Winther et al. (2007), consider the below dimensional advection equation,

$$\frac{\partial \psi}{\partial t} - U\frac{\partial \psi}{\partial x} = 0 \tag{2.4}$$

where U is a velocity field and ψ a tracer, which can also be the velocity field itself if we consider the momentum equation. Equation 2.4 can be solved using centered schemes, however these numerical discretisations induce inaccuracies, or numerical noise (e.g. Webb et al., 1998). This results in the fact that the numerical propagation speed of a perturbation ($\hat{U}$) is different from the analytical propagation speed (U). In order to decrease this error, we can either increase the order of the finite difference approximation, or increase the resolution of the model.

For constant grid spacing, $\Delta x = L/N$, where L is the total length of the domain and N is the number of grid points, the wave number, k, is only defined for discrete values, $k = 2\pi/n\Delta x$, and $n \in [2, ..., N]$. For the second order scheme the numerical approximation of the spatial derivative term is

$$\frac{\partial \psi^{O2}}{\partial x} = \frac{\psi(x + \Delta x) - \psi(x - \Delta x)}{2\Delta x} \tag{2.5}$$

and for the fourth order theme it is

$$\frac{\partial \psi^{O4}}{\partial x} = \frac{1}{(3/2)\Delta x}\left[\psi(x + \Delta x) - \psi(x - \Delta x) - \frac{1}{8}(\psi(x + 2\Delta x) - \psi(x - 2\Delta x))\right] \tag{2.6}$$

Equations 2.5 and 2.6 can be used to calculate the numerical propagation speed of a perturbation $\psi(x) = e^{ikx}$ with $k = 2\pi/n\Delta x$, $n \in [2, ..., N]$. If the time discretisation is perfect, this results in

$$\hat{U}^{O2} = U\frac{\sin(k\Delta x)}{k\Delta x} \tag{2.7}$$

$$\hat{U}^{O4} = U\frac{2\sin(k\Delta x) - (1/4)\sin(2k\Delta x)}{(3/2)k\Delta x} \tag{2.8}$$

This shows that the cost of increasing the spatial scheme increases with the higher order spatial discretisation scheme. However, the increase remains lower compared to doubling the resolution of the model grid, which results in a factor of 4 increase of the cost, due to the CFL condition associated with the explicit time stepping schemes. The gain, in terms of improving the model simulation is discussed in Chapter 4.

The higher order scheme used in the experiment discussed in Chapter 4 is approximated to the 4^{th} order and is based on the quadratic upstream interpolation for convective kinematics (QUICK; Leonard, 1979) scheme. A version of the QUICK scheme is applied, with the built in bi-harmonic viscosity modified to minimise the viscosity coefficient proportional to the modulus of the velocity field and the grid spacing (as in Winther et al., 2007).

Solving the momentum equation (2.4) numerically, leads to non-physical dispersion at small scales, which leads to noisy fields. In order to negate the numerical noise, diffusive terms need to be added to dampen this effect. As in Winther et al. (2007), we have chosen bi-harmonic diffusion, which is built into the fourth order advection scheme:

$$Diff(U) = \frac{\partial}{\partial x}\left(v\frac{\partial^3 U}{\partial x^3}\right) + \frac{\partial}{\partial y}\left(v\frac{\partial^3 U}{\partial y^3}\right) \tag{2.9}$$

Choosing the viscosity coefficient v is a delicate issue. In some cases it is chosen to be constant, with a variable part proportional to the deformation tensor (see Smagorinsky, 1963). Since the goal is to counter the dispersive nature of the advection scheme, it can be chosen more precisely. It can be shown that

$$U\frac{\partial U^{O4}}{\partial x} = U\frac{\partial U}{\partial x} - U\frac{\Delta x^4}{30}\frac{\partial^5 U}{\partial x^5} + O(\Delta x^5) \tag{2.10}$$

The first order correction term is proportional to $\frac{\partial^5 U}{\partial x^5}$ and is the dispersive term which needs to be countered by diffusion. The aim is then to add a diffusion term which overcomes this dispersive effect.

Winther et al. (2007) discuss that the critical wavelength L_w determines which dynamics are correctly represented by a numerical scheme, and the viscosity coefficient has to be chosen such that the amplitude of the wavelength L_w is significantly reduced over a time period of validity of its dynamics, $\Delta t = 10L_w/ \mid U_0 \mid$. The rate of decrease associated with a bi-harmonic diffusion is $1/vk^4$, which results in

$$vk^4 \simeq \frac{\ln(2) \mid U_0 \mid}{10L_w} \tag{2.11}$$

for the fourth order scheme ($L_w = 4.4\Delta x$) this yields

$$v \simeq \frac{\ln(2) \mid U_0 \mid L_w^3}{10(2\pi)^4} \simeq 5 \times 10^{-3} \mid U_0 \mid \Delta x^3 \tag{2.12}$$

In practice, shocks develop because of the non-linearity of the momentum advection equation. A shock is a discontinuity with the scale of a grid cell. The previous calculations are not valid in this case, but using a Smagorinsky viscosity (Smagorinsky, 1963), these shocks can be dealt with efficiently. Generally viscosity of the below form is chosen:

$$v = \Delta x^3 max(C_1\sqrt{U^2 + V^2}, C_2\Delta x t_d) \tag{2.13}$$

where $t_d = \sqrt{\left(\frac{\partial U}{\partial x} - \frac{\partial V}{\partial y}\right)^2 + \left(\frac{\partial U}{\partial y} - \frac{\partial V}{\partial x}\right)^2}$ is the deformation tensor.

The coefficients C_1 and C_2 are chose to be as small as possible, but large enough to overcome the development of noise because of the dispersive nature of the fourth order centered scheme. In the QUICK scheme

(e.g. Farrow and Stevens, 1995; Holland et al., 1998), $C_1 = 1/16$ and $C_2 = 0$. The previous calculations suggest $C_1 \simeq 0.005$ to overcome dispersive effects, and Winther et al. (2007) show that in academic configurations $C_2 = 0.05$ yields good results. These are also the values that have been chosen for the fourth order momentum advection scheme in the experiments presented in this thesis.

Chapter 3

Analysis of the Agulhas system using the Hybrid Coordinate Ocean Model

This chapter is based on the work published as:

Backeberg, B. C., J. A. Johannessen, L. Bertino, C. J. Reason (2008). The greater Agulhas Current system: An integrated study of its mesoscale variability. *Journal of Operational Oceanography*, 1(1):29-44(16).

Abstract

For the purpose of developing an operational oceanography system for the greater Agulhas Current regime, a high resolution Hybrid Coordinate Ocean Model (HYCOM) has been set in a nested configuration. The intense and complex current regime poses a challenge in modelling. However, access to satellite and in-situ data with strong and persistent signals of the dynamics and mesoscale variability ensure that adequate model validation is feasible. The study concludes that HYCOM reproduces the general larger scale circulation of the greater Agulhas Current reasonably accurately in addition to the regionally specific characteristics and mesoscale variability. Furthermore, strong anticyclonic eddies occurring in the Mozambique Channel at a frequency of $5-6$ yr^{-1}, are found to drift southward and merge with the northern Agulhas Current. Evidence of these eddies can also be tracked further southwestwards into the southern Agulhas Current and sometimes all the way towards the Agulhas retroflection region. Operational forecasting of the greater Agulhas Current, and in particular the retroflection, must therefore adequately account for the presence and influence of the Mozambique Channel eddies, in order to forecast their evolution on time scales from days to weeks.

3.1 Introduction

The Agulhas Current has been described as one of the strongest western boundary currents in the world's oceans (Lutjeharms, 2006). Forming part of the South-West Indian Ocean sub-gyre, the current flows polewards along the southeastern coast of Southern Africa from 27°S, eventually retroflecting and flowing eastward back into the South Indian Ocean south of Africa between 40° and 42°S (Gordon, 1985; Stramma and Lutjeharms, 1997).

The upstream source region for the Agulhas Current has distinct contributions from the flow through the Mozambique Channel, the poleward flowing East Madagascar Current (EMC), and recirculation from the South-West Indian Ocean sub-gyre, which supplies the greater part of the volume transport in the Agulhas Current, i.e. 40 Sv of a total 60 Sv in the upper 1000 m (Stramma and Lutjeharms, 1997). The flow in the Mozambique Channel is dominated by southward moving anticyclonic eddies (Sætre and da Silva, 1984; Biastoch and Krauss, 1999; de Ruijter et al., 2002). These eddies have spatial scales of approximately $300 - 350$ km and propagate southwards at speeds of approximately $3 - 6$ km.d^{-1} (Schouten et al., 2002, 2003). Concurrently, the EMC retroflects southwest of Madagascar (Siedler et al., 2006), generating cyclonic and anticyclonic eddies up to 250 km in diameter (Quartly and Srokosz, 2004). These propagate westwards towards the Agulhas Current (de Ruijter et al., 2004). Although the Mozambique Channel eddies and the EMC do not form a continuum with the Agulhas Current, they both affect its dynamics (Lutjeharms, 2006) and contribute to the fluxes of volume, heat and salt.

Mesoscale variability in the northern Agulhas Current (Gründlingh, 1983) occurs in the form of intermittent cyclonic meanders, known as Natal Pulses. These form at the Natal Bight, between 29°S and 30°S, where the gentler continental slope and wider shelf present favourable conditions for the occurrence of instabilities and subsequent growth of meanders (de Ruijter et al., 1999b). Natal Pulses form approximately six times per year and propagate downstream at rates of 10 km.d^{-1} (Lutjeharms and Roberts, 1988). A further source of variability is the Mozambique Channel eddies. Their propagation into the source region of the Agulhas Current has been confirmed by previous altimetry studies (Biastoch and Krauss, 1999; Schouten et al., 2002). Additionally, their interaction with the Agulhas Current has been shown to influence the timing and frequency of Agulhas ring shedding events at the retroflection. Schouten et al. (2002) suggest this to occur via two mechanisms. Firstly, the southward progressing Mozambique Channel eddies trigger the formation of the aforementioned Natal Pulse, and these are known to precede ring shedding events at the retroflection by approximately 180 days (van Leeuwen et al., 2000). Secondly, the migration of

Mozambique Channel eddies into the Agulhas retroflection region may lead to an early occlusion of the retroflection loop allowing Agulhas Ring shedding to occur.

Numerical models need to adequately resolve the mesoscale dynamics and variability of the greater Agulhas Current regime in order to be considered for use in an operational oceanography system.

In this chapter, it is demonstrated that the intense dynamics and mesoscale variability of the greater Agulhas Current system act as an excellent natural laboratory for studies using integrated satellite and in situ observations with model simulations. As well as allowing model validation, the integrated approach also ensures advances in process understanding of this complicated current regime. The data sources and model characteristics are described in the next section, followed by an intercomparison of the model simulation results with observations, considering spatial, temporal and drift analyses of the mesoscale variability and dynamics over an 11 year period from $1996 - 2006$. The summary and conclusion of the main findings are presented in the final section of this chapter.

3.2 Data Description

The strong thermal gradients and sea level anomalies associated with the dynamics and mesoscale variability of the greater Agulhas Current system make it particularly amenable to monitoring via satellite remote sensing observations such as those from radiometry and microwave altimetry. In addition, a comprehensive database of Lagrangian surface drifter data allows complementary quantitative analyses of the surface currents.

3.2.1 Satellite data

Sea surface temperature (SST) observations from the cloud independent Tropical Rainfall Measuring Mission (TRMM) Microwave Imager and the Advanced Microwave Scanning Radiometer for EOS (AMSR-E) are used in the model validation process. TRMM follows an equatorial orbit with a 35° inclination, allowing for coverage between 40°N and 40°S, while the National Aeronautic and Space Administration (NASA) AQUA satellite follows a near polar orbit allowing for global coverage. These data are used to calculate optimally interpolated sea surface temperature fields (OI SST) on a daily basis with a spatial resolution of $\sim$ 25 km. The Microwave OI SST data are produced by Remote Sensing Systems and sponsored by National Oceanographic Partnership Program (NOPP), the NASA Earth Science Physical Oceanography

Program, and the NASA REASoN DISCOVER Project. Weekly averages have been calculated from the daily data available at `www.remss.com`.

Moreover, gridded data of sea level anomaly (SLA) and surface geostrophic velocities derived from maps of absolute dynamic topography are used for comparison against the model fields. The gridded data are merged from multiple altimeter missions, namely TOPEX/Poseidon, Jason-1, ERS-1/2, GFO and ENVISAT. They span the time period from January 1996 to December 2006. The data were obtained from the SSALTO/DUACS near-real time and delayed mode multimission altimeter data processing system at Centre National d'Etudes Spatiales (CNES; `www.aviso.oceanobs.com`). The mapping technique used to produce the gridded maps has been outlined in detail by Ducet et al. (2000). The gridded data has a horizontal resolution of $1/3^\circ$ on a Mercator grid, which therefore provides grid-resolution of 24 km to 37 km in the Agulhas region. These maps are available at weekly intervals.

3.2.2 Surface drifter data

The surface drifter data with drogues at 15 m include position and time observations. Archived data from the Global Drifter Program, formerly World Ocean Circulation experiment Surface Velocity Programme (WOCE-SVP), are available from the Marine and Environmental Data Services at Fisheries & Oceans Canada (`www.meds-sdmm.dfo-mpo.gc.ca`).

Daily average drift velocities were calculated from the successive positions and times given for the individual drifters. The data were then binned into a 1° spatial grid. For the purpose of this study only drifter data for the region of the Mozambique Channel, the Agulhas Current proper, the Agulhas retroflection and the ring shedding corridor is considered for the period $1996 - 2006$.

3.2.3 HYCOM

Details of the Hybrid Coordinate Ocean Model (HYCOM) are outlined in Chapter 2. In this first simulation experiment of the nested HYCOM of the greater Agulhas Current system, the model is run from January 1996 to December 2006 using the standard 2^{nd} order momentum advection scheme.

3.3 Observation-model intercomparison

In this section the spatial characteristics of the model surface fields are compared with observations. The discussion is arranged according to passive microwaves, satellite altimetry and surface drifter data.

3.3.1 Passive microwaves

Model validation using the microwave SST fields is shown in Figure 3.1, where maps of weekly average TMI AMSR-E OI SST (left panel) are compared to maps of weekly HYCOM surface temperatures (right panel) for a period from October to December 2002. The black contours in both panels represent the isotherms 3.4°, 7.0°, 14.2°, 17.9°, 20°, 22°, 25° and 28°C. The first four are selected to respectively represent the mean SST of the Antarctic Polar Front (APF), the Sub-Antarctic Front (SAF), the Sub-Tropical Convergence (STC) and its northern extent derived from ship-board observations (Lutjeharms and Valentine, 1984).

Comparable large scale surface temperature patterns are found including the southward progression from October to December 2002 of the warm tropical surface water, as represented by the 25°C isotherm, which reaches approximately 25°S in the Mozambique Channel. Moreover, it is apparent that HYCOM simulates the dominant wavelengths of the meandering surface temperature isotherms in reasonable agreement with the observed SST fields.

HYCOM shows a reduced southwestward extent of the Agulhas Current surface temperature signal towards the retroflection region, represented by the 20° and 22°C isotherms. This deficiency may have some implications for accurate simulation of the Indo-Atlantic inter-ocean fluxes of heat and salt.

The Sub-Tropical Convergence (STC) is the northernmost front associated with the Antarctic Circumpolar Current (ACC), and it exhibits the most prominent thermal and salinity gradients both at the sea surface and at depth (Lutjeharms, 1985). The STC surface temperature expression and its northern extent is represented by the zone between the 14.2°C and the 17.9°C isotherms and reveals its meandering nature. The Sub-Antarctic Front (SAF) displays weaker horizontal surface temperature gradients than the STC, and is demarcated by the 7°C isotherm. The Antarctic Polar Front (APF) has a less distinct surface expression with an average middle temperature expression of 3.4°C. The mean latitudinal positions of the STC, SAF and APF as outlined in Lutjeharms and Valentine (1984) of 41°, 46° and 50°S respectively agree reasonably well to locations given by the microwave SST. Moreover HYCOM is also able to reproduce agreeable mean latitudinal positions of these fronts in the southern regions except the APF which does

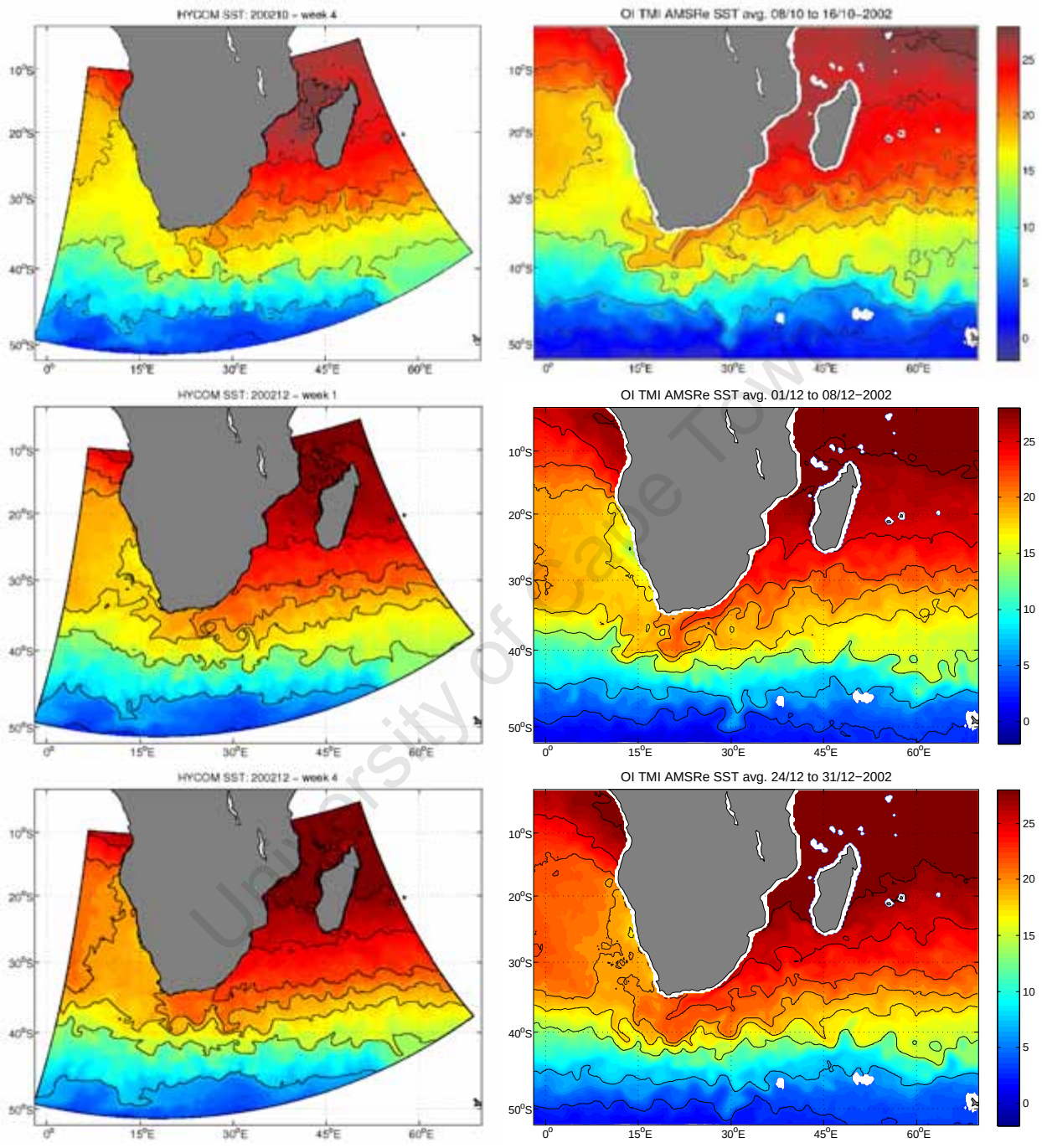

Figure 3.1: Weekly average sea surface temperature (°C) fields from HYCOM (left panel) and from passive microwave observations from the TRMM Microwave Imager and AMSR-E (right panel). The black contours represent isotherms 3.4°, 7°, 14.2°, 17.9°, 20°, 22°, 25° and 28°C.

not fall within the model domain.

3.3.2 Altimetry

Weekly model surface velocity fields in the AGULHAS HYCOM (Figure 3.2, left panel), taken from week 4 in October and from weeks 1 and 4 in December 2002, are compared to coincident altimeter-based surface geostrophic velocities (Figure 3.2, right panel). In this comparison it is found that the altimetry derived velocities may be underestimated by a factor of 1.5. This is probably due to the subsampling of the altimeter, and the fact that a-geostrophic velocities may contribute substantially to the overall flow. Furthermore, as the altimeter satellite tracks are not consistently perpendicular to the main flow direction of the Agulhas Current, the maximum slope and surface geostrophic current are not always captured. Hence, the more intense model velocity field is not necessarily unrealistic. Overall these comparisons reveal that the observed circulation features in the greater Agulhas Current system are reasonably well simulated in HYCOM.

Both the HYCOM velocity fields and the surface geostrophic velocities suggest that the flow in the Mozambique Channel is dominated by southward propagating anticyclonic eddies, as previously documented by Schouten et al. (2003). The horizontal scales of the Mozambique Channel eddies simulated in HYCOM are of comparable sizes to those observed from altimetry, and are approximately 300 km in diameter. However, in HYCOM these seem much more energetic. The model indicates that these eddies tend to form north of the Davies Ridge, near 15°S, and then move southward along the western edge of the channel. Near 30°S, they appear to merge with the northern Agulhas Current. This behaviour is strongly emphasised in HYCOM (see Figure 3.2, left panel). Biastoch and Krauss (1999) document similar results in their regional model of the Agulhas Current system, and claim that a clear connection exists between eddies in the Mozambique Channel and the Agulhas Current. The consistent merger of Mozambique Channel eddies with the northern Agulhas Current may thus be due to the fact that these eddies are more energetic in HYCOM.

HYCOM shows that the East Madagascar Current (EMC) splits into the northern and southern branches near 17°S, in agreement with previous literature (Lutjeharms et al., 2000). Surface velocities from HYCOM in the southern branch reach up to 0.7 $m.s^{-1}$, with even stronger velocities, up to 1 $m.s^{-1}$, evident at the northern tip of Madagascar. At the southern tip of Madagascar, the southern EMC reveals a tendency to undertake an anticyclonic return loop. Eddies, episodically detach from this loop and travel westward

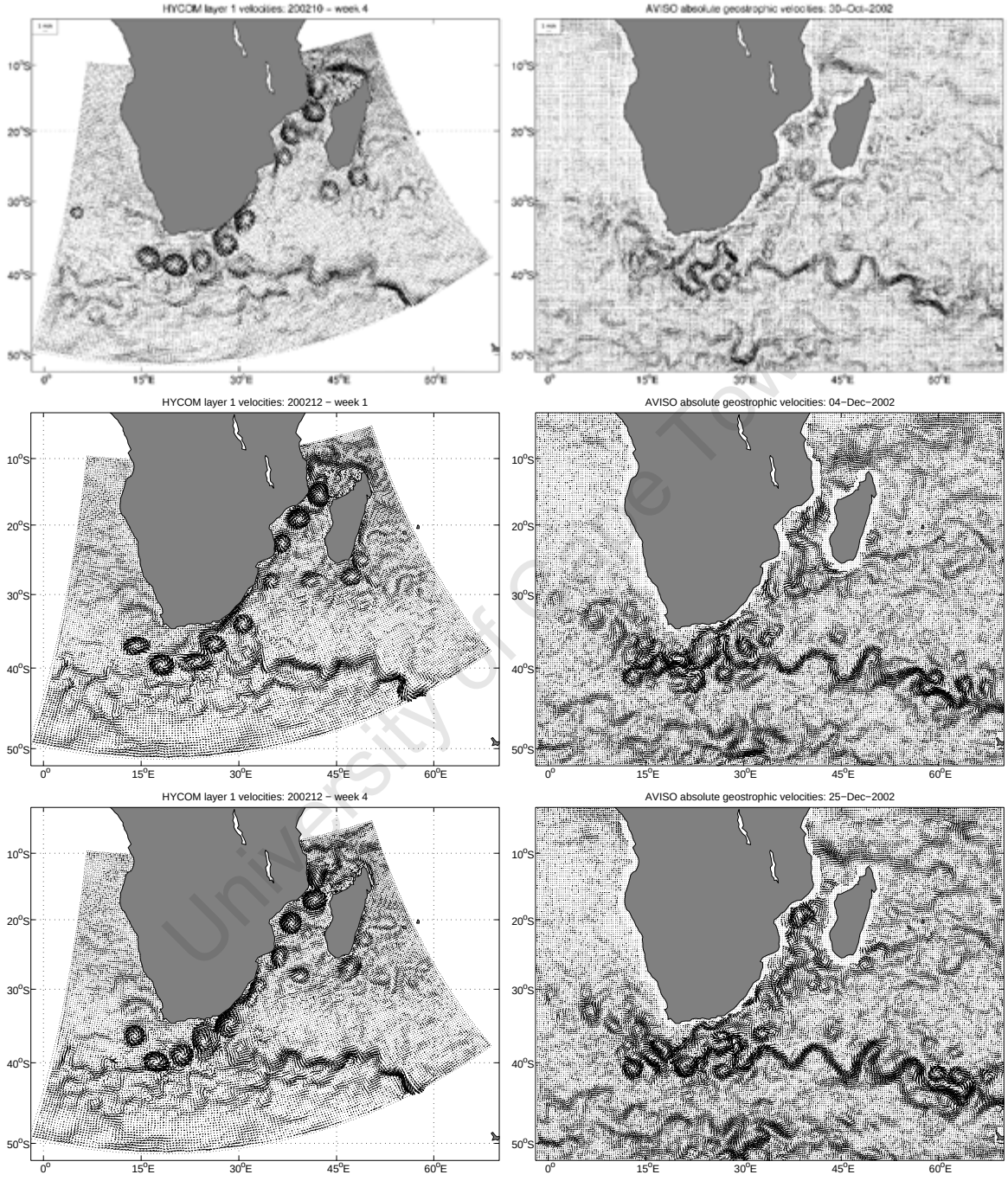

Figure 3.2: Weekly surface velocities from HYCOM (left panel), and weekly surface geostrophic velocities from AVISO (right panel).

where they eventually interact with the northern Agulhas Current. As satellite altimetry is unable to capture mesoscale ocean dynamics close to the coast, it neither reveals the EMC split, nor the strong southward flowing "mini" western boundary current. Altimetry does, however, provide evidence of a strong westward flow north of Madagascar and also strongly supports the notion of a retroflecting EMC south of Madagascar with the formation of cyclonic and anticyclonic eddies as discussed.

The main features of the Agulhas Current are well represented in the model. In the north, the Agulhas Current intensifies near 27°S and closely follows the shelf edge, which lies close to the coast, consistent with observations (Gründlingh, 1983). Weekly mean surface velocities exceeding 1.5 m.s^{-1} are simulated near the coast between 30°S and 35°S in agreement with direct current meter measurements reported in Bryden et al. (2005). HYCOM suggests that the dominant mode of variability here occurs in association with large anticyclonic eddies, approximately $300-350$ km in diameter, propagating southwestwards from the Mozambique Channel (Figure 3.2, left panel). Moreover, it seems that these eddies consistently trigger Natal Pulses as they pass the Natal Bight at 30°S. The interaction of Mozambique Channel eddies with the northern Agulhas Current is also evident in the surface geostrophic velocity observations from altimetry. However, upon approaching the northern Agulhas Current, the spatial scales of the eddies in the altimetry observations are smaller than those in the model, and they also display weaker orbital velocities.

The shelf edge separates from the coast near 33°S. As a result, the current is steered away from the coast, becoming increasingly unstable in its mean southwestward path. This growing meandering nature of the southern Agulhas Current is well represented in the surface geostrophic velocity observations from altimetry, as the core of the current is now sufficiently far away from the coast. In comparison, the mesoscale variability in HYCOM is simulated as a succession of southwestward propagating eddies in this region.

In the vicinity of the retroflection region the ocean dynamics become intense and very complex. In the weekly altimeter maps the surface current is observed to retroflect in an anticyclonic loop somewhere near 16°E and between 39° and 40°S (Figure 3.2, right panel) with a diameter exceeding 300 km, consistent with previous literature (e.g. Lutjeharms and van Ballegooyen, 1988). Complete understanding of the mechanisms that influence and control the retroflection of the Agulhas Current is lacking although a number of theories have been put forward, such as conservation of potential vorticity and inertia (summarised in de Ruijter et al., 1999a). In HYCOM, a train of southwestward propagating eddies with diameters of about $200-250$ km seem to reach the retroflection area, hence supplying mesoscale energy to the com-

plicated dynamics of the region (Figure 3.2, left panel). This train of eddies extending from the Agulhas Plateau to the retroflection has been a common feature in numerical model simulations of the region. It was first reported by Lutjeharms and Webb (1995) using the Fine Resolution Antarctic Model (FRAM). Recently, Barnier et al. (2006) showed that improved numerics, in particular of the momentum advection scheme, clearly improve the numerical simulation of this region. Although the dominant weekly surface velocity pattern induced by this train of eddies masks the position of the retroflection in HYCOM, it is fairly well represented in the longer term mean as addressed later.

Both altimetry and model data reveal that ring shedding events occur at the retroflection. Agulhas Rings are unique, because they form in association with a zonal protrusion of the parent current, and are typically larger than rings formed in association with current and frontal instabilities, such as Gulf Stream or Kuroshio rings (Pichevin et al., 1999). Furthermore, Agulhas Rings form a vital link through which warm, saline water from the Indian Ocean is transported to the Atlantic Ocean (Gordon, 1985).

In HYCOM, predominantly anticyclonic eddies with scales of approximately 300 km, can be seen propagating in a general northwesterly direction into the Southeast Atlantic Ocean. The horizontal scales and current intensities of these vortices are somewhat exaggerated. In comparison to the altimetry study by Fu (2006), HYCOM fails to simulate the broad fan of eddy trajectories into the Southeast Atlantic Ocean. Fu (2006) concluded that eddies in this region propagate in a relatively broad northwestward direction at a mean speed of $3 - 4$ km.d^{-1}.

The eastward flowing current from the retroflection region between 39°S and 40°S is known as the Agulhas Return Current. HYCOM simulates the mean position of this meandering return current in good agreement with the altimeter observations as well as the satellite SST observations reported above. The semi-permanent meanders, previously documented in Boebel et al. (2003b), are visible in the surface geostrophic velocity fields as well as in HYCOM, with their southern crests evident near 29°E, 35°E and 43°E. The gradual shift of the core of the Agulhas Return Current towards higher latitudes in the east is also evident in the model.

3.3.3 Surface drifter data

Lagrangian surface drift data usually pose a challenge for direct comparison to Eulerian velocities (Jakobsen et al., 2003). In order to benefit from these drifter data for model validation, the mean gridded velocities calculated from HYCOM and the SVP drifters were normalised against the spatially averaged standard

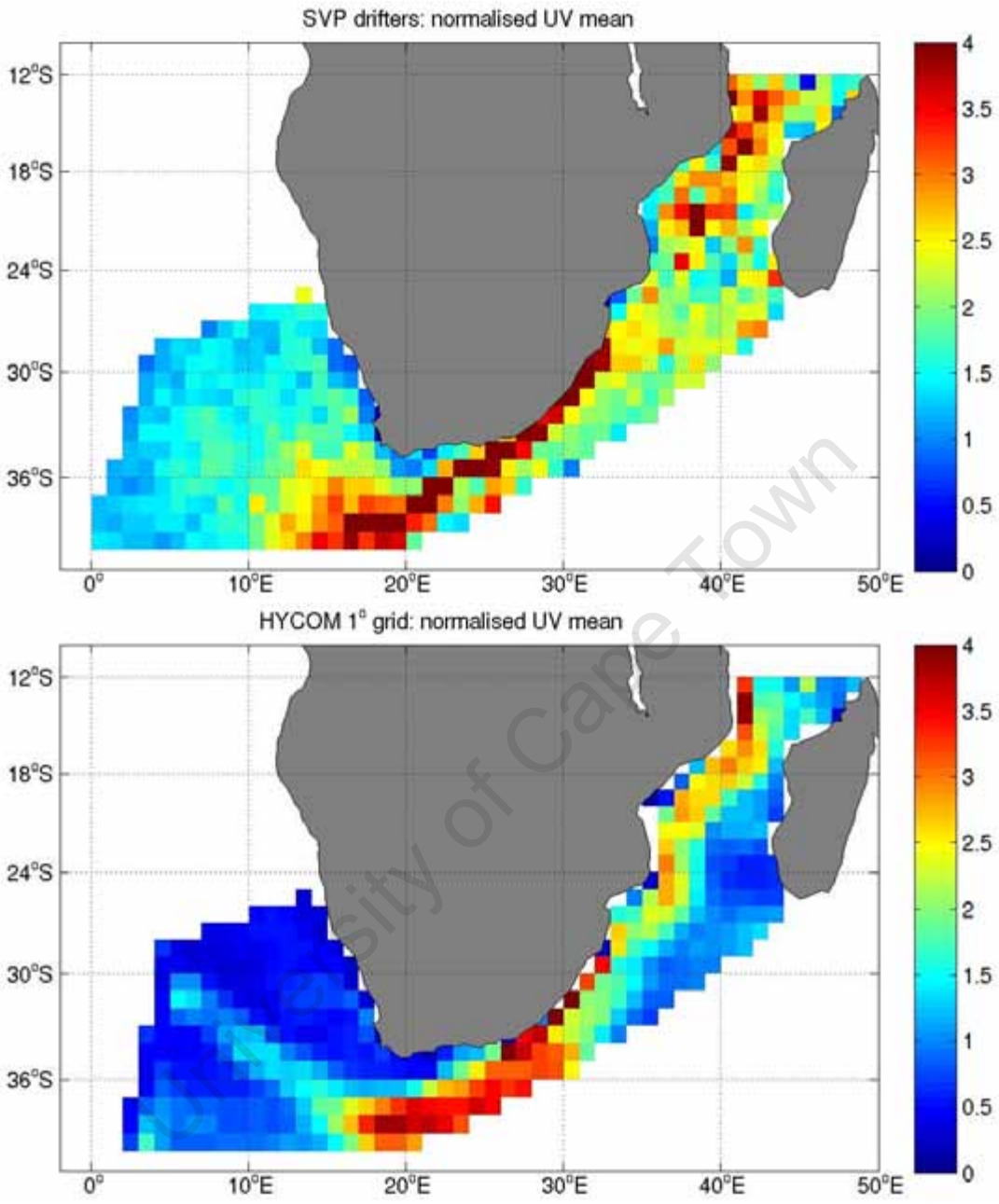

Figure 3.3: Average velocity (UV) calculated for the period $1996-2006$, and normalised against the spatial average standard deviation. SVP drift velocities gridded to 1° spatial grid (top), and HYCOM velocities sub-sampled to 1° longitude / latitude (bottom).

deviation of their respective velocities. This implies that areas where the magnitude of the normalised velocities are larger than one represent regions where the mean current is stronger than the current variability averaged over the entire region. In general the gridded mean velocities were calculated from $20-100$ daily averages. However large regional differences are encountered, e.g. in the Mozambique

Channel and northern Agulhas Current region the amount of SVP drifter data is quite sparse, whilst there were considerably more observations, some bins exceeding 200 daily averages, in the Southeast Atlantic Ocean.

Comparing the normalised velocities of these SVP drifters (Figure 3.3, top) and HYCOM (Figure 3.3, bottom) there is reasonably good agreement in the large scale patterns. In the Mozambique Channel the normalised SVP velocities exceed 1.5 to 2 and reveal a fairly broad and uniform pattern. In contrast, HYCOM displays narrower and stronger normalised velocity pattern confined to the western edge of the channel. The lack of a stronger signal southwest of Madagascar may indicate that HYCOM places comparatively less emphasis on the contribution from the EMC retroflection to the total volume flux in the Agulhas Current. This aspect was also evident when considering the zonal component of the flow.

The drifter data provides valuable information about the Agulhas Current core, which is not represented in altimetry observations due to their inability to provide accurate observations near the coast. Throughout the Agulhas Current, both the drifter data and HYCOM show that the mean current is generally stronger than the average variability. At approximately $28° - 29°$S, the mean southwestward current can be seen to intensify. This intensification is well represented in HYCOM and in good agreement with previous literature. Evidence of the strong mean currents can also be seen to extend southwestward toward the retroflection. Due to the barotropic structure of the Agulhas Current, it closely follows the shelf break, which widens near 24°E, 34°S. Further downstream, at the southern most point of the Agulhas Bank, the current separates from the shelf break. Although the number of drifters are few, this is well captured in the surface drifter data and compares relatively well with HYCOM.

The core locations of the retroflection area as depicted in the normalised velocities of the drifters and HYCOM at about $16° - 20°$E and $39° - 40°$S are in overall good agreement. This core location is also in agreement with the altimeter observations addressed above.

Distinct differences in normalised velocities are found in the ring shedding corridor. The narrow path in the normalised velocities confirms the tendency that the ring shedding in HYCOM follows a northwestward path from the retroflection. This is in contrast to the broader fan of normalised drift velocities spreading out from the retroflection in the drifter data. This is in agreement with the satellite altimetry observations above.

Overall, the comparison to the satellite and in situ observations indicates that HYCOM is able to simulate the mesoscale variability and dynamics of the greater Agulhas Current regime with satisfactory accuracy,

although some deficiencies are recognised. The large scale SST distribution in HYCOM is well represented, and with the exception of reduced southwestward penetration of the southern Agulhas Current, the characteristic SST patterns are evident. The flow in the Mozambique Channel is dominated by southward propagating eddies, and whilst the horizontal scales in HYCOM are comparable to surface geostrophic velocity observations from altimetry. The northern Agulhas Current intensification near $28° - 29°$S and its separation from the coast further south is evident in the normalised velocities of both the drifter observations as well as in HYCOM. The comparison of the model simulation to the drifter observations (Figure 3.3), suggest the position of the Agulhas retroflection is well represented in the mean. However, comparing to the weekly average data from satellite altimetry (Figure 3.2), it is evident that the Agulhas Current retroflects further upstream than observed, with a train of eddies extending from approximately 30°E, 35°S to the retroflection region and into the South Atlantic Ocean. Furthermore, these rings tend to follow a too narrow northwestward path into the Southeast Atlantic Ocean.

In the next section, this observation-model inter comparison is extended with a space-time analysis of the mesoscale features.

3.4 Space-time analysis

SLA's from HYCOM are produced by removal of the model mean dynamic topography (assumed constant). Weekly maps of SLA from altimetry and HYCOM are then used to examine characteristic spatial and temporal frequency patterns of the mesocale variability along the section marked in Figure 3.4. This analysis was adopted from the approach reported by Schouten et al. (2002). Data points along the sections are assumed to capture the mesoscale variability in the pathway of the greater Agulhas Current, extending from the Mozambique Channel (data points $111 - 152$) through the northern Agulhas Current ($75 - 111$) and southern Agulhas Current ($45 - 75$) to the retroflection area ($40 - 45$) and then into the ring shedding corridor in the Southeast Atlantic Ocean ($1 - 40$). Mesoscale feature occurrences and propagation speeds were estimated from Hovmöller plots along the section, while a fast Fourier transform (FFT) was applied to the SLA time series at locations along the section to gain further insight into the dominant variability modes in the Agulhas Current system. A limitation of the approach chosen is that the signals are interrupted whenever a mesoscale feature moves off the section. We have however taken care of picking the points on the apparent preferential paths so that the statistics should be most stable. The results from these analyses are further addressed in the next sub-sections.

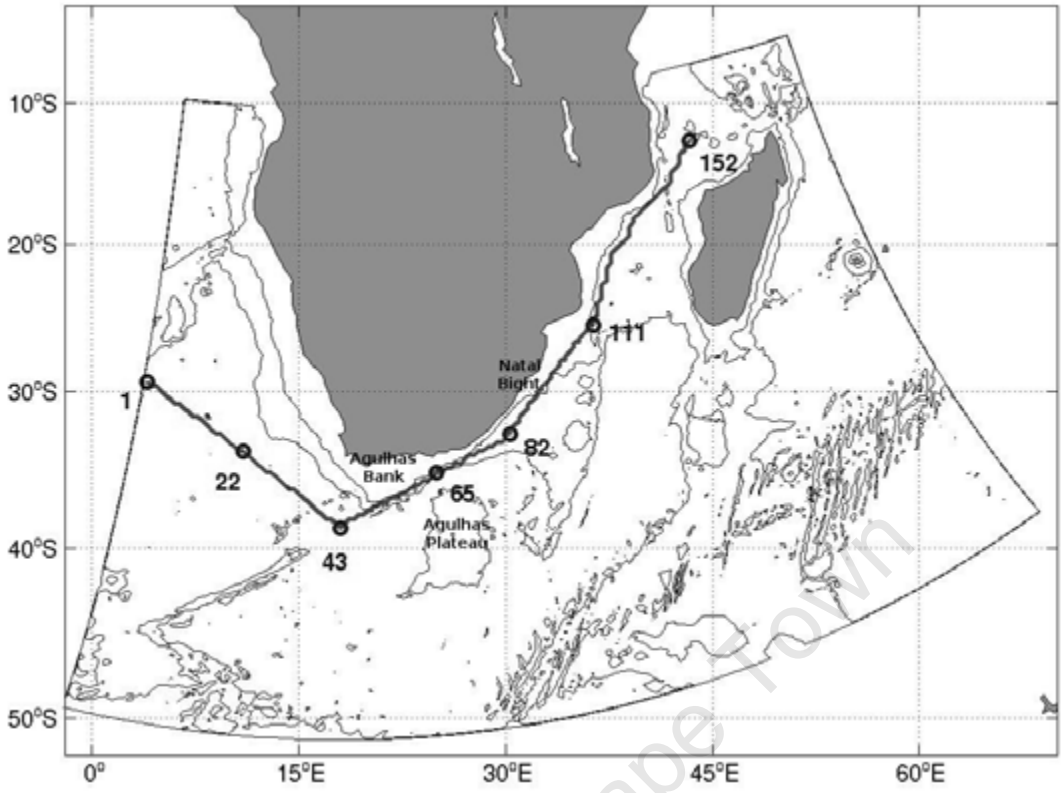

Figure 3.4: Map of section extracted from merged gridded altimeter and HYCOM SLA fields, with data point indices, model grid outline and bathymetry contoured for every 2000 m between 6000 m and the surface.

3.4.1 Hovmöller analyses

Hovmöller plots of SLA features from the altimeter and the model are shown in Figures 3.5 and 3.6 from January 1996 until December 2006. Positive SLA signals are assumed to represent anticyclonic eddies within the greater Agulhas Current system. In general, the patterns displayed in the Hovmöller plots suggest the presence of southwestward propagating mesoscale features with speeds ranging from about $7 - 10$ km.d^{-1} in the Mozambique Channel and northern Agulhas Current to approximately 5 km.d^{-1} in the southern Agulhas Current and retroflection region. In the ring shedding corridor (points $1 - 40$) the propagation speed is the same as in the southern Agulhas current while the direction shifts towards west-northwest with more distinct elongated positive SLA features depicted in HYCOM.

In the Mozambique Channel ($111 - 152$) the altimeter data shows that both positive and negative SLA features with amplitude reaching up to ± 60 cm exist. A closer look suggests a slight dominance of negative SLA features. HYCOM shows a persistent train of positive features propagating downstream from the Mozambique Channel, which compared to the altimetry seems too regular and structured. Similarily,

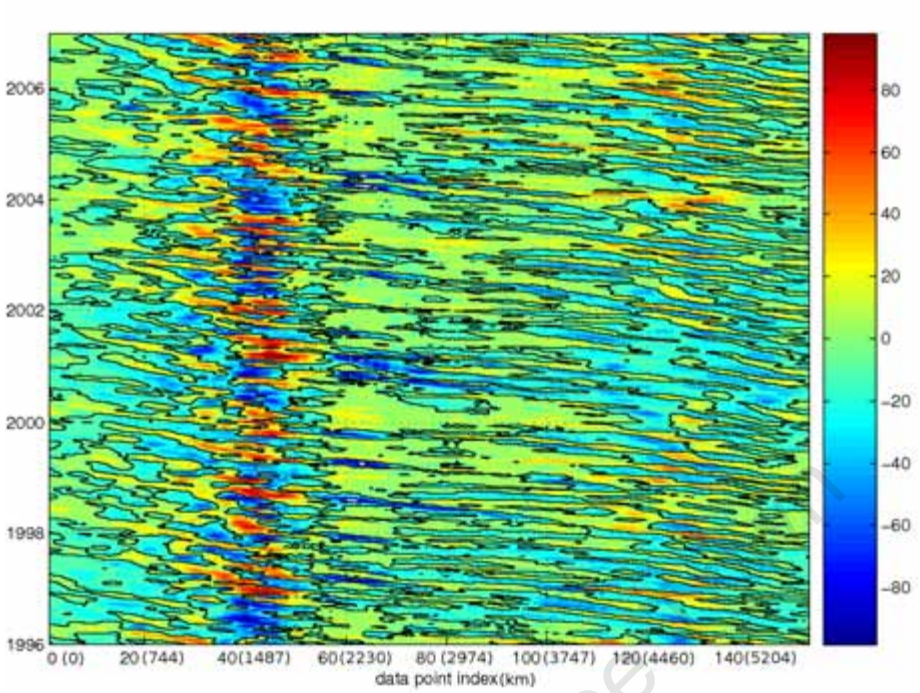

Figure 3.5: Hovmöller plot of altimeter SLA fields (SLA in cm) extracted from the section marked in Figure 3.4. The x-axis represents the data point indices along the section, with the corresponding distance in km.

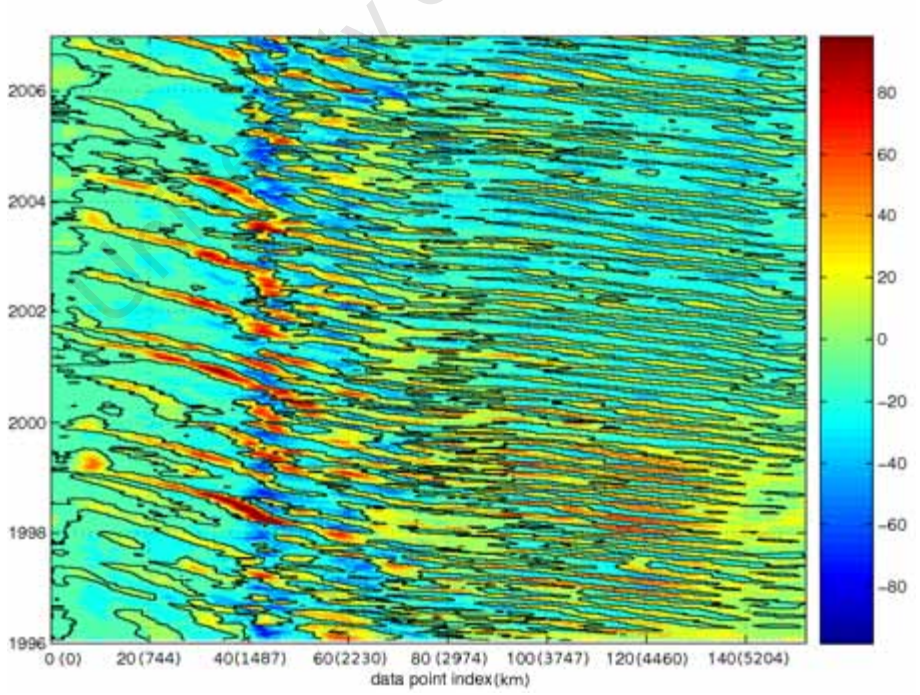

Figure 3.6: Hovmöller plot of HYCOM SLA fields (SLA in cm) extracted from the section marked in Figure 3.4. The x-axis represents the data point indices along the section, with the corresponding distance in km.

Biastoch and Krauss (1999) mention that the time and space structure simulated in their model was less complicated than in reality. Note that a weak negative trend in the model sea surface height (SSH) was encountered for this study period. This is likely associated with the spin-up period of the model. In Chapter 4 (Figure 4.1), it is shown that the model mean and eddy kinetic energies spike in the first 5 years of the simulation period, before settling at levels associated with the natural variability of the system, suggesting that a long spin-up period is required order to evacuate all the transient modes from the model domain. This probably accounts for the apparent increase in negative SLA signals upstream of index point 70 from the year 2000 onwards.

Moving into the northern Agulhas Current ($75 - 111$) the altimeter data show a shift towards weaker positive SLA features of about $10 - 20$ cm, although the continuation of negative SLA features are also visible. This shift is not clear in HYCOM for the reason explained above, where bands of narrow positive SLA signals persist throughout the northern Agulhas Current region. In the area corresponding to points $75 - 90$ (Figure 3.4), the core of the northern Agulhas Current is reported to be located mostly within 31 km of the coast (Bryden et al., 2005). Consequently, the SLA signals displayed along the section (being close to the coast) probably represent signals of meanders and anticyclonic eddies along the offshore shear zone of the Agulhas Current. This would also favour the observed tendency for the predominance of positive SLA features in the area.

In the southern Agulhas Current ($45 - 75$), predominantly positive SLA signals are present in the altimeter field, while fairly strong positive SLA signals ($50 - 60$ cm) intermittently interrupted by negative SLA signals start to develop in HYCOM. In this southern region, the Agulhas Current is sufficiently far from the coast that the extracted section is again able to capture its signal. The negative SLA signals ($20 - 30$ cm) occurring here are thought to be associated with cyclonic meanders, otherwise known as Natal Pulses. Both the negative and positive HYCOM SLA features seem to gradually reduce in their downstream propagation. The anticyclonic eddies extend to depths of 1200 m and are thus likely slowed down due to their interaction with the shallow Agulhas Bank.

In the retroflection area ($40 - 45$) and slightly upstream in the southern Agulhas Current ($45 - 55$), there is evidence of enhanced mesoscale variability in the form of increased presence of positive and negative SLA features, in particular in the altimeter data. The general agreement between the model and altimeter data supports the previous finding that HYCOM is able to provide a reasonably accurate simulation of the mesoscale dynamics associated with the Agulhas retroflection region.

Rings that are shed from the retroflection area and propagate into the Southeast Atlantic Ocean have been observed to do so in a broad, predominantly northwestward variable pathway (e.g. Fu, 2006). Hence, the extracted section in the ring shedding corridor only intermittently captures the signals associated with these features. A significant number of Agulhas Rings are seen propagating northwestward along the section in immediate vicinity of the retroflection (Figure 3.5 and 3.6, $1-40$). However, while the altimeter suggests frequent ring shedding events at the retroflection with a subsequent broadening of their pathway into the Southeast Atlantic, HYCOM underestimates the number of such events and clearly favours a distinct northwesterly trajectory of the rings.

3.4.2 Frequency analysis

In order to gain further insight into the dominant variability modes in the Agulhas Current system, a fast Fourier transform (FFT) was applied to the 11 year altimetry and HYCOM SLA time series at every point along the section (Figure 3.4). Prior to the FFT, a linear detrending function was applied, and the outer 10% of the data were smoothed by means of sinusoidal tapering function to minimise signal noise and leakage. Further details and explanation of the FFT is given in (Bracewell, 1999).

The power spectra (Figures 3.7 and 3.8) obtained from the Fourier analysis support the previous findings that there is strong and regionally distinct variability throughout the greater Agulhas Current system from the Mozambique Channel to the ring shedding corridor. A broad spectrum of frequencies is evident (Nyquist frequency is at about 24 yr^{-1}), ranging from about 21 days (18 yr^{-1}) to monthly (12 yr^{-1}), seasonal ($4-6$ yr^{-1}) and annual (1 yr^{-1}). There are differences between the two spectra, in particular manifested from region to region. In addition to the distribution, we consider the individual frequencies which clearly stand out from the background.

The northern Agulhas Current and Mozambique Channel

In the northern Agulhas Current and Mozambique Channel (indices 75 to 152), the frequency range is slightly compressed to the lower frequencies from about $2-6$ yr^{-1} in altimetry versus $4-6$ yr^{-1} in HYCOM. This suggests that the model is not able to properly represent the half-annual signal in this area as captured in altimetry. On the other hand, HYCOM simulates more high frequency variability of about $12-16$ yr^{-1} in the southern part of the Mozambique Channel and northern Agulhas Current

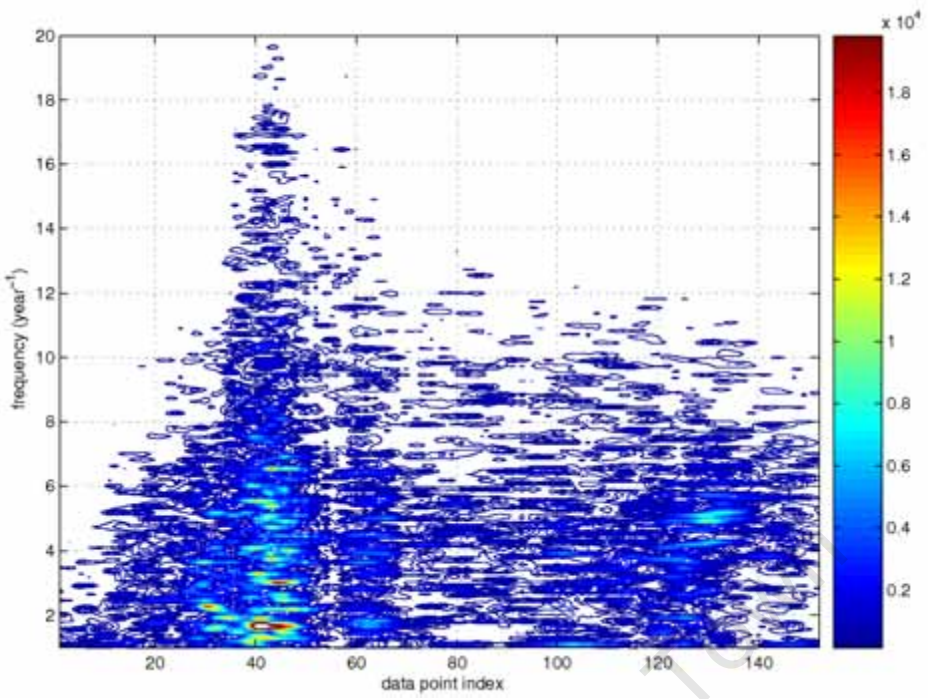

Figure 3.7: Power spectrum for the extracted section (Figure 3.4) derived from 11 years of merged gridded altimeter SLA fields.

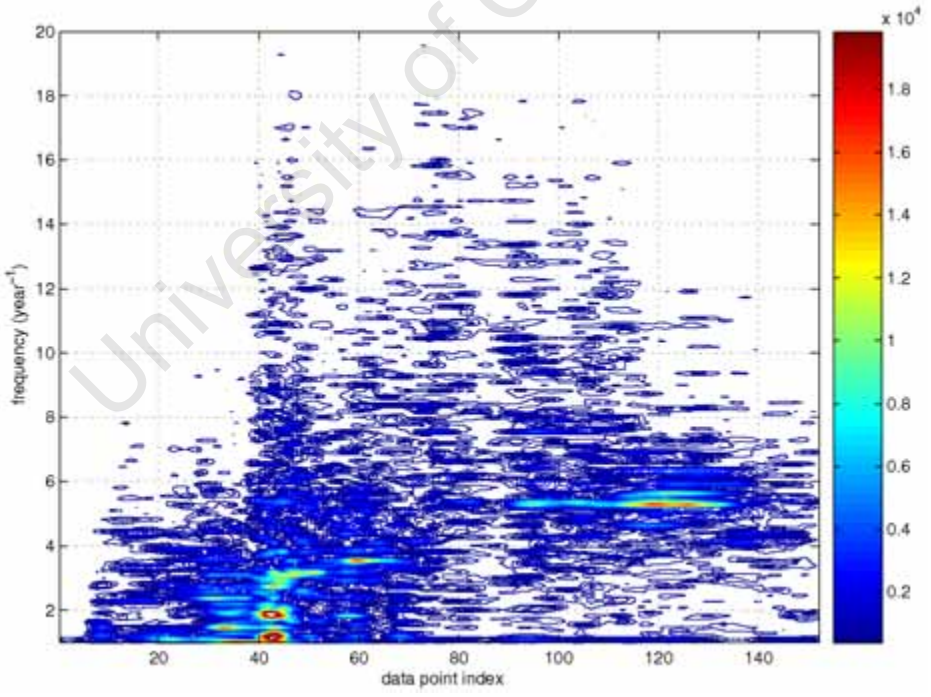

Figure 3.8: Power spectrum for the extracted section (Figure 3.4) derived from 11 years of HYCOM SLA fields.

$(75-120)$. These higher frequencies, which are not present in the altimetry SLA's, are perhaps a result of the abundant number of meanders and eddies propagating downstream from the Mozambique Channel in HYCOM as was addressed in the previous section (Figure 3.2, left panel).

A distinct frequency peak at $5-6$ yr^{-1} in the Mozambique Channel is visible in both HYCOM $(90-140)$ and altimetry (but only extending from indices $120-140$). This is consistent with the southwestward propagation of SLA features depicted in the Hovmöller plots (Figures 3.5 and 3.6) and provide statistical evidence that eddies occur $5-6$ times per year in the Mozambique Channel. Schouten et al. (2002) show that the number of anomalies per year in the Mozambique Channel reduce from 7 in the north to 4 in the south due to smaller eddies dissipating or merging with larger ones, This could explain some of the slight differences evident between HYCOM and altimetry. In HYCOM, this $5-6$ per year signal is clearly seen to extend southwestward into the northern Agulhas Current (until index 90), again in agreement with the Hovmöller plot. As mentioned previously this is an indication that an inter-connection between upstream mesoscale eddies in the Mozambique Channel and the Agulhas Current system exists at this frequency. Further downstream in the northern Agulhas Current (located at indices $85-90$), there seems to be a discontinuity of the frequency signals in HYCOM. In the Hovmöller plot (Figure 3.6), this seems to be a region where the mesoscale features are intermittently suppressed in HYCOM. This is not equally evident in the altimeter Hovmöller and power spectrum.

The southern Agulhas Current and retroflection

The southern part of the Agulhas Current system $(45-75)$ appears to maintain evidence of the southwestward extension of the frequency peak at $5-6$ yr^{-1} to about index 70 in HYCOM. In the altimeter data a southwestward extension to about the same position is observed at a frequency peak of about $4-5$ yr^{-1}. Southwestward from this position the frequency distribution in the altimeter data broadens from the annual frequency up to 7 yr^{-1}. HYCOM also shows this, in addition to a strong $3-4$ yr^{-1} signal. It remains unclear to what extent and by which mechanisms the Agulhas Plateau (south of point 65) influences the mesoscale variability in this area. While the $3-4$ yr^{-1} frequency signal seems to extend towards the retroflection area $(40-45)$ in HYCOM, there is an apparent discontinuity present in the altimeter derived frequencies at point 55. This area of the Agulhas Current $(40-45)$ is considered to have limited influence from the monsoon circulation (Ridderinkhof and de Ruijter, 2003). The annual to seasonal signals may thus be attributed to a variety of other sources including seasonal signals of the

regional wind field (Matano et al., 1999).

Southwestward from point 55 to the retroflection area both the altimeter and HYCOM contain strong signals from the annual frequency up to 8 yr^{-1}. The broadening of the frequency distribution here provides a good indication of the enhanced levels of mesoscale variability associated with retroflection region, and both the model and altimetry power spectra indicate that elevated levels of mesoscale variability occur near index 43 along the section. Whereas HYCOM lacks distinct expressions of frequencies larger than the monthly signal, the altimeter data shows strong signals in the retroflection area reaching almost up to 18 yr^{-1}. This result is consistent with the increased amount of instabilities in the southern Agulhas Current and the retroflection region observed in the Hovmöller plots (Figures 3.5 and 3.6). Similarly, the lack of the higher frequencies in HYCOM is also anticipated from the pattern of propagating SLA features seen in the Hovmöller plot (Figure 3.6).

The ring shedding corridor

In the ring shedding corridor $(1-40)$ the frequency range rapidly decreases with distance from the retroflection area, e.g. from $10-11$ yr^{-1} to 1 yr^{-1} in the altimetry and from $8-9$ yr^{-1} to $1-2$ yr^{-1} in HYCOM. This is expected for the area, where rings are known to travel along a variety of pathways, resulting in a broad fan-shaped area of ring propagation and mesoscale variability in the Southeast Atlantic Ocean (e.g. Fu, 2006). In agreement with the Hovmöller plots this frequency decrease indicates that the signals of the rings drifting into the Southeast Atlantic Ocean become less frequently captured with increasing distance from the retroflection area. In the upstream part near the retroflection $(30-40)$ the altimetry reveals northwestward extending signals of an enhanced frequency at 5 yr^{-1}, $3-4$ yr^{-1} and $1.5-2$ yr^{-1}. In comparison, HYCOM reveals signals at $3-4$ yr^{-1}, $2-3$ yr^{-1} and $1.5-2$ yr^{-1} extending northwestward into the Southeast Atlantic Ocean. These signals suggest that eddies are shed from the retroflection area up to 5 times per year in the altimetery data, while the more suppressed frequency range in HYCOM suggests that ring shedding events occur about 3 times per year. The overall suppression of mesoscale frequency signals westward of data index point 5 (20 grid cells from the HYCOM model boundary) arises from the one-way nesting scheme implemented in HYCOM, which dissipates the mesoscale signal near the western open boundary of the model.

From the above analyses, we conclude that intense instabilities and hence strong mesoscale variability is found throughout the Agulhas Current system. Furthermore, it is highlighted that mesoscale features

		Altimetry observations		HYCOM simulation	
Location observed	Data point indices	FFT	Hovmöller annual avg.	FFT	Hovmöller annual avg
Mozambique Channel	$111-152$	$5-6$	4.4	$5-6$	5.2
Northern Agulhas Current	$65-111$	N/A	4.5	$5-6$	5.3
Southern Agulhas Current	$43-65$	N/A	3.7	$3-4$	3.6
Agulhas retroflection	43	$3-4$	3.4	$2-3$	2.2
Ring shedding corridor	$1-41$	3	3.1	2	1.9

Table 3.1: Frequency estimates, from the Hovmöller analysis as well as the FFT's, of positive SLA features (anticyclonic eddies) occurring in all four regions of the section.

propagating downstream from their origin in the Mozambique Channel at approximately $5-6$ times per year play an important role in contributing to the overall mesoscale variability in the central and northern parts of the Agulhas Current. There is also evidence that upstream meanders and eddies occasionally influence the ring shedding processes at the retroflection.

3.4.3 Feature tracking and drift estimates

The annual average occurrence of southwestward propagating meanders and anticyclonic eddies, determined from the Hovmöller and FFT analyses are summarized in Table 3.1 for both altimetry and HYCOM. The results are grouped according to the different regions along the section from the Mozambique Channel in the northeast via the northern and southern Agulhas Current into the Agulhas retroflection area and ring shedding corridor in the southwest.

From altimetry, the eddy occurrence estimates of 4.4 yr^{-1}, 3.4 yr^{-1} and 3.1 yr^{-1} for the Mozambique Channel, Agulhas retroflection and the ring shedding corridor respectively are in good agreement with the associated power spectrum. In the northern and southern Agulhas Current, the respective altimeter signals in the FFT cannot be confidently isolated from the background signal. In HYCOM, on the other hand, the eddy occurrences from the Hovmöller analysis are in good agreement with the FFT analysis for all regions of the section.

The comparison provided in Table 3.1 highlight the good consistency between the results independently obtained from the FFT and Hovmöller analyses. In particular, the results indicate that Mozambique Channel eddies consistently merge with the northern Agulhas Current, thereby stimulating the formation of Natal Pulses. Furthermore, about 70% of the Mozambique Channel eddies observed in the altimetry appear at the Agulhas Plateau. While almost $^2/_3$ are advected further southwestward towards the Agulhas retroflection, where they contribute to the mesoscale variability and ring shedding processes. These

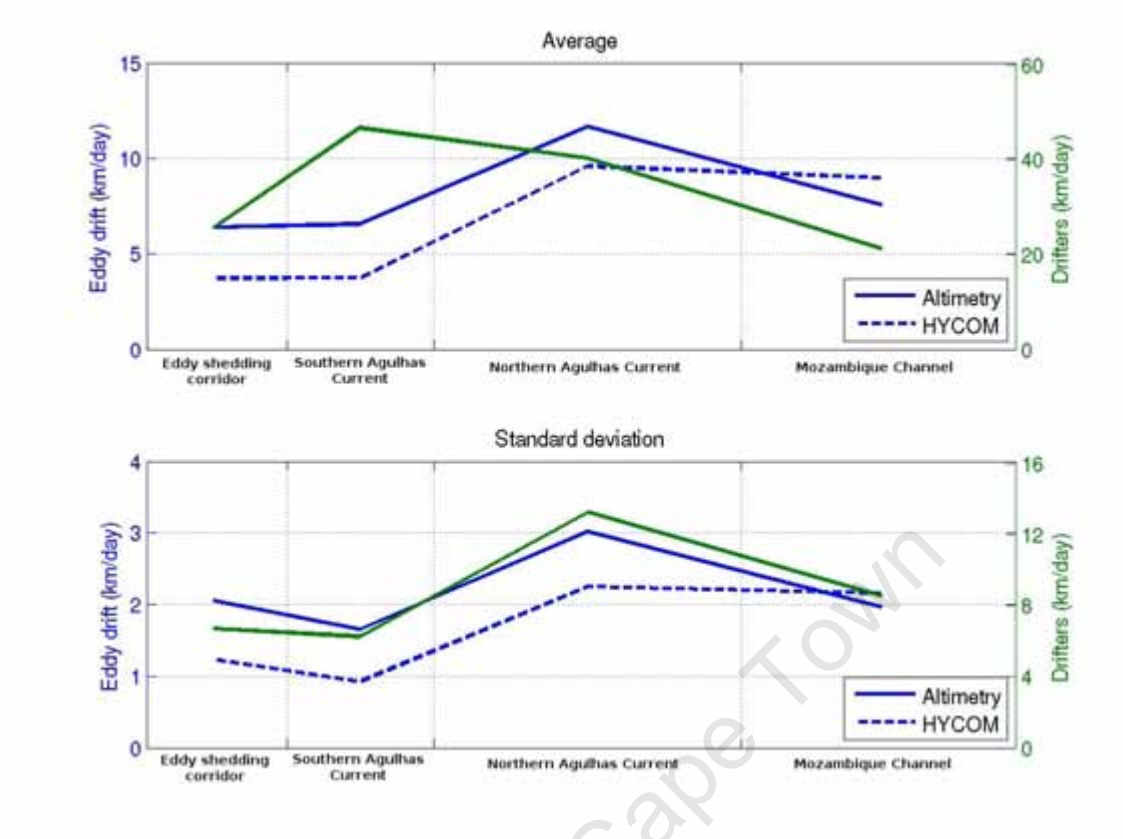

Figure 3.9: Propagation velocity estimates of positive SLA features (anticyclonic eddies) and SVP drifter velocities for the various sub-regions of the greater Agulhas Current region.

results are supported by HYCOM, except in the retroflection and ring shedding corridor the frequencies of occurrences are slightly weaker.

The mean speeds and standard deviations of the anticyclonic eddies and meanders can be estimated directly from the Hovmöller plots for the regions from the Mozambique Channel to the retroflection area and ring shedding corridor. These results are presented in Figure 3.9 together with the average surface speed obtained from the drifters for the same sub-regions.

The drift estimates range from a maximum of 12 km.d^{-1} in the central part of the northern Agulhas Current to 3.5 km.d^{-1} in the southern Agulhas Current and ring shedding corridor. On average, throughout the entire section, their propagation velocity is 7.5 km.d^{-1}. The altimeter drift estimates consistently exceed HYCOM by about 3 km.d^{-1}, except in the Mozambique Channel where HYCOM exceeds the altimeter by 1.5 km.d^{-1}. The variability of the eddy drift is also higher in the altimeter data, exceeding HYCOM by 0.75 km.d^{-1} in the standard deviation. The journey of anticyclonic eddies from the Mozambique Channel to the retroflection area, a distance of approximately 3000 km, will thus take about 400 days.

These drift estimates are slightly different to previously reported estimates (e.g. Schouten et al., 2002, 2003). For example, Mozambique Channel eddies travel at 7 ± 2 km.d^{-1} / 9 ± 2 km.d^{-1} (Figure 3.9, Altimetry / HYCOM observations) both much faster than the speed of $3-6$ km.d^{-1} reported by Schouten et al. (2003) from altimetry observations. These differences are due to the fact that the drift velocities here are estimated from the Hovmöller plots, while Schouten et al. (2003) manually tracked the eddy propagation.

In the northern Agulhas Current the drift is 11 ± 3 km.d^{-1} for altimetry and 9 ± 2 km.d^{-1} for HYCOM. This is in good agreement to the documented propagation velocity of Natal Pulses (10 km.d^{-1}). Additionally, negative SLA signals, or Natal Pulses, are periodically observed in the Hovmöller plots (Figures 3.5 and 3.6) at 30°S (index 90), and in almost all cases they are preceded by a positive SLA signal. This strongly supports that Natal Pulses are in fact induced by passing Mozambique Channel eddies, as was suggested in Schouten et al. (2002). This behaviour can be seen to occur regularly in HYCOM (e.g. Figure 3.2, left panel).

As expressed by Jakobsen et al. (2003) the direct comparison of these drift estimates to the Lagrangian current velocities calculated from the surface drifters (Figure 3.9, green curves) is not straight forward, and neither is the relationship between the mean current velocity and the propagation speed of eddies. However, we would like to examine whether the eddy propagation speed and the mean current velocities are spatially correlated. The surface drifters provide a good indication of the background mean current and its standard deviation, which ranges from 20 ± 8 km.d^{-1} (0.2 ± 0.09 m.s^{-1}) in the Mozambique Channel to 50 ± 13 km.d^{-1} (0.6 ± 0.15 m.s^{-1}) in the region of the Agulhas Current and 30 ± 6 km.d^{-1} (0.3 ± 0.07 m.s^{-1}) in the ring shedding corridor. For most parts the estimated eddy drifts and standard deviations in altimetry and HYCOM reach only a quarter of this mean surface drift and standard deviation obtained from the drifters. The anticyclonic eddies extend to depths of about 1200 m in HYCOM. It is therefore not unrealistic that the mean eddy drift in altimetry and HYCOM are less than the mean surface drift derived form the drifters. In addition, the deeper part of the eddies are expected to interact with bathymetry which will further tend to slow down their drift.

On the other hand, the spatial patterns of the standard deviations detected in altimetry, HYCOM and the surface drifters are more consistent. The variability of the eddy drift in HYCOM and altimetry therefore appears to be correlated with the variations observed in the mean surface current. Hence, the strength of the mean surface current and eddy drift correlate well with the variations in eddy drift.

3.5 Summary and conclusion

The greater Agulhas Current system known for its intense dynamics and mesoscale variability is an excellent natural laboratory for studies combining numerical ocean models with satellite and in situ observations. This is demonstrated in this study for a period of 11 years from 1996 to 2006. HYCOM reproduces the general circulation pattern with the regional characteristic spatial and temporal variability reasonably well, although some deficiencies are encountered, notably the train of eddies extending from the Agulhas Plateau to the retroflection, and the exaggerated spatial scales of Agulhas Rings that display a too narrow drift pathway into the ring shedding corridor in the Southeast Atlantic Ocean.

The space-time analyses provide quantitative means for validation of the model variability, and are also applicable to other ocean current regimes, such as the Gulf Stream and Kuroshio Current. Anticyclonic eddies occur in the Mozambique Channel at a frequency of $5 - 6$ yr^{-1}. In both HYCOM and altimetry SLA fields these anticyclonic eddies drift southwards and merge with the offshore side of the northern Agulhas Current. The model indicates that this occurs consistently at this frequency and that this merger contributes to the triggering of Natal Pulses. Furthermore, eddy propagation velocities determined from the Hovmöller analyses suggest that the anticyclonic eddies in the northern Agulhas Current propagate at approximately the same velocity as Natal Pulses, which further supports the idea that these southwestward propagating eddies induce the formation of Natal Pulses. About 70% of the Mozambique Channel eddies are tracked southwestward to the southern Agulhas Current, and ultimately nearly $^2/_3$ of these appear at the retroflection where they contribute towards the mesoscale variability and ring shedding.

Upon approaching the retroflection region, the magnitude of the SLA in altimetry and HYCOM enhances and the SLA oscillates more frequently between positive and negative signals and the power spectra indicate this through a broadening of the frequency spectrum. HYCOM and the altimetry data are moreover in very close agreement concerning the mean position of the Agulhas retroflection. The ring shedding events are revealed to occur in the altimetry at a frequency of 5 yr^{-1}. In comparison HYCOM displays ring shedding events occurring approximately $3 - 4$ times per year.

Adequate validation of HYCOM is mandatory for further investigation of the greater Agulhas Current regime. In this study the model capacity has been satisfactorily documented by intercomparison to satellite passive microwave radiometry, radar altimetry and surface drifter data. In particular, evidence of anticyclonic eddy drift from the Mozambique Channel to the retroflection area is demonstrated. HYCOM is therefore qualified for operational forecasting experiments of the greater Agulhas Current regime.

Moreover, since the Indo-Atlantic inter-ocean exchange of volume, heat and salt occurs predominantly via shedding of Agulhas Rings, it is important to accurately simulate the combination of local and upstream processes that triggers these shedding events. Operational use of HYCOM can therefore also contribute to advancing the understanding of these episodic dynamic events.

Chapter 4

Assessing the impact of a higher order numerical advection scheme on the circulation

This chapter is based on the work published as:

Backeberg, B. C., L. Bertino, and J. A. Johannessen (2009). Evaluating two numerical advection schemes in HYCOM for eddy-resolving modelling of the Agulhas Current. *Ocean Sci.*, 5, 173-190.

Abstract

A 4^{th} order advection scheme is applied in a nested eddy-resolving Hybrid Coordinate Ocean Model (HYCOM) of the greater Agulhas Current system for the purpose of testing advanced numerics as a means for improving the model simulation for eventual operational implementation. Model validation techniques comparing sea surface height variations, sea level skewness and variogram analyses to satellite altimetry measurements quantify that generally the 4^{th} order advection scheme improves the realism of the model simulation. The most striking improvement over the standard 2^{nd} order momentum advection scheme, is that the southern Agulhas Current is simulated as a well-defined meandering current, rather than a train of successive eddies. A better vertical structure and stronger poleward transports in the Agulhas Current core contribute toward a better southwestward penetration of the current, and its temperature field, implying a stronger Indo-Atlantic inter-ocean exchange. It is found that the transport, and hence this exchange, is sensitive to the occurrences of mesoscale features originating upstream in the Mozambique Channel and southern East Madagascar Current, and that the improved HYCOM simulation is well suited for further studies of these inter-actions.

4.1 Introduction

Modelling of the greater Agulhas Current regime, in particular of the very energetic retroflection region, is challenging. Ocean circulation models usually simulate the southern Agulhas Current as a train of large eddies extending from the Agulhas Plateau to the retroflection, rather than a continuous, well-defined current (e.g. Barnier et al., 2006; Backeberg et al., 2008). Consequently the simulated dynamics in the retroflection area with the periodic shedding of Agulhas Rings and maintenance of the return flow may be hampered.

Advances in model development, combined with more adequate model validation is necessary to limit this deficiency. In essence there are three ways in which ocean models can be improved (Bleck, 2006), notably by: increasing the model resolution, incorporating better model physics and implementing more adequate model numerics. Increasing the grid resolution would, in theory, allow the numerical solution to resolve finer scales. But at the border between resolved and unresolved scales of motion, the interaction of physical processes needs to be parameterised, and therefore truncation errors continue to be problematic. Improving the model physics implies better parameterisation of the physical processes which are not resolved in the model grid. Improving the model numerics, as with higher grid resolution, would lower the truncation error of the finite difference scheme used in the ocean model.

There are several ways in which model numerics can be improved. One approach is to transform the finite difference equations into a coordinate system so that they become easier to solve, and as a result the accuracy of the solutions may be improved. This approach has been adopted in isopycnic coordinate models such as the Miami Isopycnic Coordinate Ocean Model (MICOM; Bleck and Smith, 1990). In the case of isopycnic coordinate models, potential density has become the independent variable, instead of depth, which is used in Cartesian coordinate models. The advantage of using potential density as the vertical coordinate is that adiabatic flow, which is 3-dimensional in Cartesian space, becomes 2-dimensional in potential density space. This makes it easier to satisfy adiabatic constraints of temperature and salinity when estimating their lateral flow. There are two main disadvantages of having potential density as the vertical coordinate. Firstly, what is known as the outcropping problem, isopycnic coordinate surfaces intersect the sea surface and secondly, there is a lack of vertical resolution when simulating unstratified water columns. The Hybrid Coordinate Ocean Model (HYCOM; Bleck, 2002) was developed to combat these problems. It does so by reverting to fixed-depth (z-level or bottom-following) coordinates in unstratified waters, and when outcropping occurs, the layer thickness tends to zero but remains isopycnal

in nature.

Model numerics may also be improved by applying higher-order finite difference approximations. This would reduce the truncation error, much like increasing the model grid resolution, but at a lower computational cost (Sanderson, 1998). One such scheme is the quadratic upstream interpolation for convective kinematics (QUICK; Leonard, 1979). It was shown that implementing the QUICK scheme in realistic applications of ocean models generally improves their realism (Webb et al., 1998). In particular, in a case study for the Agulhas Current, where the QUICK scheme was applied to both tracer and momentum advection, the narrow, warm Agulhas Current core was significantly improved, resulting in a much better southwestward penetration of the temperature field, a deficiency noted in an application of HYCOM to the greater Agulhas Current system (Backeberg et al., 2008).

Depending on the process of interest, it is not necessary to approximate all terms to the higher-order (Sanderson, 1998). Studies have shown that applying the 4^{th} order scheme only to momentum advection improves the potential vorticity dynamics and conservation (e.g. Morel et al., 2006; Winther et al., 2007). Winther et al. (2007) conclude that with model grid spacing which is smaller than the Rossby radius of deformation, higher-order approximation need only be applied to the momentum scheme in order to yield beneficial results. Moreover, this is achieved at a fraction of the computational cost of increasing the grid resolution. An application of HYCOM for the Agulhas Current has been thoroughly evaluated in Backeberg et al. (2008). It was concluded that the simulation, using a second order momentum advection scheme, provided an adequate representation of the general circulation and mesoscale variability for the region, although some inaccuracies were recognised. Notably, a train of eddies extending from the Agulhas Plateau to the retroflection, instead of a well-defined current core.

In light of improving the model numerics, the QUICK scheme, with the bi-harmonic viscosity modified to minimise the viscosity coefficient (as in Winther et al., 2007), was applied to momentum advection in the Agulhas HYCOM. This 4^{th} order scheme (hereafter referred to as O4) is compared to the 2^{nd} order advection scheme (hereafter referred to as O2). A similar study using a high resolution model of the North Sea is documented in Winther et al. (2007). In the Agulhas Current, the regular availability of data, in particular satellite altimetry data, supports a more detailed statistical study, using skewness and spatial variograms. Although these statistical tools are very simple and classical, their use in oceanography is still marginal. We will show that they are selective tests for model validation.

Applying and validating model improvements provides a better quantitative understanding of the role and

influence of mesoscale variability and dynamics in the Agulhas Current and hence the retroflection region with its frequency of eddy shedding is obtained. Advancing the knowledge of this mesoscale variability and dynamics will in turn yield better grounds for model validation, which is essential in order to gradually progress towards establishing and implementing an operational monitoring and forecasting system for the greater Agulhas Current regime.

A description of the observations and model is outlined in Section 4.2, followed by a qualitative assessment of the two simulation experiments (Section 4.3). Mesoscale variability is studied in both simulations (Section 4.4), and compared to satellite altimetry measurements considering sea surface height variations (Section 4.4.1), sea level skewness (Section 4.4.2) and variogram analyses (Section 4.4.3). The main findings of the inter-comparisons are summarised in the conclusion.

4.2 Description of observations and model

4.2.1 Satellite altimetry

The satellite altimetry data is a very important global data set for ocean circulation studies as well as validation of models. It spans a period of more than 15 years and provides measurements of sea surface height variations or sea level anomalies (SLA) at a spatial and temporal scale of about 40 km and 7 days. This is adequate for the Agulhas Current, where the mesoscale signals are very distinct.

The absolute dynamic topography is the sum of SLA and the mean dynamic topography from Rio05 (Rio and Hernandez, 2004; Rio et al., 2005). These data are available from Ssalto/Duacs and distributed by Aviso, with support from the Centre National d'Etudes Spatiales (CNES; `www.aviso.oceanobs.com`).

Recently Aviso has developed better algorithms for data retrieval in coastal areas, where the measurement corrections are more demanding. This is very valuable for studies of the Agulhas Current, which flows very close to the coast between $30 - 34°$S.

4.2.2 Sea surface temperatures (SSTs)

Reynolds SSTs (Reynolds et al., 2002) are produced weekly on a one degree grid by the Climate Diagnostic Centre. The data are optimally interpolated, incorporating in situ and satellite SSTs and are adjusted for sea-ice cover. Before the analysis the satellite data are bias-corrected using the method described in Reynolds (1988) and Reynolds and Marsico (1994).

The Reynolds SST data is provided by the NOAA/OAR/ESRL PSD, Boulder, Colorado, USA, and is available freely from their Web site at `www.cdc.noaa.gov`.

More recently, with the launch of NASA's AQUA satellite, higher resolution ($\sim$ 25 km) near-global SST data have become available on a daily basis. These are obtained by interpolating SST measurements from the Tropical Rainfall Measuring Mission (TRMM) Microwave Imager (TMI) and the Advanced Microwave Scanning Radiometer for EOS (AMSR-E, onboard AQUA). For these sensors, missing data only occurs in regions near land or where they are influenced by sun-glitter and rain. Although these microwave SST products (hereafter referred to as MW SST) have a lower spatial resolution than full SST measurements from infrared sensors, they represent a significant improvement over the widely used weekly, one degree ($\sim$ 100 km) NCEP OI (Reynolds) SST product.

Microwave OI SST data are produced by Remote Sensing Systems and sponsored by National Oceanographic Partnership Program (NOPP), the NASA Earth Science Physical Oceanography Program, and the NASA REASoN DISCOVER Project. The MW SSTs are available at `www.remss.com`.

4.2.3 HYCOM

Two simulation experiments of the nested HYCOM of the Agulhas are discussed in this chapter. The O2 experiment uses the standard 2^{nd} order advection scheme, while in the O4 experiment a 4^{th} order advection scheme based on the QUICK scheme (Leonard, 1979), with the bi-harmonic viscosity modified to minimise the viscosity coefficient, was applied.

For a detailed description of the model setup and characteristics refer to Chapter 2. The values of the parameters chosen for the two simulation experiments are summarised in Table 2.1. Note that the viscosity parameters have been carefully adjusted at the lowermost acceptable value. Lower viscosities in the 4^{th} order scheme allow for numerical instabilities that eventually cause the model to crash, by violation of the Courant-Friedrichs-Lewy (CFL) conditions, and in the 2^{nd} order scheme they exhibit unphysical numerical noise.

Both simulations use the same nesting conditions, and in each case the same forcing fields were applied. Namely, synoptic atmospheric forcing fields from ERA40, before 2002 and then operational analyses from the ECMWF, with cloud cover data from the Comprehensive Ocean-Atmosphere Data Set (COADS; Slutz et al., 1985) and precipitation data from Legates and Willmott (1990).

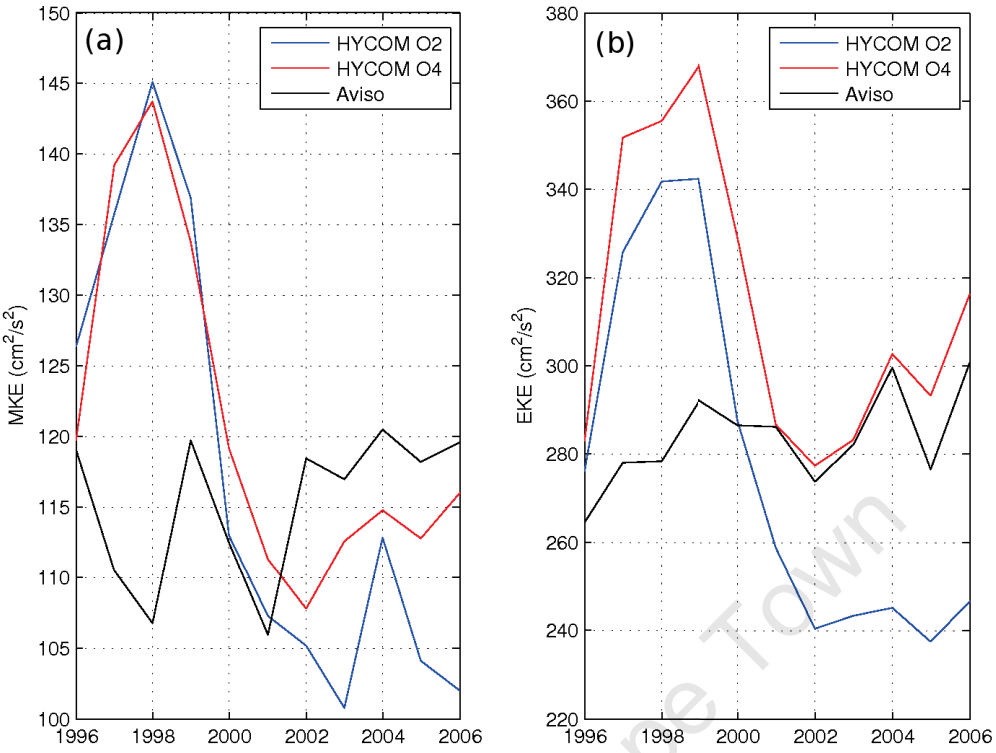

Figure 4.1: Annual averages of the mean kinetic energy (a) and eddy kinetic energy (b) for the Agulhas domain from HYCOM O2 (blue), HYCOM O4 (red) and calculated from Aviso geostrophic currents (black).

4.3 Assessment of the simulation results

Figure 4.1 shows the area averaged mean kinetic energy (MKE; a) and the eddy kinetic energy (EKE; b) for the Agulhas domain.

The simulation study is carried out over a 11-year period from 1996 to 2006, inclusive. Both experiments reveal a rapid increase during the first 2 3 years in MKE (until 1998) and EKE (until 1999). After which they decrease to a stable level in the year 2001. It takes about 1 year longer for the O2 simulation to adjust to its stable state, which in the case of EKE is about 40 cm^2.s ^{2} below, or 14% less than that of the O4 simulation and the observations.

Both simulations are able to reproduce the inter-annual changes in EKE from 2001 onwards, and the O4 experiment does so in *very* good agreement to the observed EKE from Aviso. The agreement with the MKE is a bit more sporadic, and both simulations underestimate the overall MKE for the region, although they are able to capture the general changes in the yearly MKE.

When nesting models in regions where strong boundary currents occur, such as the Agulhas Current, a

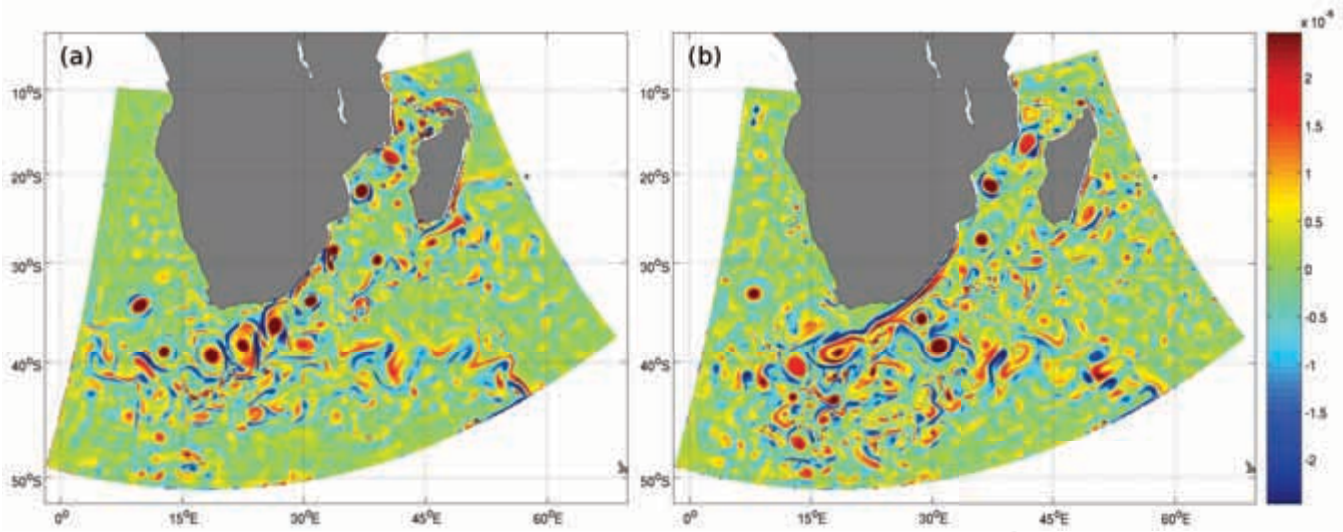

Figure 4.2: Weekly average vorticity fields for the week of 23 April 2003. Derived from current velocities at 10 m for HYCOM O2 (a) and HYCOM O4 (b).

long adjustment time seems to be needed in order to evacuate all the transient modes from the model domain. Further work is needed to address this issue, but does not lie within the scope of this study. For the purposes here, the first 5 years of the simulation are considered to represent the spin-up period. Only the latter period from 2001 2006 will be used in the analysis.

4.3.1 Vorticity analysis

As mentioned, it is expected that when applying the 4^{th} order momentum advection scheme improves the potential vorticity dynamics. To highlight the changes evident in the two simulation experiments, the weekly average vorticity fields for the week of 23 April 2003 are given in Figure 4.2.

Contrary to expectations, there does not seem to be a noticable change in the scale of the Mozambique Channel Eddies, and their intensity based on the weekly average field remains the same. The mesoscale variability in both model simulations will be examined in detail in the following sections. Note that in the O2 scheme, there is evidence of several patches of two-dimensional numerical noise, especially near the coast and the northern entrance to the Mozambique Channel, around the Comoro Islands. This is ammended by applying the higher order scheme.

The most pronounced difference is evident further downstream in the northern Agulhas Current. Here the current proper can be clearly identified in the higher order scheme, while in the second order scheme it remains poorly defined, with numerical noise evident close to the coast. The extent of the Agulhas

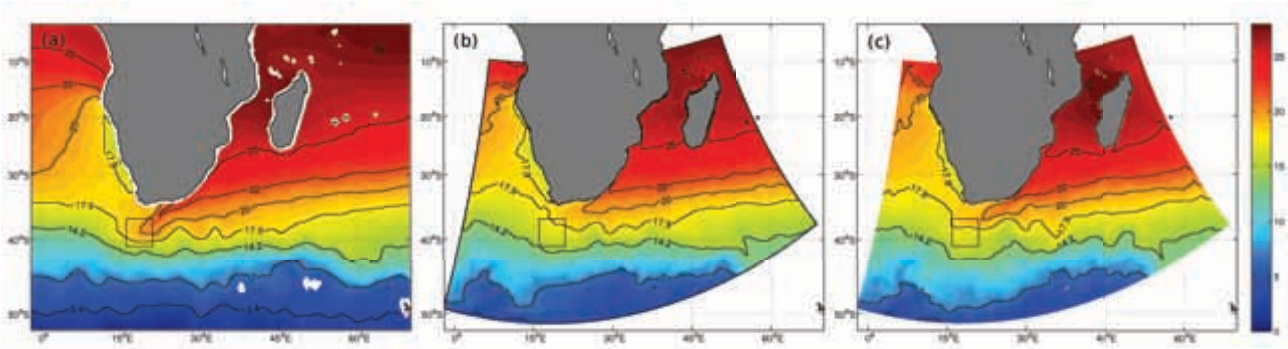

Figure 4.3: Mean sea surface temperature (SSTs, °C) fro the period 2004 2006 from MW SST (a), HYCOM O2 (b) and HYCOM O4 (c).

Current is defined by the stream of negative vorticity, cyclonic motion due to friction, close to the coast, with positive vorticity on its offshore side. In the O4 scheme, the current extends along the coast from about 27°S to about 34°S, where it separates from the coast and continues southwestward toward the retroflection region near 40°S and 15° 20°E. As noted in Backeberg et al. (2008), the O2 scheme fails to simulate the southern Agulhas Current as well-defined meandering current, and this is highlighted in the weekly vorticity field, where a train of eddies can be seen to extend from the Agulhas Plateau (near 35°S and 26°E) to the retroflection.

The retroflection region in the O4 simulation is much more chaotic, with eddies appearing to follow variable paths into the South Atlantic Ocean, a further deficiency noted of the second order scheme. Additionally, at scales smaller than the retroflection eddies, enhanced variability is evident in the the O4 scheme.

The most stiking improvement from applying the 4^{th} order advection scheme is the characterisation of the southern Agulhas Current as a well-defined meandering current and an enhancement of the mesoscale variability in particular in the retroflection region. These enhancements and their implications will be discussed in detail in the following sections.

4.3.2 Mean SST distribution

One of the deficiencies in the O2 model simulation was the extent of the southwestward penetration of the temperature field in the southern Agulhas Current. Webb et al. (1998) showed that by applying the QUICK scheme to both tracers and momentum a similar deficiency was improved in their simulation experiments. In these experiments with HYCOM, a 4^{th} order scheme was only applied to momentum advection since the horizontal grid resolution is smaller than the Rossby radius of deformation, as discussed in the Introduction of this chapter.

	Mean	Standard deviation
HYCOM O2	16.83	1.05
HYCOM O4	17.55	1.26
Reynolds SST	18.38	1.75
MW SST	18.84	1.59

Table 4.1: Statistics from the SST time series calculated for the period from June 2002 until December 2006, corresponding to the availability of the MW SST data with the launch of NASA's AQUA satellite.

Figure 4.3 shows the 3 year mean SSTs ($2004 - 2006$, inclusive) from both model simulations, which are compared to the MW SST measurements described in Section 4.2.2.

The contours represent the surface expressions of the extent of the Agulhas Current (20° and 22°C) and the three main frontal regions in the Southern Ocean: the Subtropical Convergence and its northern extent (STC; 14.2° and 17.9°C), the Sub-Antarctic Front (SAF; 7.0°C) and the Antarctic Polar Front (APF; 3.4°C). The surface expressions for the frontal bands were derived from ship-board observations (Lutjeharms and Valentine, 1984).

In general, the agreement between the model and the observations is relatively good considering that no relaxation toward observed SSTs was applied in the HYCOM simulations. SSTs are very sensitive to localised wind effects, which may not necessarily be represented in the relatively coarse resolution wind forcing used to drive the model. The latitudinal temperature gradient as well as the positions of the frontal bands are in good agreement with the observations. The extent of the Benguela upwelling system is well represented in both model simulations.

The southwestward penetration of the Agulhas Current, as represented by the 22°C isotherm, extends approximately 390 km further southwestward in the O4 experiment than the in the O2 experiment (Figure 4.3). Suggesting a better representation of the Agulhas Current core, but the extent of the southwestward penetration still does not completely agree with the MW SSTs.

In terms of heat transport into the South Atlantic Ocean, the gap between the southern tip of Africa and the 17.9°C isotherm to the southwest is broader in O4, suggesting a significant improvement of the heat flux into the South Atlantic Ocean.

In order to quantify the differences between both model simulations and the SST observations in the retroflection region, weekly data has been averaged for the area $16 - 21$°E and $37 - 41$°S (indicated by the boxes in Figure 4.3). The resulting time series were re-gridded to $1° \times 1°$ spatial resolution and averaged weekly in the case of the MW-SSTs. The mean and standard deviation are given in Table 4.1. The area

was chosen such that an underestimate of the mean SST reflects a reduced southwestward penetration of the southern Agulhas Current.

There are some discrepancies between the Reynolds SST and the MW SST (Section 4.2.2). It has been shown that a horizontal resolution the $1^\circ \times 1^\circ$ resolution of the Reynolds SST is insufficient to capture the variability of narrow western boundary currents such as the Agulhas Current, and that observations of the Agulhas Current are significantly improved with the MW SSTs (Rouault and Lutjeharms, 2003). Nevertheless, in terms of model validation of SST for long time periods, the Reynolds SST provides a useful data set, especially since the optimally interpolated MW SST only became available in June 2002.

During the period from June 2002 to 2006, there is an average difference of 1.55°C between the O2 SST and the Reynolds SST (Table 4.1), which suggests that the O2 experiment underestimates the southwestward extent of the Agulhas Current significantly. There is a marked improvement in the O4 simulation, which compared to the Reynolds SSTs underestimates the temperatures by only 0.83°C. Taking into account that the MW SSTs provide better observations of the Agulhas Current, the discrepancy is in fact 2.01°C for O2 and 1.29°C for O4.

The standard deviation for the O2 simulation is also significantly lower than the observations, 34% lower, and notably is also 17% less than O4, indicating that the 4^{th} order advection scheme improves the variability in the retroflection region.

The improved southwestward penetration of the temperature field in the O4 simulation suggests that the Agulhas Current core is stronger in this simulation experiment. To further investigate this, the vertical structure of the northern Agulhas Current, where good observations have been made, will be evaluated in the following section.

4.3.3 The vertical structure of the northern Agulhas Current

The Agulhas Current near 32°S closely follows the narrow continental slope, and is known for its very stable, invariant, flow conditions. Gründlingh (1983) showed that the current, in this northern region, does not meander more than 15 km from its mean path. de Ruijter et al. (1999b) in their study of the generation and evolution of Natal Pulses explain that the unusual stability of the current is due to the steepness of the continental slope. Natal Pulses are large cyclonic meanders in the northern Agulhas Current, which periodically interrupt its stable flow condition.

Mooring	A	B	C	D	E	F
Latitude (°S)	31 05.03	31 05.30	31 10.38	31 20.55	31 34.46	31 54.51
Longitude (°E)	30 22.08	30 25.44	30 32.22	30 64.60	31 06.00	31 28.24
Current meter depths (m)	138	384	403	353	353	388
	238	790	809	753	753	789
	439.5	1190	1209	1154	1154	1189
	740	1391	2010	1963	1963	1997
Water depth (m)	849	1480	2498	2900	2900	3446

Table 4.2: Mooring positions and current meter depths deployed during the RSS Discovery Cruise 214 (Bryden et al., 1995).

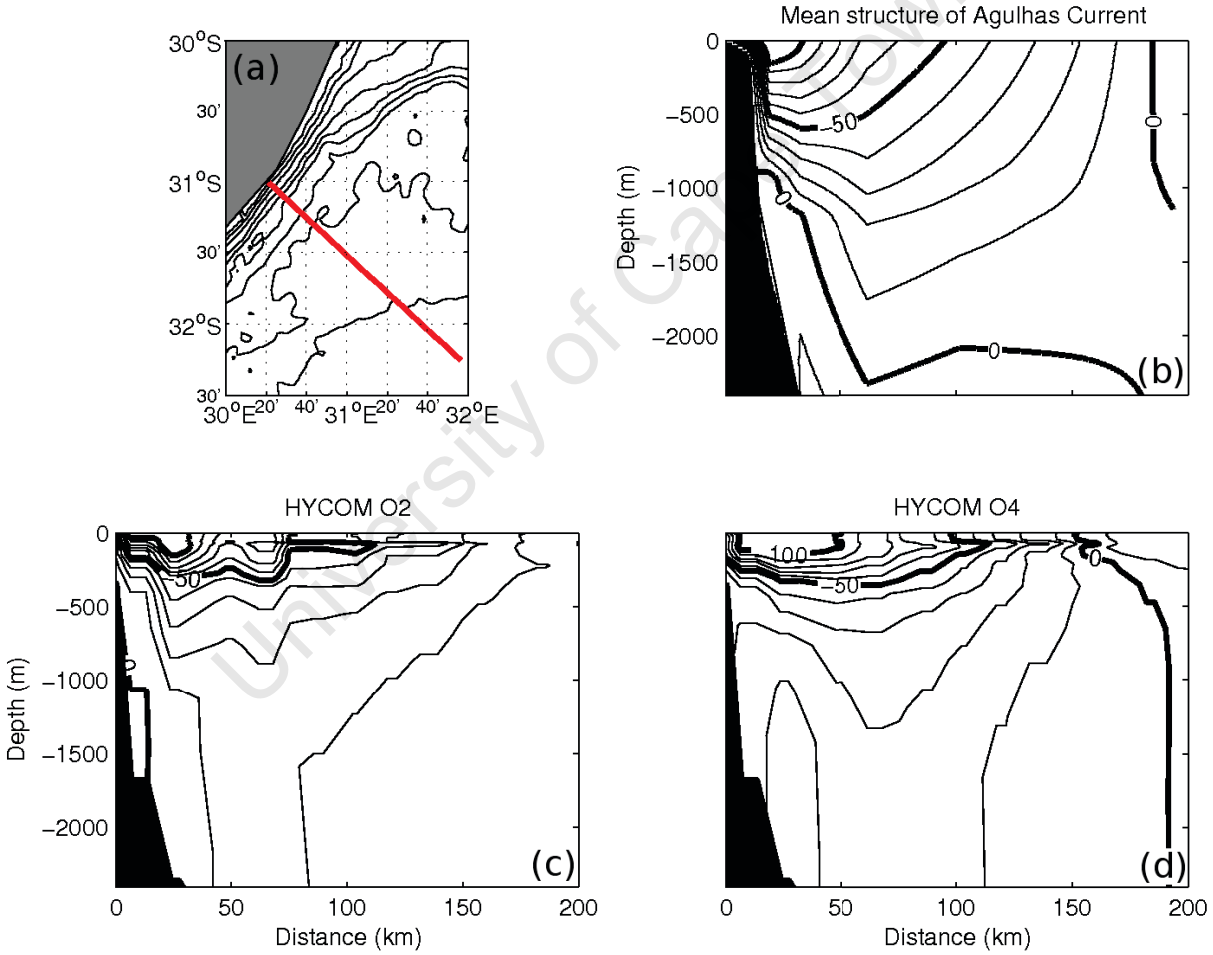

Figure 4.4: Mean vertical structure of the northern Agulhas Current from Bryden et al. (2005) (b), HYCOM O2 (c) and HYCOM O4 (d). The velocities normal to the section are given in cm.s ^{1} and are plotted at 10 cm.s ^{1} intervals. The section is indicated on the map (a) with the depth contours 100 m, 250 m, and 500 m to 4000 m at 500 m intervals from ETOPO 2 bottom topography (`http://www.ngdc.gov/mgg/fliers/01mgg04.html`) indicated.

A year long current meter mooring array was deployed during the World Ocean Circulation Experiment (WOCE; Bryden et al., 1995) southeast of Durban near 32°S from February 1995 to April 1996. These measurements provide, to date, the best estimate of the time-averaged volume flux and the vertical structure of the Agulhas Current. Position and depths of the current meter mooring array are summarised in Table 4.2.

In general the core of the Agulhas Current can be found close to the coast, lying within 31 km of the coast 79% of the time. The current penetrates to depths of 2200 m, and at its core, above 100 m, velocities exceeding 100 cm.s^{-1} are observed. The data also indicate that the offshore edge of the Agulhas Current, as determined by the position of the zero isotach, lies 203 km from the coast.

In order to compare the HYCOM simulations to the above described data, a section was defined corresponding to the positions of the year long mooring array, extending from the coast at Port Edward to 220 km offshore, and velocities normal to this section were extracted from the model (Figure 4.4). The weekly velocities were averaged over a 9 month period and compared to the mean structure described in Bryden et al. (2005), here shown as Figure 4.4b.

From the zero isotach in HYCOM O2, the outer edge of the current lies 200 km from the coast, while in HYCOM O4 the current lies closer, between $150 - 200$ km from the coast.

The characteristic V-shaped structure of western boundary currents is much better represented in the O4 simulation, with the maximum current velocity moving away from the coast with depth. In both HYCOM simulations, the current extends all the way to the bottom, with 10 cm.s^{-1} velocities evident at depths of 3000 m. This is deeper than indicated by the observations by Bryden et al. (2005), where according to the zero isotach the current extends to 2200 m, and this is most likely due to a lack of vertical resolution in the model. The model representation of the vertical structure is limited to 30 vertical hybrid layers. In particular for the deeper regions, where density changes are small, more vertical layers may have provided a better solution. Nevertheless, the 20 cm.s^{-1} isotach lies at $1200 - 1300$ m approximately $60 - 70$ km offshore in HYCOM O4, in very good agreement with the observations. The 20 cm.s^{-1} isotach in the O2 experiment only extends to about $800 - 900$ m depths. The 50 cm.s^{-1} isotach can be found at about 400 m depth in both simulations, while it is 300 m deeper in reality, which again may be attributed to the limited vertical resolution in the model. Furthermore, the vertical discretisation in the AGULHAS model mimics that of the INDIA model, both models have the same target densities ascribed to the individual vertical layers. Using the same reference densities ascribed to a basin-scale model in a regional model may

not have been ideal.

Velocities exceeding 100 cm.s^{-1} above 100 m are evident in both simulations, but are more strongly defined in the 4^{th} order advection scheme. The outer edge of the 100 cm.s^{-1} velocities extend offshore to 50 km compared to 30 km in the O2 simulation. In general this indicates that the current velocities are weaker in the O2 simulation, which has implications in terms of the southwestward penetration of the Agulhas Current, which was shown to be reduced in the SST comparison (Sections 4.3.2).

Overall, the O4 simulation provides an improved representation of the vertical structure of the Agulhas Current in better agreement with the observations, although it is noted that the relatively shallow depth of the 50 cm.s^{-1} isotach is not corrected much by applying the higher order horizontal advection scheme. The transports derived from this section will be discussed in relation to the observations in the following Section (4.3.4).

4.3.4 Transport in the northern Agulhas Current

Bryden et al. (2005) calculated the time-averaged volume transport, by integrating the velocities from the coast to 203 km offshore and to a depth of 2400 m. The daily transports were averaged over 267 days from 5 March to 27 November 1995 to yield a mean poleward transport of 69.7 ± 21.5 Sv ($1\ \text{Sv} = 1 \times 10^6 \text{m}^3.\text{s}^{-1}$).

For the comparison to HYCOM, the weekly transports were calculated across the same section (Figure 4.4a) and integrated to a depth of 2400 m. The mean transports and their standard deviations were calculated for HYCOM for the entire period from the beginning of 2001 to the end of 2006, as well as for 9 months of each year, corresponding to the 267 days over which the mooring data transports were calculated (Table 4.3).

On average, the O2 simulation underestimates the observed poleward volume transport by 21.4 Sv. This is improved in the O4 experiment, where the transports are only 12.2 Sv less than estimated by Bryden et al. (2005), within one standard deviation of the observed mean.

The yearly running mean transports (Figure 4.5) of HYCOM O4 oscillate around $\sim$ 60 Sv, while in HYCOM O2 they decrease by approximately $\sim$ 20 Sv between 2001 and 2006, indicating that the second order advection scheme is subject to a degree of model drift throughout the simulation. This may be related to the fact that the 4^{th} order advection scheme is better than the 2^{nd} order scheme at conserving potential vorticity (Winther et al., 2007), or it may be related to the definition of the viscosity term close to the land boundary.

	Period	Mean	Std
Bryden et al. (2005)	05/03 – 27/11/1995	69.7	21.5
HYCOM O2	2001 – 2006	48.3	19.6
	2001	52.9	19.7
	2002	52.4	17.7
	2003	52.3	21.7
	2004	48.3	16.8
	2005	42.4	13.3
	2006	37.7	17.8
HYCOM O4	2001 – 2006	57.5	19.9
	2001	56.9	22.2
	2002	54.1	17.1
	2003	60.7	18.1
	2004	64.4	27.5
	2005	55.6	19.6
	2006	51.8	17.56

Table 4.3: Northern Agulhas Current transport statistics. Note the inverted convention from Bryden et al. (2005), the maximum transport was considered to be positive and poleward.

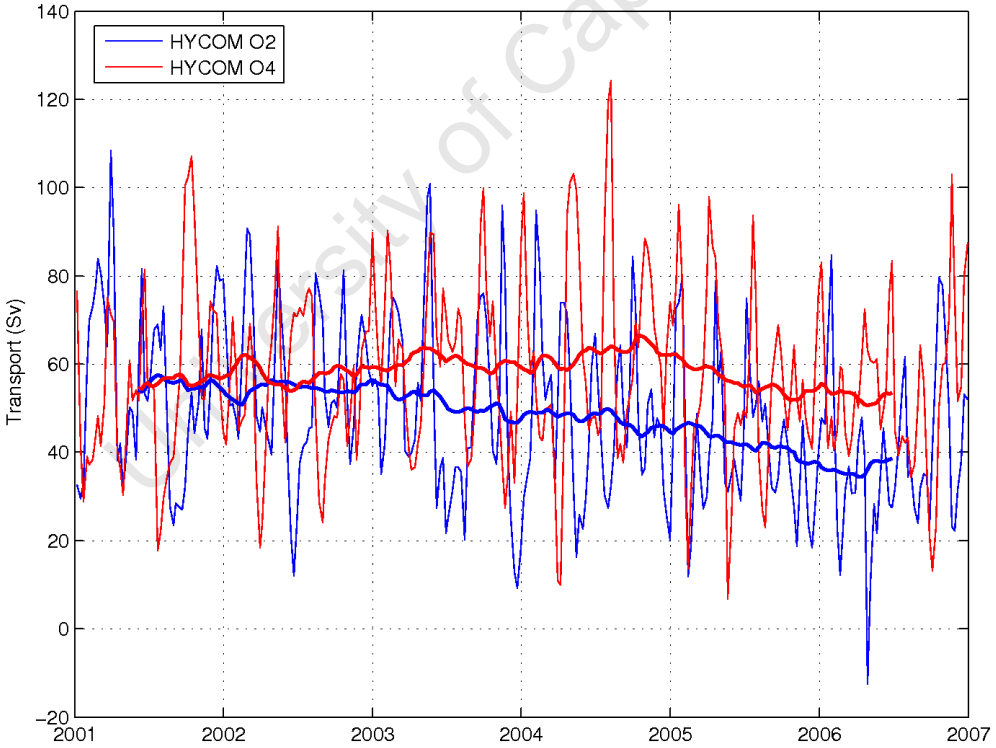

Figure 4.5: Agulhas Current weekly transports at 32°S integrated to 2400 m from HYCOM O2 (blue) and O4 (red), with the corresponding yearly running means. The running means for the first and last 6 months have been excluded due to edge effects of the running mean window.

In the discussions of the vertical structure of the Agulhas Current (Section 4.3.3) it was shown that the vertical characteristics of the Agulhas Current are much improved in the O4 scheme. A much deeper and well-defined current is evident, which (partially) accounts for an increase in the transports. Additionally, there is a 1°C increase in the vertical temperatures of the upper 100 m and a 0.2 psu increase in salinity in the upper 200 m in the O4 scheme (not shown). This results in enhanced temperature and salinity gradients of the upper 500 m, and according to the thermal wind equation an increased density gradient will result in an increased transport. Furthermore, as will be shown in Section 4.4, there is an overall increase of mesoscale variability in the O4 scheme. The Agulhas Current transport is sensitive to mesoscale eddies, and their enhancement also acts to increase the average transport.

In HYCOM there is no indication of a seasonal signal of the transports, although some interannual signals seem to be evident.

The volume flux in the Agulhas Current is always poleward, varying between 8.9 Sv and 121.0 Sv (Bryden et al., 2005). Apart from the last week in April 2006 in HYCOM O2 where the transport is negative (equatorward currents in this instance were caused by the passage of a mesoscale eddy), both experiments simulate predominately poleward transports (Figure 4.5), ranging from 9.4 Sv to 108.4 Sv (HYCOM O2) and from 6.9 Sv to 124.2 Sv (HYCOM O4). The weekly transports are generally stronger (poleward) in HYCOM O4 than in HYCOM O2, in particular the extremes (not shown).

The minimum and maximum velocities in both simulation experiments are always associated with the southwestward passage of anticyclonic eddies. These transport fluctuations occur between $4-6$ time per year, in good agreement with the occurrence of southwestward propagating Mozambique Channel eddies. They were previously shown to appear in the Mozambique Channel $5-6$ times per year, frequently interacting with the northern Agulhas Current (Backeberg et al., 2008). The advection of these eddies are clearly responsible for the large fluctuations in Agulhas Current transport.

From these comparisons, it is evident that the O4 simulation provides stronger poleward transports within the Agulhas Current core. Additionally, it seems that these are significantly contributed toward by upstream mesoscale variability. An increase in mesoscale variability in the O4 scheme seems to be the cause of the enhanced transports, considering that the 4^{th} order scheme has been documented to increase the eddy kinetic energy in model simulations (Winther et al., 2007). According to previous studies (e.g. Backeberg et al., 2008) these also have an impact on the dynamics at the retroflection, influencing the heat transport and therefore the Indo-Atlantic inter-ocean exchange. Assuming that these fluxes are predominantly

influenced by the mesoscale variability, it is therefore important to examine and quantify the eventual relationship between the upstream and downstream dynamics.

4.4 Analyses of the mesoscale variability

In this section mesoscale variability associated with sea surface heights are analysed using the satellite altimetry data as well as the two model simulations. Due to the fact that the mesoscale signals in the greater Agulhas Current region are quite strong the inter-comparison with altimetry measurements yields a good opportunity to validate model simulations.

4.4.1 Sea surface height variations

To convert altimeter measurements into dynamically meaningful quantities, the exact position of the sensor with respect to the geoid is required. To date the precision of the geoid is insufficient to allow for useful dynamical calculations of wavelengths shorter than about 2000 km (Le Traon, 2002). In terms of comparing the mean flow, the mean dynamic topography of the model simulation differs from the observations, there is an offset of about 150 cm between the AGULHAS HYCOM and Rio05 (Rio et al., 2005) mean dynamic topography but the gradients are similar (not shown), therefore they are comparable. From the geostrophic assumption, the mean SSH contour lines (Figure 4.6, black) depict the mean surface circulation pathway.

Altimeter based sea level anomalies and estimation of eddy kinetic energies (or its proxy: standard deviation of SSH) are routinely used to assess the performance of eddy-resolving / -permitting ocean models

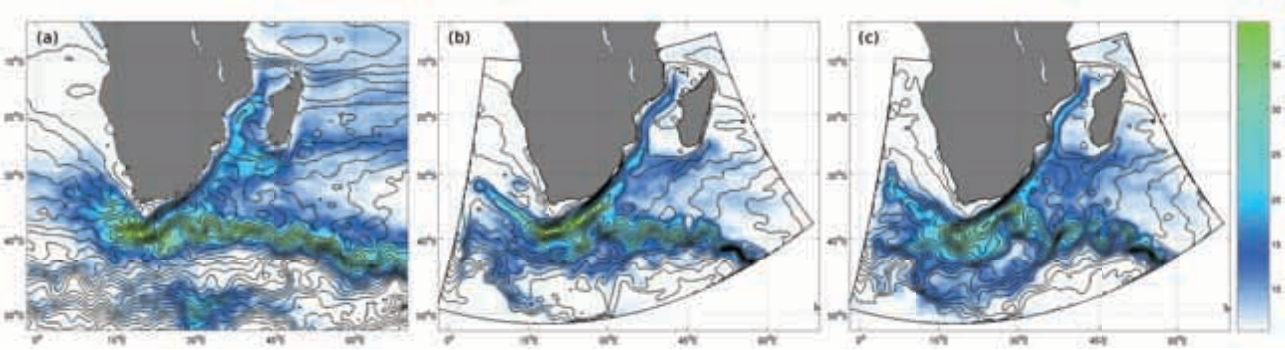

Figure 4.6: Sea surface height (SSH) mean (black contours, spaced every 7.5 cm) and standard deviation (∇, colour scheme in cm) from Aviso MADT (a), HYCOM O2 (b) and HYCOM O4 (c) for the period from 2001 to 2006, inclusive.

(Treguier et al., 2003). The standard deviation (∇, Equation 4.1, Figure 4.6, colour scheme) is the variability about the time mean, and hence differences in the mean dynamic topography do not come into play.

$$\nabla = \sqrt{\frac{1}{n}[\sum \eta^2 - \frac{1}{n^2}(\sum \eta)^2]} \tag{4.1}$$

where n is the number of observation and simulation weeks, and η is the sea surface height.

North of Madagascar, near the open boundary, the jet associated with the South Equatorial Current (SEC) seems to be slightly stronger in the O4 versus the O2 simulation, while the jet in the altimetry observations appears to be stronger than the model experiments. This is most likely due to inherent weaknesses from the parent model.

In the Mozambique Channel, there is no clearly defined current indicated by the streamlines from the altimetry SSH. The high levels of variability indicate, in agreement with the previous literature, that the flow here is dominated by the passage of eddies. Both model runs are able to simulate these high levels of mesoscale variability. Slightly stronger variability is evident in the O4 experiment, suggesting that suggesting that more energetic mesoscale variability is simulated in the 4^{th}order advection scheme.

Both model simulations depict the mean path of the southern extension of the East Madagascar Current (SEMC). The mean SSH streamlines retroflect in an anticyclonic direction to flow eastward into the South Indian Ocean. Higher levels of mesoscale variability are encountered due to this retroflecting current, with occurrences of both cyclonic and anticyclonic eddies as reported by Siedler et al. (2009). The variability in the O4 simulation is slightly broader and more energetic but remains lower than observed from altimetry.

In the northern Agulhas Current, the simulation experiments overestimate the current strength in comparison to the altimetry. In particular north of 34°S, the narrow separation between SSH streamlines indicate a strong gradient and hence an intensification of the mean geostrophic current. However, as mentioned previously, the quality of the data from Aviso close to the coast is questionable and the Agulhas Current is known to remain within 31 km of the coast 79% of the time in this region (Bryden et al., 2005).

The mesoscale variability in this northern part of the Agulhas Current, is predominantly confined to the offshore side of the current. This is evident from the enhanced variability offshore of the northern Agulhas Current, in both model simulations as well as the altimetry.

In the southern Agulhas Current, the current is again sufficiently far away from the coast for the altimetry

data to recapture its flow. Comparing the trajectories of the southern Agulhas Current mean flow, between $20° - 28°$E and $34° - 38°$S, the core of the current is too far south in HYCOM O2, suggesting that it separates from the continental shelf prematurely. In the 4^{th} order simulation, the southwestward extent of the Agulhas Current core is much narrower and extends further southwestward than in the 2^{nd} order experiment. Its trajectory is also slightly further north.

As the southern Agulhas Current separates from the coast, following the continental shelf break, it continues southwestward as an unstable, meandering current. In turn the SSH standard deviation reveals a narrow band of high variability, along the continental shelf break north of 36°S between 22° and 26°E. In the O2 simulation this narrow band is completely masked by excessively high and broad standard deviation values assumed to be caused by the distinct train of eddies extending from the Agulhas Plateau to the retroflection (Backeberg et al., 2008). In the O4 scheme a narrow band of high variability is encountered, suggesting that it is able to simulate the southern Agulhas Current as a meandering current, rather than a train of eddies. This will be confirmed later using sea level skewness (Section 4.4.2.2).

The distribution and pattern of the standard deviation in the retroflection area is improved in HYCOM O4. The maximum variability associated with the retroflection in HYCOM O2 is confined in its latitudinal distribution, lying between 37° and 40°S. Whereas in HYCOM O4 it extends further south in better agreement with the altimetry observations. Furthermore high values of standard deviation are focussed about the mean postion of the retroflection (17°E and 39°S), in good agreement with variability seen in the altimetry.

The Agulhas Ring shedding corridor in HYCOM O2 is confined to a very narrow band extending northwestward from the retroflection. This indicates that eddies and rings shed from the retroflection prefer to travel along this one trajectory. The strength and pattern of the standard deviation distribution is less focused in the northwest direction in the O4 experiment. In comparison this agrees better with the spatial distribution of variability observed from altimetry suggesting that, although the higher-order momentum advection scheme seems to underestimate the variability for the region compared to observations, it is able to simulate more variable eddy trajectories in the ring shedding corridor.

The meandering pathway of the Agulhas Return Current, is represented by the narrowly spaced band of mean SSH contours and high standard deviation at about 40°S between 20° and 60°E in the altimetry. It is known to have three main quasi-stationary meanders (e.g. Boebel et al., 2003b) and these are well represented in the simulated mean SSH field. Although slightly lower levels of variability are observed.

The second and third meanders, with their northern troughs near 33° and 39°E, are more clearly defined in the O4 experiment.

In summary there are marked improvements from applying the 4^{th} order advection scheme in HYCOM for the Agulhas Current simulations. In particular the strength and distribution of the mean flow (mean SSH) and variability (∇) in the southern Agulhas Current associated with the transition from a more stable current upstream to a strongly meandering and retroflecting current downstream appears to be more reliable in HYCOM O4 when compared to altimetry.

4.4.2 Sea level skewness

The above comparisons are qualitative, and more quantitative analyses need to be performed in order to objectively assess these simulation results.

Sea level skewness has been proposed by Thompson and Demirov (2006) as a new method for using SSH measurements from altimetry in model validation and mesoscale variability studies.

Skewness is a measure of the asymmetry of the distribution of a variable, or just the normalised third moment about the mean. It is given by γ_1 (Equation 4.2), of which we will consider the classical unbiased estimate (Equation 4.3).

$$\gamma_1 = \frac{\frac{1}{n}\sum_{i=1}^{n}(x_i - \overline{x})^3}{[\frac{1}{n}\sum_{i=1}^{n}(x_i - \overline{x})^2]^{\frac{3}{2}}} \tag{4.2}$$

$$\gamma_\eta = \frac{\sqrt{n(n-1)}}{n-2}\gamma_1 \tag{4.3}$$

γ_η denotes the unbiased skewness of SSH (η) for a sample of n values, x_i is the i^{th} value and $\overline{x}$ the sample mean.

Thompson and Demirov (2006) show that in an idealised example of a meandering current, standard deviation of SSH is a function of position, with the maximum variability occurring at the mean position of the current, where the sea surface gradient is greatest.

Similarly, skewness is also a strong function of the cross current position. It is zero at its mean position, where changes in the sea surface height induced by the meandering current are symmetric. Therefore in a meandering current it is possible to infer its mean position from the zero line of the skewness. Moreover, as

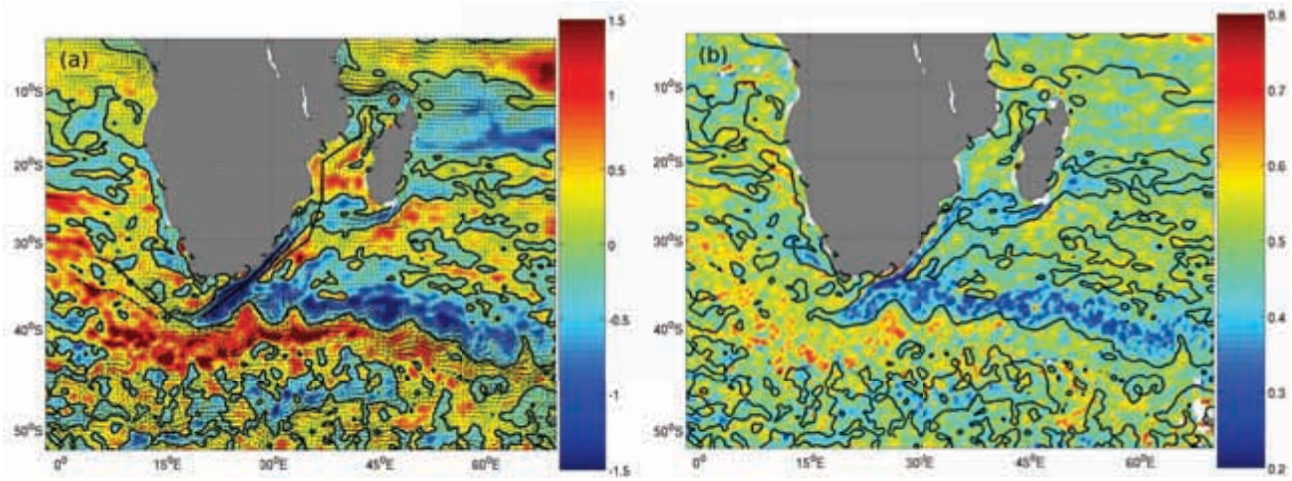

Figure 4.7: (a) Sea level skewness (colour scheme indicates positive and negative) with mean geostrophic currents derived from altimetry SSH measurements (vectors). (b) The fraction of anticyclonic EKE from the total EKE. The data period spans from 2001 to 2006, inclusive. The solid black contour indicates zero skewness.

the skewness increases toward lower mean sea levels, a geostrophic flow to the left (right) can be inferred in the southern (northern) hemisphere.

In regions with an abundance of eddies, the skewness field allows for the preferred sense of rotation to be determined. Consider the following two situations: (1) one large anticyclonic eddy and one large cyclonic eddy of the same dimension, and (2) one large anticyclonic eddy and two small cyclonic eddies. For the two situations, the mean SSH and its standard deviation may be the same but the skewness will be zero in situation (1) and negative in situation (2). Therefore negative (positive) skewness indicates a preference for cyclonic (anticyclonic) rotation.

Thompson and Demirov (2006) conclude that the skewness analysis is a useful statistical method for validating high resolution ocean models. In the following section sea level skewness determined from altimetry is assessed for greater Agulhas Current region and then used to assess the model simulations. To our knowledge, this is the first time that sea level skewness is used in model validation.

4.4.2.1 Assessment from altimetry measurements

In order to evaluate the sea level skewness field it is compared to the mean geostrophic currents derived from altimeter SSH measurements (Figure 4.7a) and to the fraction contribution of anticyclonic eddies toward the total EKE (Figure 4.7b). The method of distinguishing between cyclonic and anticyclonic rotation by calculating the fraction from total EKE was used in the study of the southern extension of

the East Madagascar Current (Siedler et al., 2009), but here was applied to the entire greater Agulhas Current domain.

The zero skewness line seems to indicate the mean positions of meandering currents northwest of Madagascar, in the southern Agulhas Current, and in the Agulhas Return Current (Figure 4.7a). The fraction of anticyclonic EKE from the total seems to explain most of the pattern evident in the sea level skewness field (Figure 4.7b).

The flow in the Mozambique Channel is dominated by southward moving anticyclonic eddies (e.g. Sætre and da Silva, 1984; Biastoch and Krauss, 1999; de Ruijter et al., 2002), and most of the variability associated with these eddies is located toward the centre of the channel (Figure 4.6a), contributed to mostly by anticyclonic eddies (Figure 4.7b). The skewness field (Figure 4.7a) is predominantly positive here in good agreement with the fraction of anticyclonic EKE. Near the Mozambican coast there is a preference for cyclonic rotation, consistent with cyclonic shear edge eddies forming from friction at the continental shelf edge. However, the skewness field does not indicate the presence of cyclonic shear. This may be related to the fact that skewness cannot distinguish between an eddy field with an equal mix of cyclonic and anticyclonic eddies of the same intensity and a region with no eddies.

The two modes of the southern extension of East Madagascar Current (SEMC) described by Siedler et al. (2009) are clearly evident in the skewness field. The current consistently retroflects southwest of Madagascar near 42°E, with anticyclonic motion (and eddies) favoured during a southwestward extension of the SEMC, while cyclonic motion (and eddies) occurs during westward flow along the south Madagascar continental shelf edge. For the SEMC the zero skewness line (Figure 4.7a) does not seem to indicate the mean position of the westward outflow. The mean geostrophic currents are located within the area of negative skewness, indicating that the SEMC outflow is not a meandering current.

The tongue of positive sea level skewness, extending from south of Madagascar toward the Agulhas Current, was suggested to represent anticyclonic eddies propagating westward (Thompson and Demirov, 2006). Moreover, these are thought to be one of the mechanisms by which Natal Pulses are triggered in the northern Agulhas Current (Schouten et al., 2002). The occurrence of anticyclonic eddies in this region has been confirmed by (e.g. Siedler et al., 2009), and is also clearly evident in the fraction of anticyclonic EKE (Figure 4.7b).

Natal Pulses are large cyclonic meanders, that form at the Natal Bight, on the east coast of South Africa near 29°S. Their average offshore extent is 170 km and they form approximately 6 times per year

(Lutjeharms and Roberts, 1988). These periodically interrupt the stable flow conditions of the northern Agulhas Current as they propagate southwestward along the South African east coast.

The band of negative skewness extending about 150 km offshore along the east coast of South Africa from $26° - 35°$S indicates that there is a preference for cyclonic disturbances in the mean current, consistent with what is known of Natal Pulses. The fraction of anticyclonic EKE (Figure 4.7b) is low, and confirms that up to 80% of the variance is from cyclonic meanders. However the total EKE (cyclonic + anticyclonic; Figure 4.6a) is very low, suggesting a rather stable current with relatively infrequent occurrences of Natal Pulses. In fact, most of the EKE, between 26° and 35°S is located on the offshore side of the Agulhas Current, and is mainly due to anticyclonic eddies. These EKE maxima might be connected with anticyclonic eddies frequently originating at the SEMC and the Mozambique Channel.

Upon approaching the Agulhas retroflection, between $21° - 27°$E and $35° - 40°$S, the skewness field as well as the fraction of anticyclonic eddies in total EKE, indicate predominantly cyclonic rotation in the southern Agulhas Current. This might be related to the arrival of Natal Pulses in combination with westward propagating cyclonic eddies pinched off from the northern extremities of the meandering Agulhas Return Current.

The zero skewness line in the southern Agulhas Current closely follows the mean position of the current. In particular southwestward of 22°E / 37°S, at the southern termination of the Agulhas Bank, where the current separates from the continental shelf break and continues southwestward as a meandering current. As such the skewness field is able to determine the mean position of a meandering current, and approaching the Agulhas retroflection region, is in good agreement with the fraction of anticyclonic EKE.

In the ring shedding corridor the tongue of positive skewness extending into the South Atlantic Ocean, indicates a preference for anticyclonic eddies. Thompson and Demirov (2006) discuss that it has been shown that cyclonic eddies which occur closer to the South African west coast travel west-southwest from this position, while anticyclonic Agulhas Rings travel west-northwest from the Agulhas retroflection (e.g. Richardson and Garzoli, 2003; Matano and Beier, 2003; Treguier et al., 2003). They argue that if the relative contributions of cyclonic and anticyclonic eddies are equal, the skewness will be zero (as in situation 1, Section 4.4.2). It may be possible that these cancel each other out closer to the coast and hence cause the southward displacement of the ring shedding corridor.

In the meandering Agulhas Return Current the zero skewness line provides a really good indication of the mean position of the current, and its quasi-stationary meanders.

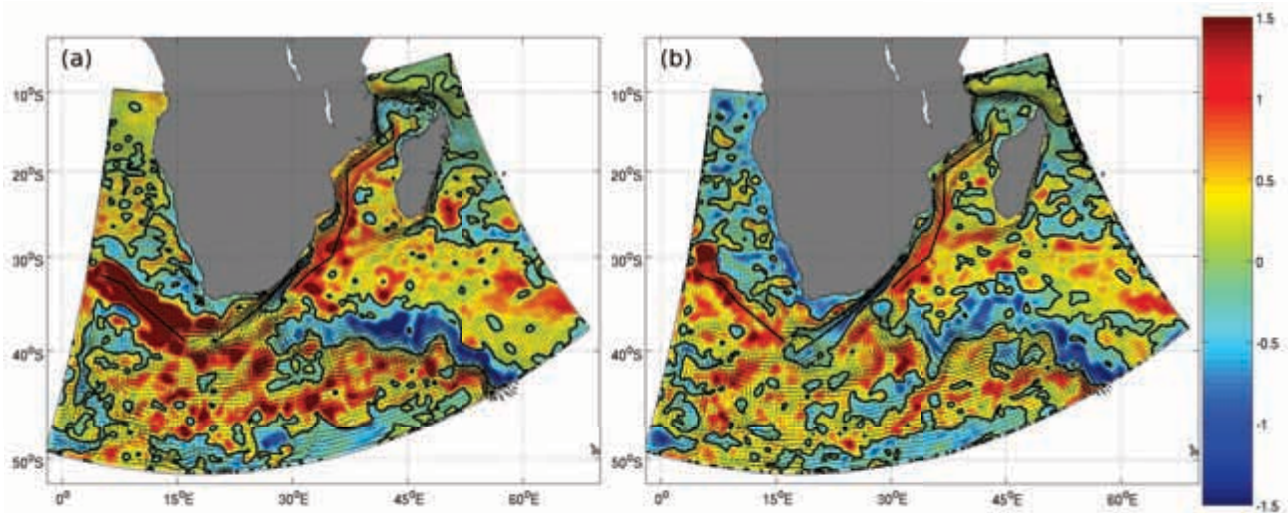

Figure 4.8: Sea level skewness (colour scheme) with the black contour indicating zero skewness and mean surface currents (vectors) from HYCOM O2 (a) and O4 (b). The data period spans from 2001 to 2006, inclusive.

4.4.2.2 Comparison to HYCOM simulations

The skewness field has been calculated from HYCOM O2 and O4 SSH fields (Figure 4.8) as a means to validate and compare the two simulations as well as provide new insight into mesoscale dynamics simulated in the model.

The current to the northwest of Madagascar is well represented in both simulations, the zero skewness line indicating the mean path at 10°S, in agreement with the altimetry skewness field (Figure 4.7).

Moreover, a preference for anticyclonic eddies in the Mozambique Channel is well represented in both HYCOM simulations, in good agreement with the observations.

In the SEMC, contrary to the altimetry sea level skewness, there is a preference for anticyclonic rotation in the model simulations. However, a band of negative skewness extending toward Mozambique west of Madagascar's southern tip in the O4 scheme suggests that it is able to reproduce the bimodal pattern discussed in Siedler et al. (2009). Although this pattern is not as pronounced as in the altimetry skewness field, it is completely absent in HYCOM O2.

The most striking improvement from applying the 4^{th} order advection scheme can be seen in the Agulhas Current proper. The band of negative skewness along the east coast of South Africa extends all the way to the retroflection region, near 40°S, in good agreement with the observations from altimetry. This indicates that the O4 scheme is able to simulate the Agulhas Current as a well defined current core, with the periodic occurrence of cyclonic disturbances or Natal Pulses. This band of negative skewness is much shorter in

O2 extending from 32°E / 29°S to 25°E / 35°S, the northern tip of the Agulhas Plateau.

In the southern Agulhas Current the zero skewness line from the O4 scheme lies within the centre of the mean position of the current. According to Thompson and Demirov (2006), the zero skewness line will *only* indicate the mean position of a current, when it freely meanders. The O4 simulation results therefore suggest that the southern Agulhas Current is represented as a meandering current, as opposed to a train of eddies evident in the O2 scheme (Backeberg et al., 2008).

The skewness distribution of the O4 scheme at the Agulhas retroflection is generally in better agreement with the altimetry skewness field. Along the continental shelf of the Agulhas Bank, for instance, there is a narrow band of positive skewness north of the negative skewness band, which continues westward at the southern termination of the Agulhas Bank. The ring shedding corridor is less focussed in O4, indicating a more realistic representation of the variability associated with the Agulhas retroflection ring shedding.

In both simulations the meandering Agulhas Return Current is only represented by the zero skewness line east of 30°E, which seems to indicate that not enough flow is returning eastward from the retroflection. In particular, the second meander, with its southern trough near 35°E extends too far south in the O4 simulation, while it seems to be more realistically portrayed in the 2^{nd} order advection scheme. Moreover, the negative (positive) skewness north (south) of the mean position of the return current is well pronounced in both simulation experiments, although not as strong or persistent as found in the altimetry analyses.

In summary, the 4^{th} order advection scheme significantly improves the dynamic characterisation of the southern Agulhas Current, revealing a well-defined meandering current, with distinct bands of cyclonic and anticyclonic eddies.

4.4.3 Variogram analysis

In this section the spatial scales of mesoscale features are discussed. The (semi-)variogram, is a geostatistical technique which characterises the spatial correlation within a data set and quantifies variability as a function of scale (Wackernagel, 1998).

In geostatistics, analyses of spatial data often rely on the assumption of stationarity for the random process (Gneiting et al., 2001). In the stationary case, the variogram can be simply deduced from the covariance as $C0 - C(h)$, where $C0$ is the variance and $C(h)$ the covariance. The variogram averages squared differences of the variable, which filters the influence of a spatially varying mean. Therefore, the variogram can be

defined in some cases where the covariance function cannot. For example in the non-stationary case, the variance may keep increasing with increasing lag, rather than leveling off, corresponding to an infinite global variance. In this case the covariance function is undefined, while the variogram remains valid. This also holds true for auto-correlation functions.

Dissimilarities (γ) between sample pairs are calculated by computing the squared difference between the values (Equation 4.4), and these are plotted against the separation of the sample pairs in geographical space, or lag (h), to form the variogram cloud. The lag distances are grouped into classes (H_k), and within each class the dissimilarities are averaged to form the sequence of values of the experimental variogram. The dissimilarities depend on the spacing and on the orientation of the point pair described by the lag vector, and because it is a squared quantity, the order in which the points in space are considered does not come into play. Therefore the variogram is symmetric with respect to h.

$$\gamma(H_k) = \frac{1}{2n_c} \sum_{\alpha=1}^{n_c} (\eta(x_\alpha + h) - \eta(x_\alpha))^2 \quad with \quad h \, \epsilon \, H_k \tag{4.4}$$

n_c are all the point pairs that can be linked by a vector, h. The average dissimilarity with respect to a vector class within a specific interval H_k, is a value of the experimental variogram $\gamma(H_k)$.

Usually the average dissimilarity between values increases with distance between point pairs, as near samples tend to be more alike. If the variable is stationary, at large distances between point pairs the experimental variogram may reach a sill, its maximum. When this occurs the expression converges to twice the variance, therefore dividing by 2 means that the sill approximates the variance within the data. At scales exceeding the natural scale of the phenomena in question, harmonic effects may be noted, in which the variogram peaks and dips at lag distances that are multiples of the natural scale, this is known as cyclicity.

An abrupt change of the slope of the dissimilarity function at a specific scale indicates that an intermediate level of variation has been reached, this is known as the range. It identifies the distance from the origin where the variogram reaches its maximum value (the sill), at which point the sampled variable exhibits its maximum variance.

The behaviour of the variogram near the origin is important to note, it characterises the very small scales within a dataset and indicates the type of continuity of the variable: differentiable, continuous but not differentiable, or discontinuous. A discontinuous variogram at the origin is known as a nugget effect, which

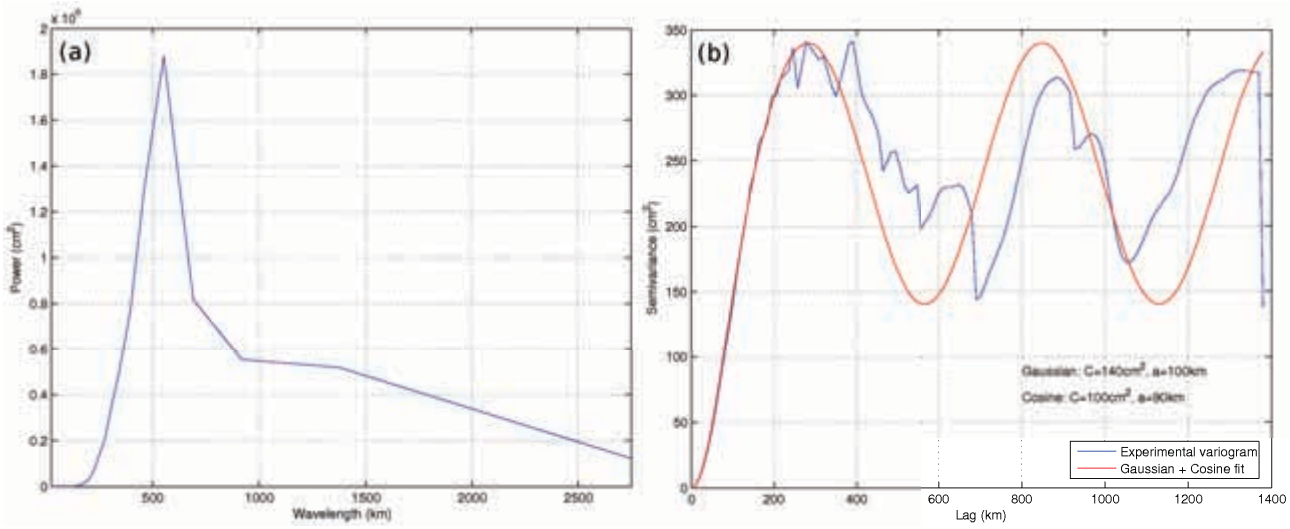

Figure 4.9: Spatial FFT spectrum (a) and variogram analysis (b) of model SLA data from HYCOM OW along a section in the Mozambique Channel. The section data was extracted from gridded data and interpolated to 10 km.

indicates that the values of the variables change abruptly at very small scales, it may also arise when data is sparse or from measurement error.

A theoretical curve is fitted to the variogram in order to attribute a physical meaning to them. The fit is done by eye, because emphasis is not placed on how well the variogram function fits the the sequence points, but rather what type of continuity is assumed near the origin. The fit therefore implies an interpretation of the behaviour of the variogram at the origin and its behaviour at large lag distances.

4.4.3.1 Comparison to a spatial Fourier analysis

A spatial Fourier and variogram analysis of modelled SLA data (HYCOM O2) are compared in order to confirm for an oceanographic application, that the variogram indicates the scale up to which a spatial correlation exists between data points, thus giving an indication of the size of mesoscale features. The comparison is done for modelled SLA data along a section in the Mozambique Channel where large anticyclonic eddies, up to 300 km in diameter, are known to occur frequently (HYCOM O2; Backeberg et al., 2008).

Figure 4.9a is the time averaged spatial FFT spectrum for the modelled SLA data along the section indicated in Figure 4.8a. Notice the peak near $L_w \cong 560$ km, which for a Fourier analysis typically corresponds to two eddies (cyclonic and anticyclonic) with diameters of about 280 km, in agreement with the simulated eddies observed in HYCOM O2 for the Mozambique Channel (Backeberg et al., 2008).

The blue curve (Figure 4.9b) indicates the corresponding experimental variogram calculated using Equation 4.4, and the red curve is the theoretical variogram fitted to the sequence (Equation 4.5), which in this case is a combination of a Gaussian and a cosine function. Other functions were tested (cardinal sine, cubic, exponential) with less success.

$$\gamma(h) = C_g[1 - exp(-\frac{h^2}{a_g^2})] + C_c[1 - cos\frac{2\pi h}{a_c}] \tag{4.5}$$

C is the amplitude of the Gaussian / cosine function, h the distance between points and a the range, or radius. In Equation 4.5 the subscripts g and c refer to the Gaussian and cosine variables respectively. Note that in a Gaussian model the range a_g corresponds to a length scale of $a_g \times 2.5$, which in this case is 275 km ($a_g = 110$ km).

Mozambique Channel eddies in HYCOM O2 are all of very similar sizes. Therefore, the typical mesoscale size indicated by the Fourier analysis should be of a similar size to the maximum mesoscale estimated by the variogram. In this case, the mesoscale estimate from the variogram is 275 km and the estimate from the Fourier analysis is 280 km, in good agreement with each other as expected.

In addition to this, the combined Gaussian and cosine fit indicates a mixture of periodic (cosine) and other (Gaussian) signals. Here the periodic signal suggests a succession of eddies. The cosine range ($a_c = 90$ km) indicates that successive eddies are typically ~ 560 km ($a_c \times 2\pi$) apart.

Both the spatial Fourier and variogram analyses reflect the whole range of spatial scales related to mesoscale currents for a given region. Therefore it may be prudent to refer to "mesoscale features" rather than "eddies" when discussing these results. However, due to the dominance of anticyclonic eddies (in HYCOM O2) in the Mozambique Channel it may be safe to conclude that these results provide an indication of the typical (Fourier) and maximum (variogram) eddy diameters. For consistency, discussions hereafter will refer to "mesoscale features" only, and these are defined to include both eddies and meanders in mesoscale currents.

The information contained in a variogram is in principle equivalent to that contained in a Fourier transform, but the variogram is more practical for testing the stationarity of a variable and for examining small scales. In addition to this the Fourier transform relies on the assumption that the data domain is periodic rather than infinite. Furthermore, when calculating the experimental variogram the data does not need to be preprocessed. Before calculating the Fourier transform, trends in the data have to be removed, and

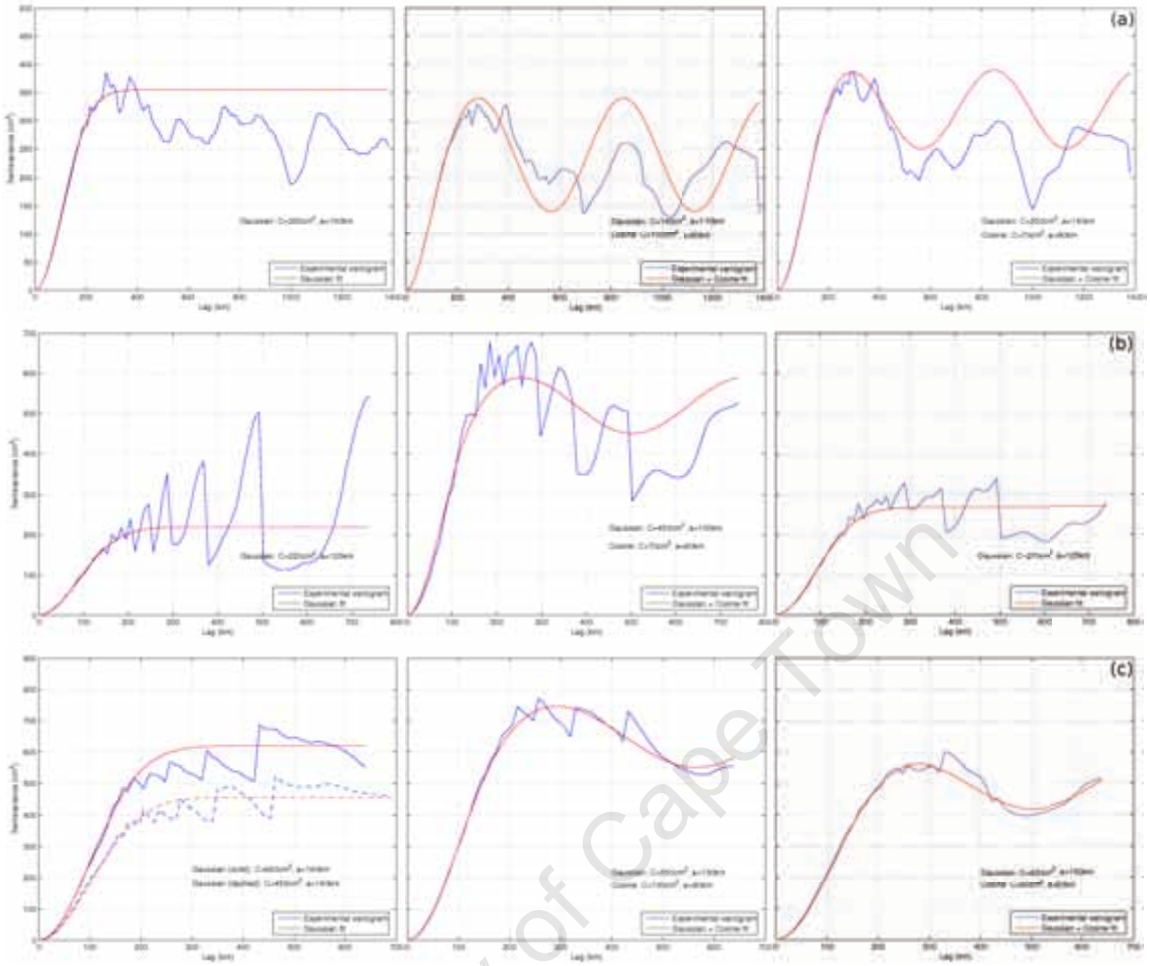

Figure 4.10: Variogram analysis for Aviso (left colum), HYCOM O2 (middle column) and HYCOM O4 (right column). SLA data was extracted from gridded data along sections for the Mozambique Channel (a), the Agulhas Current (b), and the Agulhas ring shedding corridor (c) and interpolated to 10 km. See straight black lines in Figures 4.7a and 4.8.

tapering functions need to be applied at the edges. Moreover, the physical meaning of the semivariance is easy to interpret. In the case of mesoscale variability in the ocean, it represents the amplitude of the differences, and like eddy kinetic energy, high values represent regions with high mesoscale variability. The major advantage of the variogram, is that it is easy to calculate, requiring only a few lines of code.

These results confirm that the variogram indeed provides an indication of the size of mesoscale features for a given region, and in addition to this is able to determine the presence of periodic signals, as well as comparable magnitudes of the variance.

4.4.3.2 Quantifying spatial scales of mesoscale variability

To quantify the spatial scale of mesoscale variability in key regions of the greater Agulhas Current system, three sections were defined along which SLA data from Aviso, HYCOM O2 and HYCOM O4 was extracted (see Figures 4.7 and 4.8).

The Mozambique Channel section, extending southward from 43°E / 14°S to 30°E / 33.5°S, was chosen to represent the path along which predominantly anticyclonic eddies propagate southward from the Mozambique Channel toward the northern Agulhas Current. This path can be clearly identified in both HYCOM O2 and O4 simulations, and is also evident in the altimetry field.

The Aviso SLA experimental variogram (Figure 4.10a, left) was fitted with a Gaussian function (the first term in Equation 4.5), indicating that a maximum variance (or sill) of 355 cm^2 is reached at a radius (or range) of 150 km. This suggests that mesoscale features (eddies or meanders) along this section have diameters up to 375 km, somewhat larger than previously documented.

As discussed previously (Section 4.4.3.1), the HYCOM O2 variogram (Figure 4.10, middle) was fitted with a curve combining a Gaussian and cosine function (Equation 4.5). The respective Gaussian and cosine ranges, (a_g and a_c) indicate that, contrary to previous findings (Backeberg et al., 2008), the Mozambique Channel eddies in HYCOM O2 are smaller and less intense than in reality, with diameters of 275 km, and a semivariance 60% less than observed from altimetry. In addition to this the periodicity, with successive eddies $\sim$ 560 km ($a_c \times 2\pi$) apart, is not evident in the altimetry SLA section, indicating that the formation of eddies in the O2 simulation is too regular / periodic.

Applying the 4^{th} order advection scheme in HYCOM improves some of the deficiencies of the O2 scheme in the Mozambique Channel. The amplitude of the Gaussian sill (C_g) is much higher, and the range has increased to 140 km, corresponding to a diameter of 350 km, in better agreement with the altimetry observations. There is also some improvement in the (artificial) periodicity, in that the amplitude of the cosine function (C_c) is slightly lower, suggesting a reduction of the periodicity.

The second section extends from 32°E / 30°S along the South African east coast toward the retroflection region at 20°E / 39°S and lies within a band of negative skewness thought to be associated with periodic cyclonic disturbances or Natal Pulses.

The Aviso variogram analysis, with C_c = 220 cm^2 and a_c = 125 km, here indicates mesoscale diameters of up to 312.5 km, in agreement with the documented scale of the Agulhas retroflection loop (340 km;

Lutjeharms and van Ballegooyen, 1988).

The amplitude of the sill in O2 is much higher (C_c = 450 cm^2), with a shorter range (a_g = 100 km) corresponding to diameters of 250 km. A periodicity of 80 km (corresponding to eddies $\sim$ 500 km apart) confirms the successive train of eddies simulated in O2.

The HYCOM O4 variogram is in much better agreement with the altimetry, and no periodicity is evident. A Gaussian function provides the theoretical fit. The amplitude of the sill is slightly higher, but the range of 125 km is in good agreement with the altimetry. A train of eddies (as in O2) will result in a variogram with a higher variance at the sill, due to the enhanced variability associated with an eddy field, but with a smaller spatial scale compared to a well defined current extending southwestward with a large retroflection loop at its termination, as in Aviso and O4. This result presents an additional indication that the O4 scheme provides a much more realistic simulation of the southern Agulhas Current.

From the skewness analysis two sections were defined in the altimetry for the northwestward passage of Agulhas Rings. The first (solid line, Figure 4.10c, left) corresponding to the track along which rings seem to preferentially propagate in HYCOM (Figure 4.8) and the second where according to the skewness field from altimetry (Figure 4.7), predominantly anticyclonic eddies are found in the observations (dashed line).

The Aviso variogram shows that the northern section has a variance of 620 cm^2, with a scale of 140 km, corresponding to diameters of 350 km. The variance in the southern section is 40% lower, but the length scales are similar (135 km corresponding to a diameter of 337.5 km). This indicates, that eddies shed from the retroflection tend to preferentially propagate along the northern track, and that the altimetry skewness field is unable to indicate this path as pointed out by Thompson and Demirov (2006). Note that Agulhas Rings have been documented to have diameters of up to 320 km (Lutjeharms and van Ballegooyen, 1988), in good agreement with the variogram analysis.

While in both model simulations the spatial scales are in good agreement with the altimetry observations, the amplitude of the variance in O2 is too large. A periodic (cosine) signal is also evident in both simulations, suggesting an artificial regularity of Agulhas Ring shedding. This amplitude is somewhat lower in the O4 scheme.

In conclusion, using the variogram tool, the spatial scales of mesoscale features for three sections in the greater Agulhas Current system were quantified. In addition to this, the variogram analysis, provides an objective tool for comparing and validating the two model simulations. It was able to identify (unrealistic) periodic signals in the model simulations, as well as provide a good quantitative comparison of the scales

of the ocean features. A major improvement of the O4 simulation is that the periodicity evident in all the sections for the O2 scheme, is reduced in the Mozambique Channel and ring shedding corridor, and significantly, absent for the section through the Agulhas Current. Moreover, the spatial scales and amplitudes of the variances in HYCOM using the 4^{th} order advection scheme are much more realistic, and in better agreement with the altimetry observations.

4.5 Conclusions

From this inter-comparison of the two numerical advection schemes in HYCOM it was clearly shown that applying higher order numerics (the 4^{th} order momentum advection scheme) significantly improve the model simulation of the greater Agulhas Current regime.

The most significant improvement in the O4 simulation is the change in the southern Agulhas Current, from a train of successive eddies, to a well-defined meandering current. Stronger poleward transports and a much improved vertical structure of the Agulhas Current near 32°S in HYCOM O4 is evident. These improvements may contribute toward a better southwestward penetration of the temperature field, and implies a stronger leakage of warm, saline Indian Ocean waters into the South Atlantic Ocean vital for the Meridional Overturning Circulation.

Satellite altimetry measurements of the sea surface are used in model validation techniques. The sea surface height variations, sea level skewness and variogram analyses quantify the improvements evident in the simulation, as well as providing some new perspectives in terms of studying mesoscale variability in the ocean.

Sea level skewness was shown to be an ideal tool for studying flows with meanders that become unstable and change into eddies. In an eddy field it is able to distinguish between a preference for cyclonic or anticyclonic rotation. The zero skewness line in the southern Agulhas Current confirms that throughout the O4 model simulation, the current is represented as a well defined meandering current.

The variogram analysis confirms that the O4 scheme simulates more realistic scales and variances of mesoscale features. Additionally, it is able to identify (unrealistic) periodic signals such as too regular Mozambique Channel eddies and successive eddies in the southern Agulhas Current, which are pronounced deficiencies of the O2 scheme.

Finally, the Agulhas Current transport, and hence the Indo-Atlantic inter-ocean exchange, is sensitive to

mesoscale features that originate upstream in the source regions. HYCOM O4, in particular with the improved simulation of the southern Agulhas Current, is well suited for application in further studies of this exchange.

Chapter 5

On the formation of Mozambique Channel Eddies

This chapter is based on the work published as:

Backeberg, B. C. and C. J. C. Reason (2010). A connection between the South Equatorial Current north of Madagascar and Mozambique Channel Eddies. *Geophys. Res. Lett.,* 37, L04604, doi:10.1029/2009GL041950.

Abstract

Mozambique Channel eddies cause disturbances in the Agulhas Current that may trigger the shedding of Agulhas rings from the retroflection south of Africa. This ring shedding is the predominant mechanism by which warm, saline water flows from the Indian into the South Atlantic Ocean, which is important for the Meridional Overturning Circulation. Combining output from a high resolution ocean model and geostrophic current observations derived from satellite altimeter measurements, a mechanism is proposed that connects the formation of mesoscale eddies in the Mozambique Channel to positive vorticity anomalies associated with westward transport pulses in the South Equatorial Current. In this way interannual signals associated with large-scale changes in the gyre circulation of the South Indian Ocean may enter the channel and modulate the eddy formation frequency, which ultimately affects the Agulhas leakage.

5.1 Introduction

Only recently was it shown that the flow in the Mozambique Channel (MZC) is dominated by mesoscale anticyclonic eddies, rather than a well-defined poleward western boundary current (de Ruijter et al., 2002). Eddies with spatial scales of approximately 300–350 km, and southward propagation velocities of approximately 3–6 km.d^{-1} have been observed from altimetry (Schouten et al., 2002, 2003), and most modern eddy-resolving models are able to simulate these reasonably well (e.g. Penven et al., 2006a; Backeberg et al., 2008, 2009).

Eddies originating in the source regions of the Agulhas Current, namely the MZC and the region south of Madagascar, have been implicated in generating disturbances in the current proper that ultimately affect the Indo-Atlantic inter-ocean exchange by triggering the shedding of Agulhas rings from the retroflection (e.g. van Leeuwen et al., 2000; Schouten et al., 2002; Penven et al., 2006b).

Wind anomalies over the Indian Ocean are known to affect the greater Agulhas Current system and its eddy activity, and MZC eddies play an important role (e.g. Biastoch and Krauss, 1999; Biastoch et al., 1999; Hermes et al., 2007). Sea level anomaly (SLA) analyses from both satellite altimetry as well as modelling studies indicate that $4 - 6$ eddies per year occur in the channel. The dominant frequencies of eddy occurrences experience latitudinal variations, ranging from 7 yr^{-1} in the north, associated with the extension of the South Equatorial Current (SEC), to 4 yr^{-1} in the southern limit of the channel (Schouten et al., 2003). It has been suggested that westward propagating Rossby waves related to the Indian Ocean Dipole cycle affect the intensity of the mesoscale activity in the channel, through a weakening / strengthening of the SEC and its branches at the Madagascar and African coast (Palastanga et al., 2006).

Mesoscale eddies originating in the MZC play an important role in contributing to the mesoscale variability of the Agulhas Current and its retroflection. Yet, the eddy formation mechanism in the MZC is, to date, not well explored. Observations from a current meter mooring array indicate MZC eddies form near the narrows of the channel at 16°S, subsequent to strong poleward currents (Ridderinkhof and de Ruijter, 2003). Furthermore, it has been suggested that their formation is associated with barotropic instabilities of the SEC north of the MZC (Quadfasel and Swallow, 1986; Biastoch and Krauss, 1999), and the subsequent shedding of an eddy is due to the geometry of the narrows, although no clear consensus has been reached in terms of the dynamics causing eddies to form.

From previous studies, it appears that a connection between the SEC and the MZC exists through which mesoscale, seasonal as well as interannual signals are able to propagate into the channel and hence modulate

the frequency of eddy occurrences. However, it remains unclear as to the mechanism by which such signals propagate into the channel and how they affect the eddy formation process. To address this issue, the focus of this study is to analyse vorticity entering the MZC from the north, relating this to the variability observed in the SEC north of Madagascar and to show how it may contribute toward eddy formation in the channel. The model system and satellite altimetry data used, as well as the analysis technique applied are outlined in Section 5.2. Finally the results are discussed and our main findings concluded in Section 5.3.

5.2 Data and methods

In Chapter 3 it was shown that a $1/10^{th}$ of a degree Hybrid Coordinate Ocean Model (HYCOM; Bleck, 2002) of the greater Agulhas Current system adequately resolves the general circulation in the region. Following this a 4^{th} order momentum advection scheme was implemented, and in Chapter 4 it was shown that the new scheme significantly improves the realism of the model simulation of the region. In particular, the MZC and its eddies have been shown to be realistically represented in terms of their dimensions, the associated current velocities as well as their formation frequency. For this study, data from the years $2001 - 2006$ from the second simulation experiment, using the 4^{th} order momentum advection scheme was used.

To complement the model results, surface geostrophic velocities are derived from satellite altimetry sea surface height measurements combined with the mean dynamic topography from Rio05 (Rio and Hernandez, 2004; Rio et al., 2005). The gridded data are merged from multiple altimeter missions, including TOPEX / Poseidon, Jason-1, ERS and Envisat and these are mapped to a $1/3°$ Mercator grid (Ducet et al., 2000). The data are available at weekly intervals from Ssalto/Duacs and distributed by Aviso, with support from the Centre National d'Etudes Spatiales (CNES; `www.aviso.oceanobs.com`).

It should be noted that there is a shortage of altimetry data close to the coast, which is due to a number of factors. Firstly, the radar echo reflected from water is different from the radar echo reflected from a combination of water and land. Satellite altimetry data closer than 50 km from the coast is flagged as poor quality data and thus not included in the Aviso product. Secondly, the computation of error corrections is limited by knowledge of the local tides, which are much more complex close to the coast compared to the open ocean, and rapid variations of tides and atmospheric pressure must be accounted for. Finally, wet tropospheric corrections, computed from radiometer measurements are also less precise, or even missing, near the

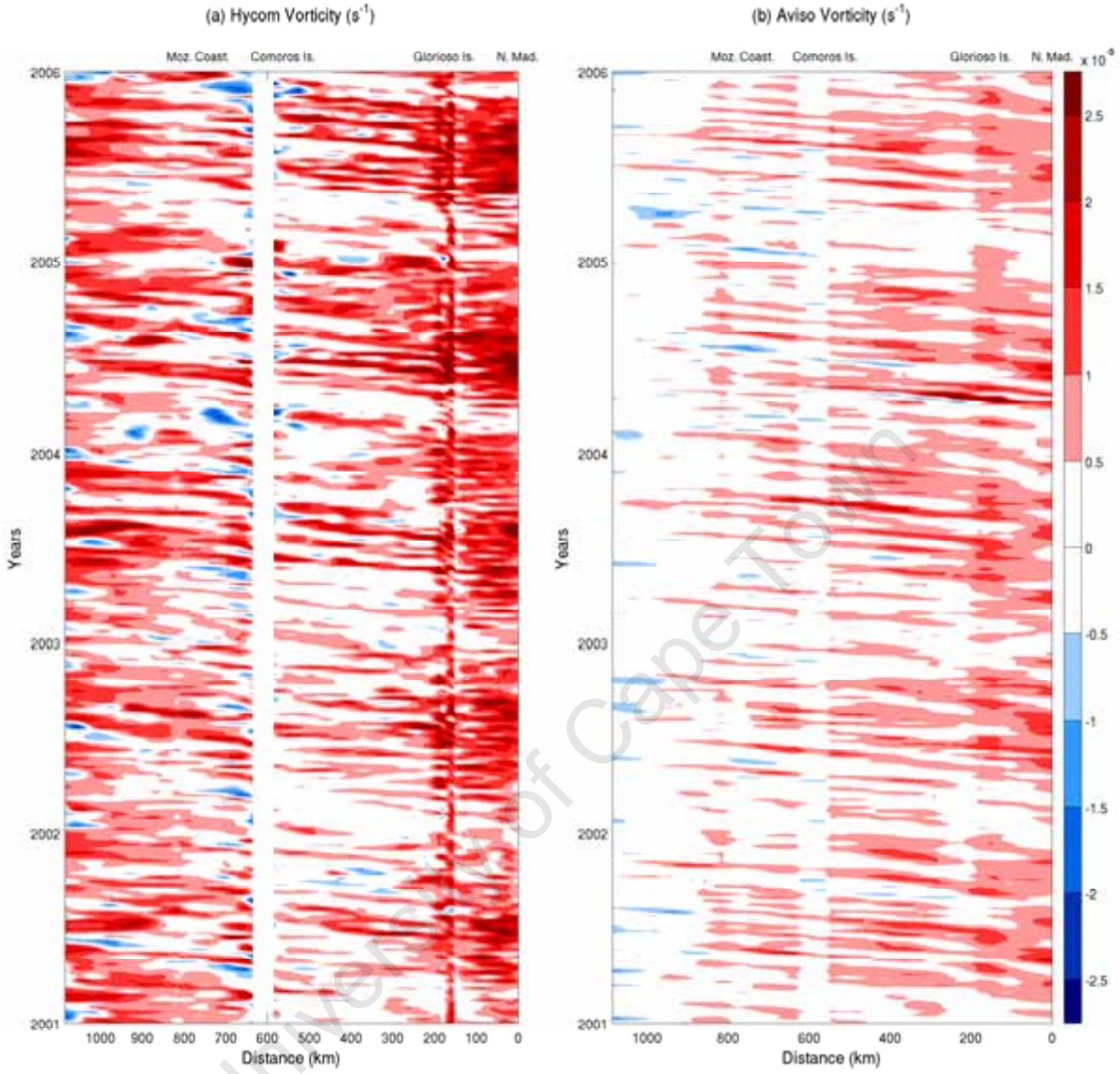

Figure 5.1: Hovmöller plot of vorticity (s^{-1}) for the section from the northern tip of Madagascar along 11.5°S to the Mozambiçan coast and southward along the coast to 14°S. Section data was extracted from the gridded HYCOM (a) and Aviso (b) vorticity fields and interpolated to 10 km.

coasts (source: `www.aviso.oceanobs.com/no_cache/en/applications/coastal-applications/`). The model data forms an integral addition to this study due to its superior spatial resolution as well as its ability to provide data close to the coast.

To investigate the eddy formation process in the MZC, model vorticity was calculated from the gridded HYCOM current velocities at 10 m and compared with the vorticities derived from the Aviso surface geostrophic currents for the years $2001 - 2006$. Next, a section was defined across the entrance of the

channel at 11.5°S, extending from the northern tip of Madagascar westward toward the Mozambiçan coast, then continuing southward along the coast to 14°S, and data along the section was extracted and interpolated to 10 km. The resulting Hovmöller plots are given in Figure 5.1. The positions of the northern tip of Madagascar (0 km), the Gorioso Islands ($\sim$ 180 km), the Comoros Island ($\sim$ 600 km) and Mozambiçan coast ($\sim$ 800 km) are indicated on the plots at the top of each panel.

In order to relate the westward propagating vorticity signals evident in the Hovmöller plots to variability in the SEC north of Madagascar, an additional section was defined to extend from the northern tip of Madagascar to 11°S across which weekly transports were extracted from HYCOM (Figure 5.2a; solid line). The mean transport from this section in HYCOM for the years $2001-2006$ is 33 ± 7 Sv (positive westward), which is in good agreement with previous observational estimates of 27 ± 9 Sv (current meter; Schott et al., 1988) and 29 Sv (1100 m reference level; Swallow et al., 1988). Plotted on the same panel (Figure 5.2a, dashed line) are the weekly vorticities from the first data point in the Hovmöller plot, located at 49°E, 11.5°S. Figure 5.2b shows the corresponding 5 month running mean of the transports and vorticities in HYCOM. For the Aviso geostrophic currents, weekly U component velocities were extracted from the section north of Madagascar and plotted together with the weekly vorticities at 49°E, 11.5°S (Figure 5.2c), and the corresponding 5 month running mean (Figure 5.2d).

A lagged cross-correlation of the currents north of Madagascar and vorticity near the Mozambiçan coast provides an indication of the time-scale at which signals propagate across the entrance of the channel and into the narrows (Figure 5.3). Two locations along the Hovmöller plot near the Mozambiçan coast were selected: (1) where the Hovmöller section meets the Mozambiçan coast at 43.6°E, 11.5°S and (2) further south along the Hovmöller section near the narrows at 41.5°E, 13.9°S. These are indicated by the solid and dashed line respectively.

Finally, using the current output at 10 m from HYCOM, weekly vorticity fields were calculated, and the seasonal cycle removed. A region in the MZC between $41^\circ - 42.5^\circ$E and $15^\circ - 17^\circ$S was selected and the area average vorticity time series computed. From this time series, events exceeding the 95^{th} percentile were selected to calculate the mean composite vorticity anomaly and corresponding currents (T_0; Figure 5.4f). This represents the mean of the periods during which particularly strong eddies were simulated in the narrows of the MZC. Following this, composite maps of the weeks preceding these eddy events were calculated for T_{-20}, T_{-15}, T_{-9}, T_{-7} and T_{-5} weeks before T_{-0} (Figures 5.4a-e, respectively). The same analysis was attempted using the Aviso data, however the results are not very clear. The discrepancy may

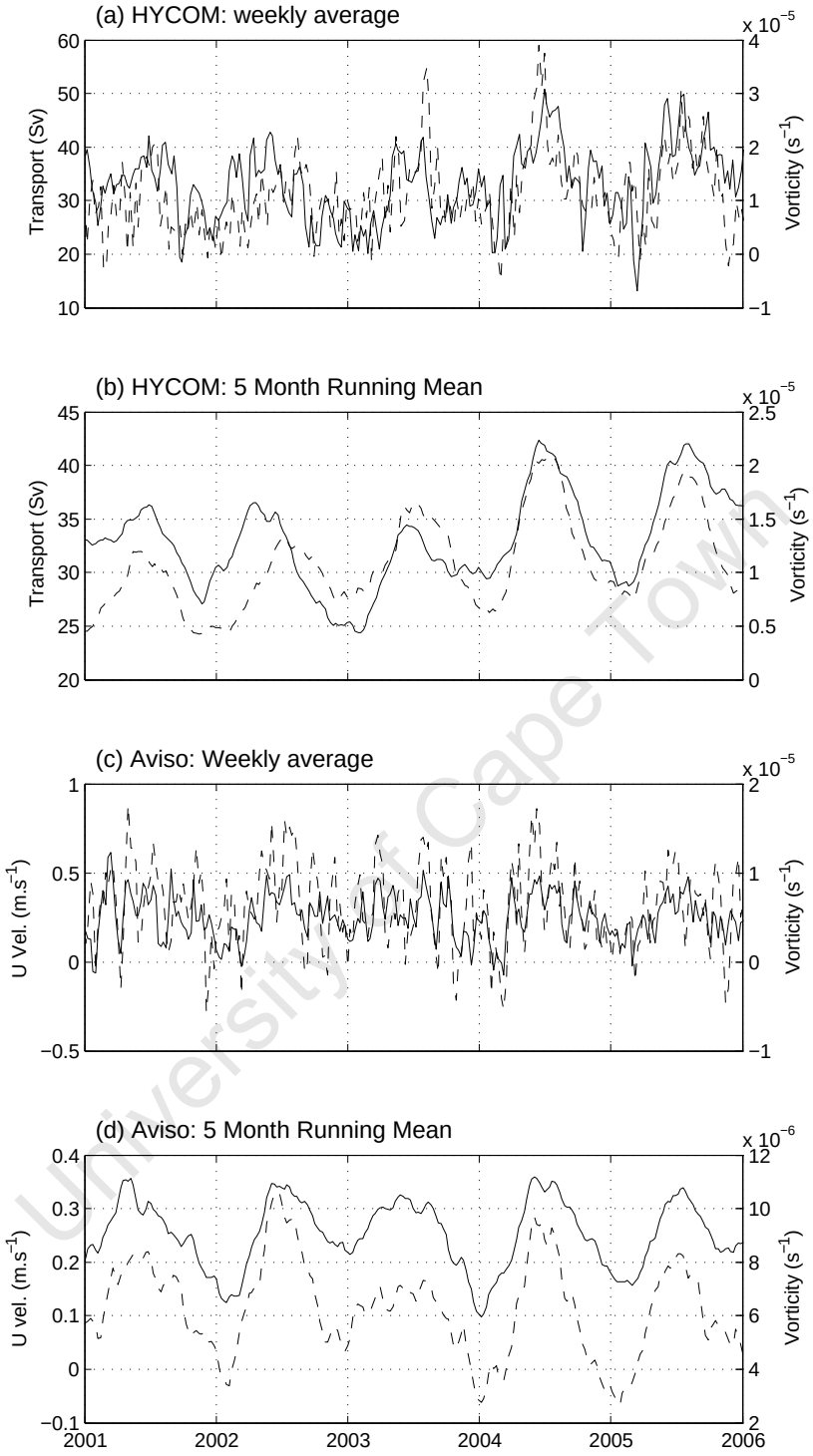

Figure 5.2: (a) Time series of weekly transports (Sv, solid line) from HYCOM for a section extending to 11°S from the northern tip of Madagascar, with weekly vorticity (s^{-1}; dashed line) for the first data point of the the Hovmöller series (Figure 5.1a). (b) Corresponding 5 month running mean from HYCOM. (c) Weekly Aviso U velocities ($m.s^{-1}$; solid line) for the section north of Madagascar with weekly vorticity (s^{-1}; dashed line) for the first data point of the the Hovmöller series (Figure 5.1b). (d) Corresponding 5 month running mean from the Aviso data.

have to do with the relatively low resolution of the altimetry data set as well as loss of information due to interpolation in the generation of the gridded data product. Furthermore, a shortage of altimetry data close to the coast may further impede the ability to track the vorticity signal as it propagates southward into the MZC.

5.3 Results and discussion

Both the HYCOM and Aviso vorticity Hovmöller plots (Figure 5.1) clearly show positive vorticity signals propagating westward from the northern tip of Madagascar to the Mozambiçan coast. The predominantly positive vorticity is due to friction at the inshore edge of the SEC, which drives anticyclonic motion as it flows westward past the northern tip of Madagascar. This behaviour is similar, but in the opposite direction, to cyclonic motion occurring in the southern extension of the East Madagascar Current as it flows westward past the southern tip of Madagascar (de Ruijter et al., 2004; Siedler et al., 2009). The vorticity signal in HYCOM is significantly stronger than observed in Aviso, due to the aforementioned differences in resolution, and the signals propagating southward along the Mozambiçan coast are barely evident, which is likely due to the poor quality of the altimetry data close to the coast.

The positive vorticity signals are estimated to propagate across the northern entrance to the MZC channel at approximately $5-9$ km.d^{-1} (HYCOM) and $6-10$ km.d^{-1} (Aviso), which agrees well with documented eddy propagation velocities at these latitudes (Chelton et al., 2007). The Glorioso and Comoros Islands, interfere with the westward propagating signals. At the Comoros Islands in particular, the vorticity signals seem to become enhanced, and in some cases additional westward propagating signals are formed.

In addition to the mesoscale pulsing, both the model and altimetry data show a strong seasonal cycle east of the Comoros Islands, with maximum (minimum) vorticities occurring in the austral winter to spring (summer to autumn). The model suggests there to be some evidence of seasonality on the Mozambiçan side of the channel, but it is weaker, and not at all apparent in the Aviso data product.

From the Hovmöller plots alone, it seems clear that the mesoscale signals propagating into the channel as well as their seasonal cycle is related to variability at the same time-scales in the SEC north of Madagascar. Comparing the weekly transports and vorticities from HYCOM (Figure 5.2a), there is good correlation between the two data, $r = 0.48$ and statistically significant at the 95% confidence level. This indicates that strong westward volume fluxes are frequently associated with positive vorticities. Similarly, for the

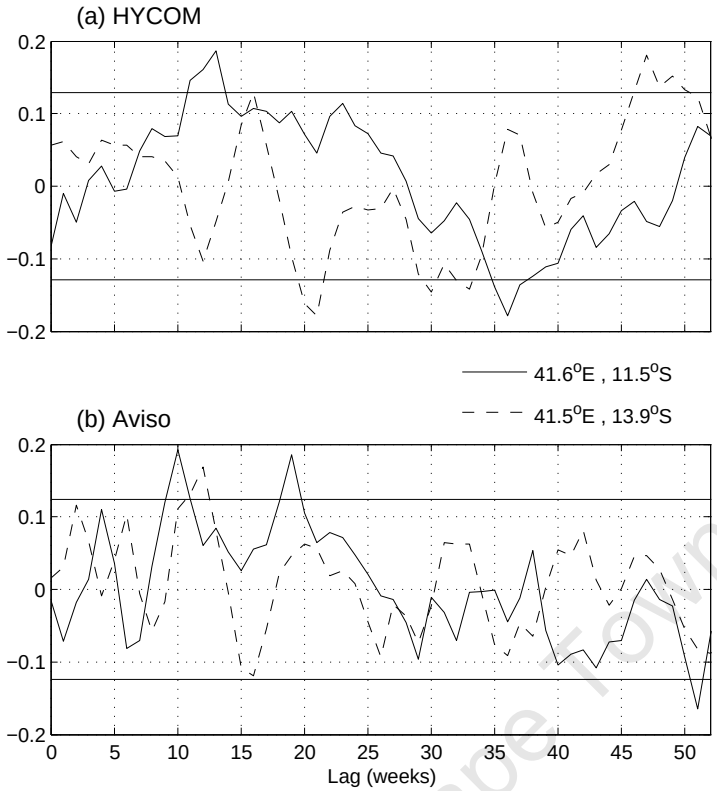

Figure 5.3: (a) Lagged cross-correlation sequence of HYCOM transports north of Madagascar and vorticity at 41.6°E, 11.5°S (solid line) and 41.5°E, 13.9°S (dashed line). (b) Lagged cross-correlation sequence of Aviso U velocities and vorticity for the same locations.

Aviso U velocities (Figure 5.2c), during westward current pulses, positive vorticity features are observed. The correlation coefficient for the two Aviso time-series is 0.57. The weekly model and Aviso data confirm a strong relationship between the SEC north of Madagascar and vorticity features which then propagate westward to the MZC.

At the seasonal time-scale (Figure 5.2b and d), there is very close agreement between the fluctuations observed in the SEC north of Madagascar and vorticity propagating toward the Mozambiçan coast. This agreement indicates that the seasonal cycle of the SEC is transmitted into the MZC, with maximum (minimum) currents and vorticity occurring during the austral winter (summer). An autocorrelation sequence of vorticities along the section confirms that seasonal signals occur, they are strongest east of the Glorioso Islands and reduce westward toward the Mozambiçan cost. This result suggests that eddy formation in the MZC has a seasonal cycle, which in fact has been documented previously using satellite observations (Heywood and Somayajulu, 1997) as well as modelling studies (e.g. Hermes et al., 2007). Note, there is a remarkably good agreement between the timing of the seasonality in HYCOM compared to the satellite observations.

The cross-correlation sequence of the transport in HYCOM north of Madagascar and the vorticity near the Mozambiçan coast (Figure 5.3a) at 41.6°E, 11.5°S (solid line) and 41.5°E, 13.9°S (dashed line) shows peaks at 13 and 16 weeks. These peaks were expected considering the signal propagation velocity estimate of 5 km.d^{-1} from the Hovmöller analysis. The latter peak is however not statistically significant, indicating a weaker relationship between the transports of the SEC north of Madagascar and vorticity near the narrows of the channel.

For the cross-correlation sequence of the Aviso U velocities and vorticity at the northern location near the Mozambiçan coast, statistically significant peaks are observed at 10 and 19 week lags, while for the southern location a statistically significant peak is observed at a lag of 12 weeks. These peaks are in good agreement with the signal propagation velocity estimates of $6 - 10$ km.d^{-1}.

Using both model and altimetry data, the above time series analyses provides compelling evidence indicating that positive vorticity features propagate into the MZC and that these are associated with transport fluctuations of the SEC north of Madagascar at mesoscale and seasonal time-scales. The following composite analysis of the HYCOM vorticity fields provides a mechanism, or pathway, through which vorticity anomalies may reach the narrows of the MZC, where they aid in the formation of anticyclonic eddies.

It was shown that strong westward jets associated with SEC north of Madagascar cause positive vorticity anomalies to develop. Anticyclonic motion, therefore positive relative vorticity, occurs here due to friction at the inshore edge of the SEC. 20 weeks prior to an eddy being formed in the narrows of the MZC, the composite maps show a positive vorticity anomaly extending westward from the northern tip of Madagascar (Figure 5.4a). Subsequently, 5 weeks later (T_{-15}; Figure 5.4b) the vorticity anomaly has moved westward toward the Mozambiçan coast with the background flow. Upon approaching the Comoros Island at 43.5°E, 11°S further coastal shear effects causes the vorticity anomaly to intensify and expand southwestward (T_{-9}; Figure 5.4c). 13 weeks later (in agreement with the cross-correlation sequence) the vorticity anomaly reaches the Mozambiçan coast, where it acts to intensify the poleward currents (T_{-7}; Figure 5.4d). In the now enhanced poleward flow, conservation of potential vorticity generates additional anticyclonic flow curvature and serves to further intensify the positive vorticity anomaly (T_{-5}; Figure 5.4e), and an eddy begins to form. In the southern hemisphere where the Coriolis parameter (f) is negative, a poleward moving eddy experiences a decreasing f (more negative), and therefore relative vorticity (ζ) must increase in order to conserve potential vorticity. Therefore, MZC eddies intensify in their southward passage toward the narrows (T_{-5} and T_{-0}, Figures 5.4e and f). Finally, as these eddies move from the relatively shallow

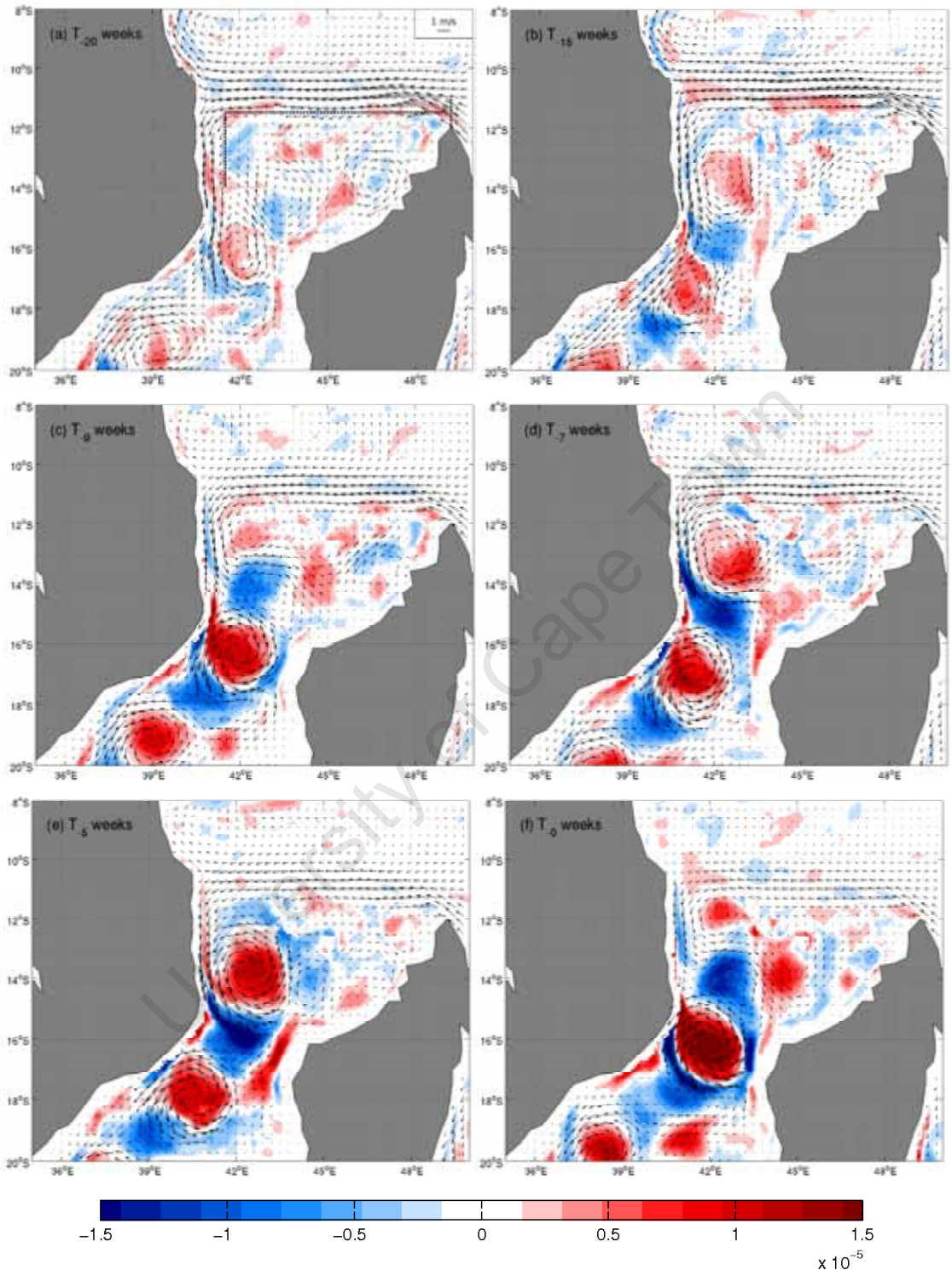

Figure 5.4: HYCOM vorticity (s^{-1}) and current ($m.s^{-1}$) composites for vorticity events in the narrows higher than the the 95^{th} percentile (T_{-0}; f). Composite maps of 20, 15, 9, 7 and 5 weeks before the events are included as T_{-20}, T_{-15}, T_{-9}, T_{-7} and T_{-5} (a-e, respectively). The dashed black line in (a) indicates the coordinates of the section along which vorticity was extracted for the Hovmöller plots (Figure 5.1).

narrows to the deeper part of the channel, they experience a vertical stretching, which reduces the relative vorticity of the water column, and as a result the eddy intensifies further. Generally, the simulated eddies in the Mozambique Channel extend to depths of 1000 m, with the 25 cm.s^{-1} isotach reaching depths of 400 m. A detailed analysis of the eddy physics, investigating baroclinic, barotropic or mixed baroclinic-barotropic instabilities is required to confirm the proposed mechanism, but is not within the scope of this study.

Combining output from an eddy resolving model and satellite altimetry data it was shown that eddy formation in the MZC is related to variability of the SEC north of Madagascar. The model composite analysis indicates that eddies form in the channel approximately 20 weeks following a vorticity anomaly north of Madagascar associated with a strong westward transport pulse in the SEC. Furthermore seasonal variability was shown to occur and is able to enter the channel via the described mechanism, accounting for the seasonal changes in the eddy activity previously noted (Heywood and Somayajulu, 1997; Hermes et al., 2007). Considering that MZC eddies have been implicated in generating disturbances in the Agulhas Current that affect the Indo-Atlantic inter-ocean exchange (Biastoch et al., 2008b), a connection of the MZC eddies to the large-scale variability of the South Indian Ocean is significant. It suggests that ultimately, variability in the Agulhas system and inter-ocean leakage is driven by changes in the gyre circulation of the Indian Ocean, which are related to interannual modes such as the Indian Ocean Dipole and El Niño Southern Oscillation.

Chapter 6

Mesoscale transport variability in the greater Agulhas Current system

This chapter is based on the work submitted as:

Backeberg, B. C., J. A. Johannessen, and C. J. C. Reason (2009). Mesoscale transport variability in the Agulhas system and its connection to leakage into the South Atlantic Ocean. *submitted to J. Geophys. Res.*

Abstract

A regional eddy resolving Hybrid Coordinate Ocean Model of the greater Agulhas Current system is used to investigate the transport variability in the source regions of the Agulhas Current, the Agulhas Current core and in the retroflection region. The contribution from eddies in the Mozambique Channel, as well as variations in the mean westward flow south of Madagascar play important roles in determining the overall poleward volume flux in the Agulhas Current at 32°S. Maximum poleward transports in the Agulhas Current core are reached when the contributions from the respective source regions are at their maximum in addition to the presence of anticyclonic eddies on the ocean side of the current. A correlation between strong transports in the Agulhas Current and westward protrusions of the retroflection loop exists at lag periods of 9 and 37 weeks. Furthermore, following periods of strong transports in the Agulhas Current comparatively more eddies are shed from the retroflection than following periods of weak transports, indicating that the condition of the Agulhas Current influences the mesoscale variability at the Agulhas retroflection. The maximum leakage of warm, saline water into the South Atlantic Ocean in the model simulation reaches up to 38 Sv, and the estimated contribution from Agulhas rings of $8 - 10$ Sv constitutes 26% of the overall westward transport.

6.1 Introduction

The Agulhas leakage of warm, saline water from the Indian Ocean into the Atlantic Ocean is thought to occur predominantly in the form of large Agulhas rings shed from the Agulhas retroflection (Lutjeharms, 2006). This is thought to be an important component of the upper limb of the Atlantic meridional overturning circulation (MOC), which plays a key role in maintaining the global overturning circulation of the ocean (e.g. Gordon et al., 1992). Moreover, the contribution of Agulhas rings toward the overall leakage is considered to be significant for the decadal variability of the MOC (Biastoch et al., 2008a), and paleo-oceanographic studies have suggested that changes in the Agulhas leakage play a crucial role in the termination of glacial / interglacial periods, which has significant implications for climate change scenarios (Peeters et al., 2004). Recently it has been shown that the sea surface temperature in the Agulhas retroflection region has increased significantly since 1980's, and the associated increase of the heat and salt fluxes into the Atlantic Ocean as well as enhanced ocean-atmosphere interaction may have significant impacts on the regional and hemispheric climate (Rouault et al., 2009).

Retroflection eddies are unique in the global ocean because they are shed primarily due to a zonal protrusion of the retroflection loop, and are typically larger than eddies pinched off from meandering currents such as the Gulf Stream (Pichevin et al., 1999). Their horizontal diameters range from $200-280$ km, and they may reach depths of up to 1100 m (Duncombe-Rae, 1991). The number of rings shed from the retroflection varies annually, but on average six Agulhas rings are observed drifting into the South Atlantic Ocean each year, and with drift velocities of $5-8$ km.d^{-1} ($0.06-0.09$ m.s^{-1}), the corresponding volume flux estimates range from $3-20$ Sv (1 Sv $= 10^6$ m^3.s^{-1}) (Gordon et al., 1992). Historically, the inter-ocean exchange due to eddies is estimated by calculating the heat, salt and transport anomaly by selecting a reference station just outside the ring (e.g. Byrne et al., 1995; Duncombe-Rae et al., 1996; Goni et al., 1997). However, the salt and heat content at the reference station has already been mixed into the background, and are implicitly subtracted, and therefore the anomalies, i.e. the fluxes associated with the rings, are underestimated with respect to what was initially injected into the Atlantic during the shedding event (Boebel et al., 2003a).

However, quantifying the Agulhas leakage remains a challenging task. The complexity of the currents and the intense mesoscale features in the Agulhas retroflection region make it difficult to directly measure the Indo-Atlantic inter-ocean exchange. Obtaining realistic model simulations is problematic due to the highly non-linear nature of the flow dynamics. Furthermore, the intermittent process of Agulhas ring

shedding is thought to be influenced by perturbations propagating downstream from the northern Agulhas Current (van Leeuwen et al., 2000), and these mesoscale features are thought to originate from the Agulhas Current source regions, namely the Mozambique Channel and south of Madagascar (Schouten et al., 2002; de Ruijter et al., 2004).

Recently, in a study using Lagrangian drifter trajectories simulated in an eddy-resolving model, van Sebille et al. (2009) showed that weaker transports in the Agulhas Current core cause the current to detach from the African continental slope further downstream. This results in a westward migration of the Agulhas retroflection loop associated with lower inertia that hinders the generation of anticyclonic vorticity, thereby enhancing the Agulhas leakage.

Conversely, a decadal warming trend observed in the Agulhas retroflection region has been attributed to an increased flux of warm, saline anomalies (i.e. eddies) into the South Atlantic resulting from an intensification of the Agulhas Current since the 1980's (Rouault et al., 2009). This latter study is in agreement with the theory that stronger transports in the Agulhas Current core generate inertia that can push the retroflection front downstream, which may force the loop to close upon itself and detach a ring (Pichevin et al., 1999). The numerical experiments of Pichevin et al. (1999) show that transport pulses in the Agulhas Current modify the periodicity of ring generation at the retroflection such that it adjusts to the periodicity of the pulses. Therefore a higher number of transport pulses, associated with a strong Agulhas Current, result in increased ring shedding frequencies and associated volume fluxes.

The objective of this study is to examine the sources of transport variability in the greater Agulhas Current system, and to quantify the downstream effect on the Agulhas retroflection and hence the Indo-Atlantic inter-ocean exchange using a regional ocean model. The model characteristics are outlined in detail in Chapter 2, a brief overview of the regional model used in this study is outlined in Section 6.2, followed by a comparison and assessment of the mean simulated transports in Section 6.3. The mesoscale transport variability simulated for the greater Agulhas Current system is discussed in context of the associated flow dynamics of the region in Section 6.4, and the findings are validated using surface drifter observations in Section 6.5. In Section 6.6 the relationship between the weekly transport variability and the occurrence of mesoscale eddies is quantified and the downstream effect on the Agulhas retroflection and hence the Indo-Atlantic inter-ocean exchange is discussed in Section 6.7. In closing, the summary and conclusion of the main findings in this study are presented in Section 6.8.

6.2 HYCOM

The ability of the regional HYCOM of the greater Agulhas Current system to realistically simulate the region has been documented in Chapters 3 and 4. In particular the importance of a 4^{th} order momentum advection scheme is highlighted, which greatly improved the dynamics of the model, especially in the retroflection region. The models suitability for studying the transport variability throughout the greater Agulhas Current system and the downstream affect on the Agulhas retroflection and the inter-ocean exchange was demonstrated.

In this study output from the second simulation experiment using the 4^{th} order momentum advection scheme is used. For a full description of the model setup and characteristics refer to Chapter 2.

6.3 Mean transports in the greater Agulhas Current system

To analyse the mesoscale transport variability of the Agulhas Current, its sources and the leakage into the South Atlantic Ocean, six sections were selected across which the transports integrated to the sea floor were calculated from the model output. The geographical locations of these sections are given in Figure 6.1. Note for all sections, positive transports are southward / poleward and westward.

Southward transports of 15 Sv in the Mozambique Channel (MZC) have been estimated using current meter moorings across the narrows of the channel at 17°S (de Ruijter et al., 2002). The transport estimated across the section at 20°S in the MZC from the model reveals a mean southward volume flux of 21 Sv somewhat larger than documented from observations, but at 21 ± 7 Sv remains within one standard deviation of the observed estimate.

The mean westward volume transport south of Madagascar has been suggested to result from a combination of the volume flux from the East Madagascar Current (EMC) and recirculation in the South West Indian Ocean sub-gyre, with a mean contribution of 25 Sv from the EMC and 35 Sv from the recirculation (Stramma and Lutjeharms, 1997). In HYCOM, two transport sections south of Madagascar were defined. The first extends from the southern tip of Madagascar to 30°S at 45°E (SEMC), where previous modelling studies have been conducted (e.g. Hermes et al., 2007; Matano et al., 2002). The second extends 2° further south to 32°S. The mean transport in the northern section from HYCOM is 35 ± 8 Sv and in good agreement with previous studies, whereas the southern extension provides an additional transport of 11 ± 9 Sv. A total mean transport of 45 ± 11 Sv may therefore feed the Agulhas Current.

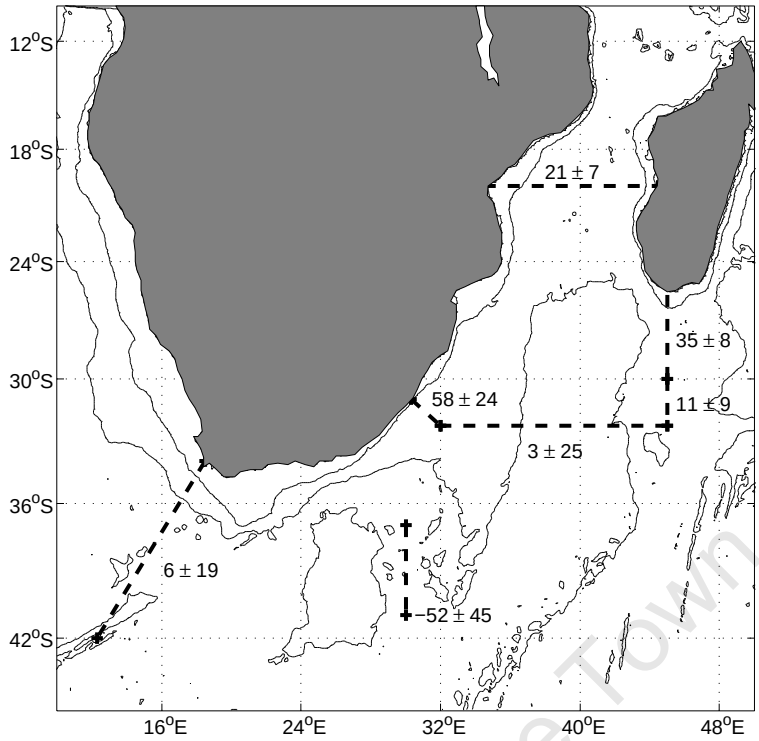

Figure 6.1: Mean transports and standard deviations from HYCOM for the period January 2001 to December 2006. Transports are given in Sv (1 Sv = 10^6 $m^3.s^{-1}$) and are positive southward / poleward and westward. The 1000 and 4000 m isobaths of the model bathymetry (GEBCO) are also plotted.

The poleward transport across the zonal section between 32° and 45°E at 32.3°S reaches 3 ± 25 Sv. The sum of the mean transports in the MZC and the SEMC minus the transports leaving the box to the south then becomes 64 ± 24 Sv. This indicates that the defined sections for the Agulhas source regions provide a good representation of the volume transport reaching the Agulhas Current. The 6 Sv deficit which is unaccounted for may be attributed to errors in the interpolation when calculating the depth integrated transports from the hybrid vertical grid in HYCOM.

For the transports in the Agulhas Current at 32°S, the same section was chosen as that for a year long current meter mooring, which was deployed during the World Ocean Circulation Experiment (WOCE; Bryden et al., 1995). The volume transport of 70 ± 22 Sv derived from these data (Bryden et al., 2005) constitutes the best estimate of the total poleward volume flux in the Agulhas Current to date. HYCOMs ability to realistically represent the observed vertical structure and transport magnitudes there was documented in Backeberg et al. (2009). For this study, the transports for Agulhas Current were integrated to the sea floor. With a mean and standard deviation of 58 ± 24 Sv, HYCOM lies within one standard deviation of the observed estimate.

The eastward volume flux in the Agulhas Return Current from geostrophic current estimates relative to

1500 m is 54 Sv (Lutjeharms and Ansorge, 2001). The volume transport extracted from HYCOM for a meridional section extending from $37° - 41°$S at 30°E is eastward at 52 ± 45 Sv, in good agreement with the observations. This value indicates that a significant volume is transported eastward into the South Indian Ocean. However, quantitatively it is unclear how much of the eastward transport is respectively originating from Agulhas Current and the South Atlantic Current.

To assess the weekly and seasonal transport variability of the Indo-Atlantic inter-ocean exchange via the Agulhas retroflection (AR), a meridional section extending southward from Cape Town at 18°E to 42°S (similar to Rouault et al., 2009) was chosen. The mean westward volume transport across this meridional section in HYCOM is 6 ± 19 Sv, which is weaker but within one standard deviation of the 15 Sv estimated from subsurface floats and surface drifters (Richardson, 2007).

In summary, the mean transports extracted from HYCOM across the selected sections are in good agreement with reported observations of the transports in the Agulhas system. Throughout the region variability of the transports occurs, which is evident in the respective standard deviations. It varies in strength compared to the mean, depending on the flow regime of the region in question. These will be discussed in detail in the following section.

6.4 Mesoscale transport variability

Weekly transport estimates from four of the sections in the Agulhas Current system (Figure 6.2) are further examined in order to determine the relationship between the mean flow and its variability as influenced by eddy induced volume transports. To assess this relationship the mean and standard deviation of volume transports in the MZC, the SEMC (including the southern extension), the Agulhas Current, and the AR are considered together with the 95^{th} and 5^{th} percentile transports (Table 6.1). Note that for the MZC and SEMC the 95^{th} and 5^{th} percentile transports are calculated for the period January 2001−December 2004 only, due to the fact that from January 2005−December 2006 the transports increase and decrease significantly in the MZC and SEMC respectively.

Table 6.1 includes the maximum wind speed and stress (N.m^{-2}) in the sections, and the associated estimates of Ekman surface current and Ekman layer depth. The Ekman surface current (V_0) and Ekman layer depth (D_E) are calculated using the below equations discussed in Pond and Pickard (1983):

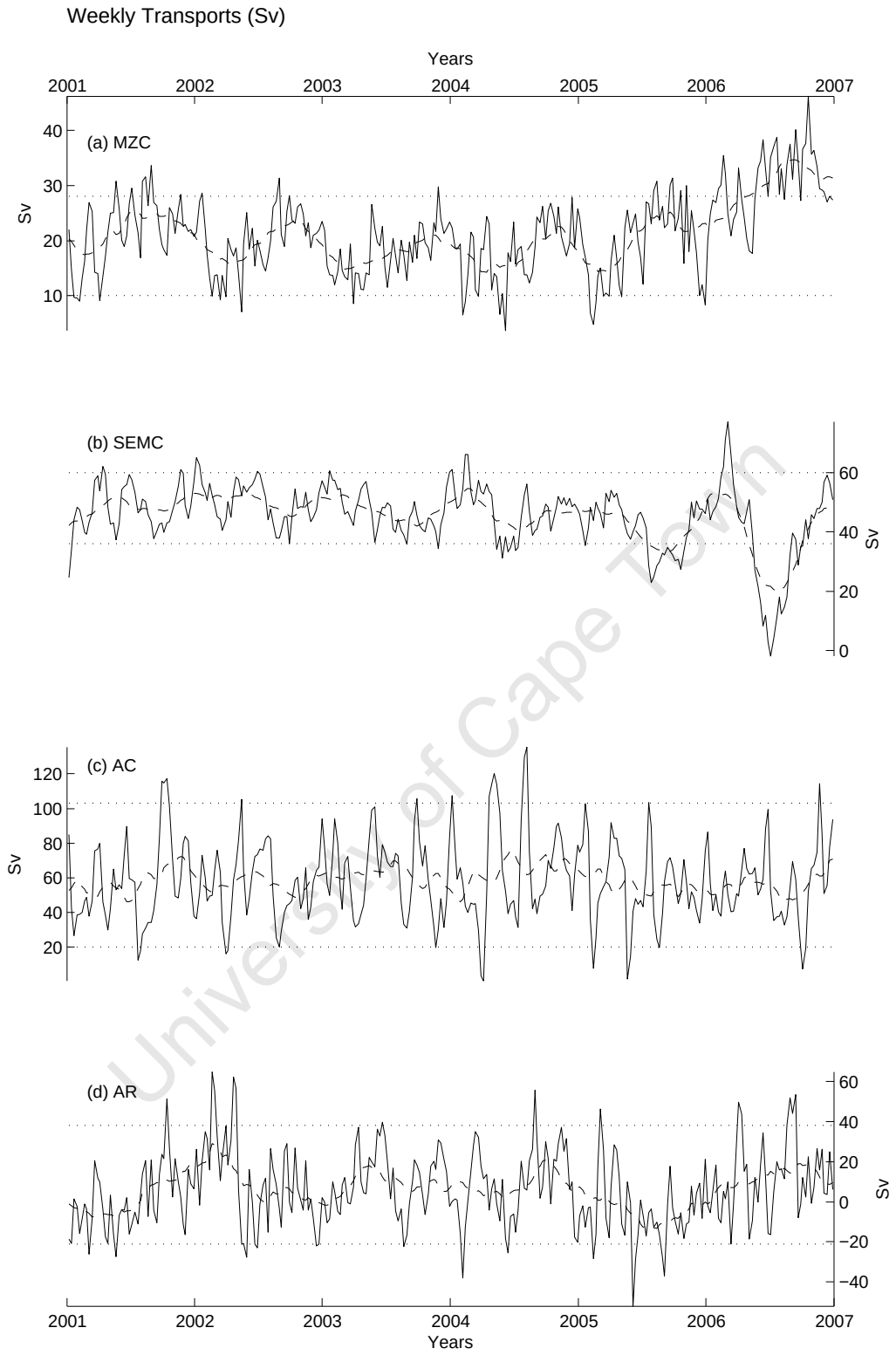

Figure 6.2: Weekly transports (Sv) across sections in (a) the Mozambique Channel at 20°S, (b) south of Madagascar at 45°E including the southern extension to 32°S, (c) the Agulhas Current at 32°S, and (d) the Agulhas retroflection which represents the Agulhas leakage into the South Atlantic Ocean. In each case the dashed line indicates the 5 month running mean transport for the period, and the dotted lines indicate the 95^{th} and 5^{th} percentiles.

$$V_0 = \frac{\sqrt{2}\pi\tau}{D_E \rho \mid f \mid} \tag{6.1}$$

where τ is the magnitude of the wind stress on the sea surface, $\mid f \mid$ is the magnitude of f, and $D_E = \pi\sqrt{\frac{2A_z}{|f|}}$ is the Ekman depth.

The wind stress magnitude is defined as $\tau = \rho_a C_D W^2$, where ρ_a is the density of air, C_D is the drag coefficient, approximately equal to 1.4×10^{-3}, and W is the wind speed in m.s^{-1}. Pond and Pickard (1983) substitute these values into equation 6.1, and by considering the field observations analysed by Ekman, determine that the surface currents and wind speeds are related as

$$V_0 = \frac{0.0127W}{\sqrt{\sin \mid \phi \mid}} \tag{6.2}$$

which is valid outside $\pm 10^\circ$ latitude (ϕ) from the equator.

Using this information, they subsequently derive an expression for the Ekman layer depth

$$D_E = \frac{4.3W}{\sqrt{\sin \mid \phi \mid}} \tag{6.3}$$

Detailed knowledge of the Ekman layer is difficult to obtain, the estimates of Ekman drift velocity and associated transport provided in Table 6.1, are based on the length of the respective transport section, an Ekman layer thickness of 50 m, and an Ekman drift velocity of 0.1 m.s^{-1}, which are considered to be conservative considering the strength of the maximum winds.

The corresponding eddy volume transports given in Table 6.1 were estimated by determining the average eddy diameters and depths for the respective regions and multiplying these with their respective mean drift. The velocity threshold at depth chosen to represent the depth to which the eddies extend is 0.3 m.s^{-1}. The drift of the eddies and mesoscale features in the greater Agulhas Current system used in these estimates were previously determined from the model and discussed in detail in Backeberg et al. (2008).

Finally, to characterise the circulation pattern that persists in the region during the periods when the transports exceed the 95^{th} percentile, the corresponding mean composite currents were calculated from the model velocity fields at 10 m (Figure 6.3).

	MZC	SEMC	AC	AR
Mean flow transport	21 ± 7	45 ± 11	58 ± 24	6 ± 19
95^{th} percentile transport	28	60	103	38
5^{th} percentile transport	10	36	20	-21
Max. Wind speed ($m.s^{-1}$)	12	16	19	18
Max. Wind stress ($N.m^{-2}$)	0.26	0.47	0.66	0.59
Max. Ekman surface current ($m.s^{-1}$)	0.16	0.21	0.25	0.24
Max. Ekman layer depth (m)	54	72	86	81
Estimated Ekman transport	5	4	1	5
Eddy transport	$6-7$	9	$11-16$	$8-10$
Eddy diameters ($\times 10^3$ m)	$270-340$	280	$300-350$	$250-300$
Eddy depths (m)	270	380	$400-600$	700
Eddy drift velocities ($m.s^{-1}$)	0.08	0.08	$0.07-0.10$	0.05

Table 6.1: The transport (Sv) of the mean flow, and at the 95^{th} and 5^{th} percentiles of the Mozambique Channel (MZC), the southern extension of the East Madagascar Current (SEMC), the Agulhas Current (AC) and the Agulhas retroflection (AR) transport sections. The maximum Ekman transports are based on the length of the respective transports section, an Ekman layer thickness of 50 m, and an Ekman drift velocity of 0.1 $m.s^{-1}$. Estimates of the eddy volume transports are based on the dimensions and drift velocities of the eddies simulated in HYCOM for each of the regions. The eddy depths were determined by considering the depth of the 0.3 $m.s^{-1}$ isotach of the eddies in the model, and the drift velocity estimates are taken from Backeberg et al. (2008) where available.

In the MZC, the weekly transports are predominantly poleward and range over $10-28$ Sv between January 2001 and December 2004 (Figure 6.2a). A maximum poleward transport of 46 Sv is reached in October 2006, which coincides with a strong increasing trend of the poleward transports between January 2005 and December 2006. Large fluctuations at monthly to bi-monthly time-scales are evident, and these are probably due to mesoscale anticyclonic eddies that dominate the flow regime in the channel (e.g. de Ruijter et al., 2002). A seasonal cycle of the transports in the MZC is also observed in the model simulation, with maximum transports occurring in the austral winter to spring (Figure 6.2a, dashed line). This behaviour is in agreement with previous studies suggesting that eddy activity in the channel has a seasonal cycle (e.g. Heywood and Somayajulu, 1997; Hermes et al., 2007). Moreover, recently a connection between the eddy formation in the MZC and the transport variability of the South Equatorial Current (SEC) has been proposed, by which seasonal variability associated with the SEC may propagate in the channel and modulate the eddy formation frequency (Backeberg and Reason, 2010).

The size of the eddies in the MZC from our model simulation range from $270-340$ km in diameter and extend to depths of 270 m (Table 6.1). With poleward drift velocities of 7 $km.d^{-1}$ (0.08 $m.s^{-1}$) this corresponds to a volume flux of approximately $6-7$ Sv which is in very good agreement to the standard deviation of the transport calculated across the section (Table 6.1). This indicates that maximum poleward

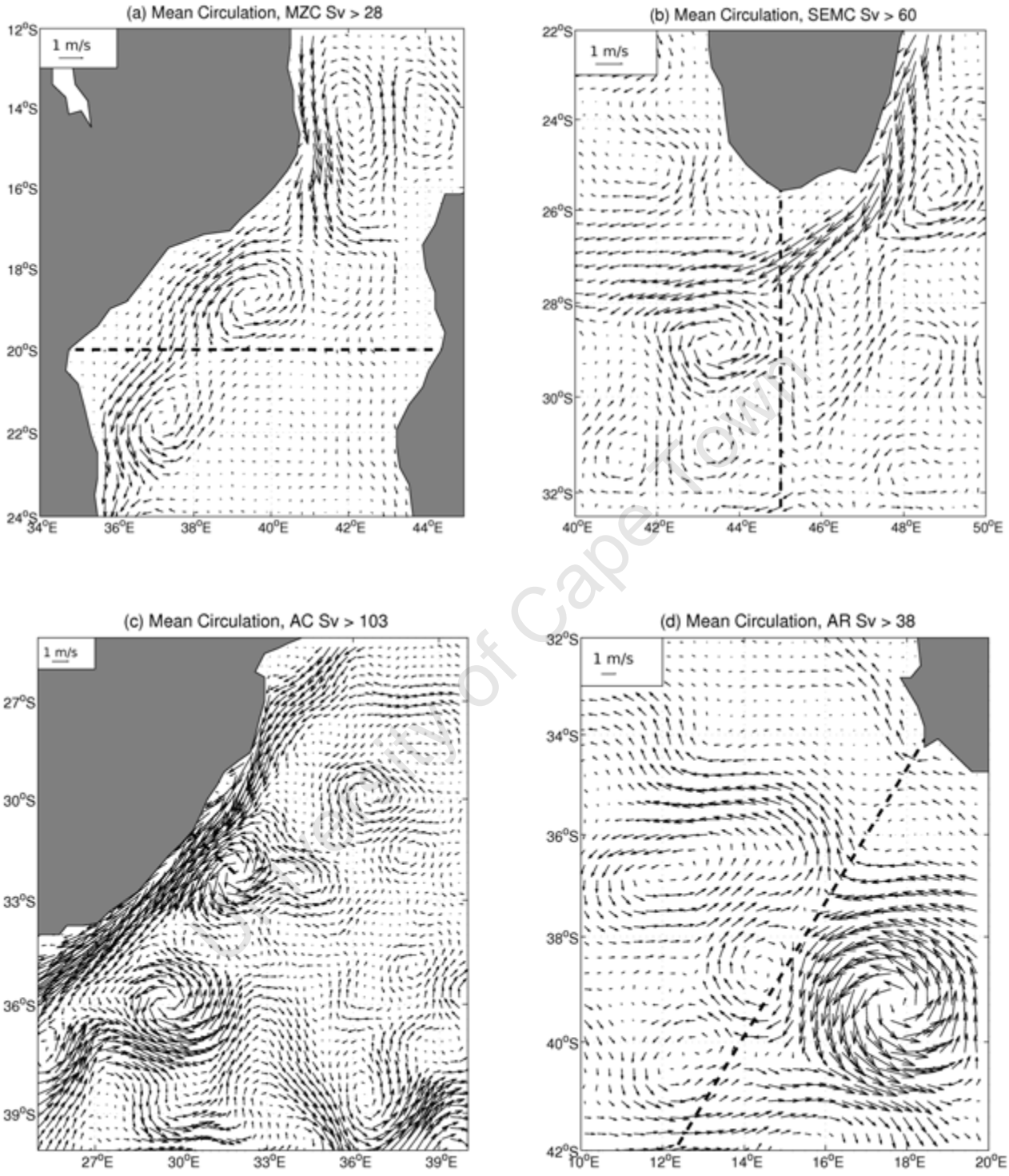

Figure 6.3: Mean circulation when the transports exceed the 95^{th} percentile for (a) the Mozambique Channel at 20°S, (b) the outflow from the southern extension of the East Madagascar Current at 45°E, (c) the Agulhas Current at 32°S and (d) the Agulhas retroflection at 18°E. The dashed black line in each case indicates the geographical extent of the section across which weekly transports were calculated.

transports in the channel consist of a mean flow plus the volume flux associated with the poleward passage of mesoscale eddies.

The circulation pattern which persists in the MZC when the poleward transports exceed the 95^{th} percentile of 28 Sv (Figure 6.3a) shows a strong current flowing poleward along the Mozambican shelf as well as strong eddy activity throughout the channel. Two eddies are evident at 19°S and 22°S, with a third one in the process of being formed north of the narrows at 14°S. In contrast, during poleward transports below the 5^{th} percentile which is less than 10 Sv, the poleward current along the coast of Mozambique weakens and only one clearly defined eddy is present in the channel south of 20°S. Furthermore, wind stress curl anomalies during weak poleward transports are slightly less negative than during periods of strong transports, and the mean wind is orientated to the north which further slows the poleward transports. The maximum poleward Ekman transport across the MZC section, which is approximately 1045 km long, is 5 Sv (Table 6.1). Local winds may therefore play a contributing role toward the overall volume transport through the MZC. However the fact that a strong (weak) presence of eddies coincides with high (low) poleward transports confirms that the dominant drivers of transport fluctuations in the channel are the mesoscale eddies.

South of Madagascar the weekly transports are predominantly westward (Figure 6.2b). Between January 2001 and December 2004, the transports range from $36 - 60$ Sv. In the last two years of the simulation experiment strong transport fluctuations at the seasonal time-scale are evident, coinciding with the previously mentioned increasing transport trend through the MZC. In 2006, a maximum westward transport of 77 Sv occurs in March followed by a sharp decline to -2 Sv in July. The large changes evident in the source regions of the Agulhas system in the last two years of the simulation experiment may suggest that large scale changes have occurred in the Indian Ocean gyre circulation affecting these regions (e.g. Palastanga et al., 2006). The weekly fluctuations of the transports, as evident in the standard deviation, may be due to mesoscale variability associated with the retroflecting current south of Madagascar (Siedler et al., 2009). Compared to the MZC, the 5 month running mean transports for the SEMC (dashed line) indicate that there is no well-defined seasonal cycle.

The average diameter of the eddies associated with the retroflection of the SEMC may reach up to 280 km and extend to depths of 380 m in the model. With an eddy drift velocity of 7 km.d^{-1} (0.08 m.s^{-1}), which is appropriate for these latitudes (Chelton et al., 2007), these eddy dimensions correspond to an eddy volume flux of approximately 9 Sv. This value is slightly less than the standard deviation of the

transports across the section south of Madagascar, and adding / subtracting the eddy volume flux from the mean transport fails to reach the transport values of the the 95^{th} and 5^{th} percentiles, suggesting the existence of additional sources of variability.

Considering the circulation pattern during which the transports in the SEMC exceed 60 Sv, strong currents extending southwestward from the southeast tip of Madagascar can be seen (Figure 6.3b). Centred at 43°E, 29°S an anticyclonic eddy possibly shed from the SEMC retroflection is evident. North of this feature, strong westward currents persist and the return flow feeding the South Indian Ocean Countercurrent (SICC; Siedler et al., 2006) is weak, suggesting that most of the flow is westward toward the Agulhas Current. The sum of the transport from the mean flow and the eddy contribution is 54 Sv, while the transport of the 95^{th} percentile is 60 Sv (Table 6.1), leaving a difference of 6 Sv. Considering the local effect of winds, the Ekman transport across the section south of Madagascar, which is 750 km long, is approximately 4 Sv. During the strong westward transports south of Madagascar, positive wind stress curl anomalies with strong westward winds persist in the region, which confirms that the local winds contribute to the overall westward transport toward the Agulhas Current.

Conversely, during periods when the transports are less than 36 Sv (5^{th} percentile), the flow of the SEMC is weaker and there is an absence of eddies in the region. Furthermore, the retroflection south of SEMC is well-defined, and a strong eastward flow feeding the SICC persists, contributing to an overall weaker westward volume transport toward the Agulhas Current. Also, the wind stress curl and the westward winds in the region are weaker when the westward transports are reduced.

Hence, while mesoscale eddies, and the persistence of a well-defined retroflection south of Madagascar dominate the variability of the strength of the westward volume flux feeding the Agulhas Current, the influence of the local winds seems to play a stronger role for the SEMC transport variability compared to the MZC transport variability.

The weekly fluctuations of the transports in the Agulhas Current are nearly an order of magnitude larger than in its source regions. Ranging from about $20 - 120$ Sv, the transport is entirely poleward (Figure 6.2c). Transport pulses, that occur on average 4 times per year, are evident but there is no apparent seasonal signal in the fluctuations (Figure 6.2c, dashed line).

The horizontal diameters of the eddies observed near the Agulhas Current range from $300 - 350$ km, and have depths of $400 - 600$ m (Table 6.1). These dimensions are somewhat larger than the dimensions of the eddies simulated in the source regions. Using eddy drift estimates of $6 - 9$ km.d^{-1} ($0.07 - 0.10$ m.s^{-1}),

the eddy volume flux associated with these eddies is approximately $11 - 16$ Sv, which is significantly lower than the calculated standard deviation of the transports suggesting the existence of additional sources of transport variability.

The 95^{th} percentile transport in the Agulhas Current is 103 Sv (Table 6.1) and the circulation pattern in the region when the transports exceed this value show a very strong Agulhas Current core with an anticyclonic eddy feature located just offshore of the current near the section across which the transports were calculated from the model (Figure 6.3c). The sum of the volume flux in the MZC and SEMC when their respective transports exceed the 95^{th} percentile reaches 88 Sv. Combined with the mean eddy volume flux of 13 Sv, a maximum of 101 Sv is obtained. The agreement of this combination with the magnitude of the 95^{th} percentile transport in the Agulhas Current suggests that the largest transports in the Agulhas Current are reached when the volume fluxes from the Agulhas source regions are at their maximum, and occur simultaneously with the passage of anticyclonic eddies on the ocean side of the current core.

Following the above argument, the sum of the 5^{th} percentile transports in the source regions is 46 Sv, and assuming an absence of eddies, a further 13 Sv may be deducted (Table 6.1). This value amounts to a minimum volume transport in the Agulhas Current of 33 Sv, which is in good agreement with the standard deviation calculated for the section, although it remains significantly higher than the 5^{th} percentile transport of 20 Sv in the Agulhas Current. The circulation pattern during which the transports in the Agulhas Current are less than 20 Sv indicates that in addition to the absence of anticyclonic eddies in the region and a weaker Agulhas Current, a cyclonic circulation feature is located offshore of the Agulhas Current core. This feature imposes weak equatorward currents at the outer edge of the transport section and may account for the remaining 13 Sv difference.

Finally, the wind direction and curl anomalies for periods of strong and weak transports do not show significant differences, and the Ekman transport across the section is comparatively small (Table 6.1). Therefore, these results indicate that the presence or absence of mesoscale eddies in addition to the strength of the volume fluxes from the source regions are the dominant drivers of the transport variability evident in the Agulhas Current.

These results may be somewhat sensitive to the length of the section across which the transports are calculated. Extending the transport section to 34°E, 34°S and performing the same analyses as discussed above yields similar results, with high (low) eddy activity near the current core during transports greater than (smaller than) the 95^{th} (5^{th}) percentile.

At the AR the mean transport is fairly weak while the variability is relatively strong and more complex than upstream in the Agulhas Current as revealed in Figure 6.2d and Figure 6.3d. Stronger westward leakage of the Agulhas Current into the South Atlantic Ocean occurs in association with ring shedding, while periods during which the transports are predominantly eastward returning to the South Indian Ocean implies no leakage. There is no clearly defined seasonal cycle, while a weak bi-annual signal appears to exist (Figure 6.2, dashed line).

Agulhas rings shed from the retroflection loop in the model simulation may have diameters of up to 300 km and extend to depths of 700 m. With a drift velocity of 4 km.d^{-1} (0.05 m.s^{-1}) this corresponds to an eddy volume transport of up to 10 Sv (Table 6.1), which falls within the range of previous eddy volume flux estimates ($3 - 20$ Sv, e.g. Gordon et al., 1992), but is weaker than the calculated standard deviation across the AR transport section (Table 6.1). This suggests that in addition to the shedding of Agulhas rings from the retroflection, a mean flow contributes toward the Agulhas leakage into the South Atlantic Ocean.

The circulation pattern described when the transports across the AR exceed the 95^{th} percentile of 38 Sv (Figure 6.3d) shows that a very large anticyclonic eddy is centred at 18°E, 39°S which has been occluded from the retroflection loop. The sum of the mean and eddy volume transport in the retroflection region is 16 Sv, which is 22 Sv less than the 95^{th} percentile. During the strong leakage into the South Atlantic, a westward current to the north of the the anticyclonic feature is evident. This current crosses the transport section and meanders northwestward into the South Atlantic Ocean. With a width of $\sim$ 150 km, extending to a depth of 1000 m, and a mean depth averaged westward current velocity of 0.1 m.s^{-1}, this current constitutes a volume transport estimate of 15 Sv. Furthermore, during these periods when the transport into the South Atlantic Ocean exceeds the 95^{th} percentile, a positive wind stress curl anomaly together with northeastward winds occurred in the region. Northeastward winds generate a northwestward Ekman transport. As the transport section defined for the AR is approximately 1050 km long, the corresponding Ekman transport across the section is 5 Sv (Table 6.1). The addition of the transport in the northwestward meandering jet as well as the wind induced Ekman transport then constitutes 20 Sv, and together with the mean and eddy contribution approximate the 95^{th} percentile transports. This result indicates that in addition to the eddy volume flux, a northwestward jet as well as local wind induced transports provide important contributions toward the overall westward volume transport into the South Atlantic Ocean.

During periods when the AR transport is less than the 5^{th} percentile of -21 Sv, eastward transports toward

the South Indian Ocean dominate. The corresponding circulation pattern indicates that the anticyclonic feature associated with the retroflection loop has shifted eastward and the northwestward meandering currents to the north of the loop are weaker. Furthermore, the eastward flowing South Atlantic Current south of 40°S, which previously was weak, is much stronger and extends further north. Although weak leakage into the South Atlantic ocean persists, in the form of a northwestward meandering current, the intensification and northward shift of the South Atlantic Current induces a net eastward transport across the selected transport section. This highlights the difficulty of determining the Agulhas leakage into the South Atlantic Ocean from mean circulation patterns. Finally, the wind stress curl anomalies during these periods are weaker and the wind direction is orientated east-southeastward which induces north-northeastward Ekman transport. These conditions combine to reduce the overall eastward transport and in these situations the eddy induced leakage into the South Atlantic Ocean has shut down.

The importance of mesoscale eddies in transport variability has been well documented in the literature (e.g. van Leeuwen et al., 2000; Schouten et al., 2002; Biastoch et al., 2008b). The above analyses quantify the eddy contribution toward the transport variability throughout the greater Agulhas Current regime. In summary, the model simulation indicates that in the MZC, the variability of the transport is dominated by the southward passage of anticyclonic eddies, while south of Madagascar variations in the mean flow, and the presence or absence of a well-defined retroflection are key contributors toward the volume flux reaching the Agulhas Current. In the Agulhas Current, strong poleward transports are frequently associated with eddies. However, variations in the mean flow and their relation to the strength of the transports from the source regions also play an important role. Finally, concerning the volume flux into the South Atlantic via the Agulhas retroflection it was found that a well defined northwestward current as well as Ekman transports contribute towards the westward volume transport in addition to the ring shedding.

6.5 Surface drifter observations

In the previous section the contribution of mesoscale eddies toward the variability of the transports in the different regions of the Agulhas system was analysed and discussed. To validate these findings and characterise the distinctly different flow regimes from an observational perspective, surface drifter data are analysed.

Archived surface drifter data with drogues at 15 m from the Global Drifter Program, formerly World Ocean Circulation experiment Surface Velocity Programme (WOCE-SVP), was made available from the Marine

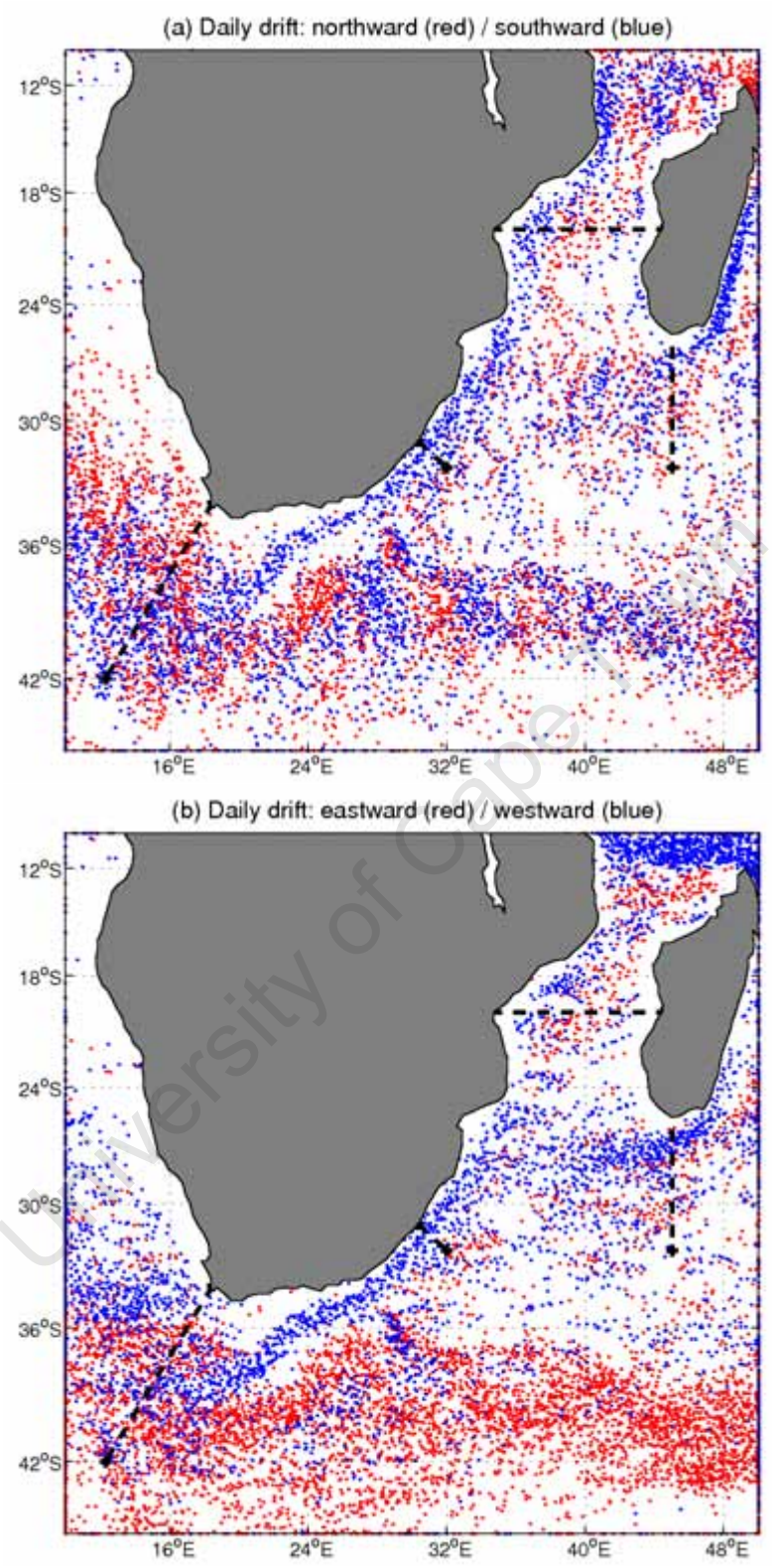

Figure 6.4: Daily average of the (a) meridional and (b) zonal surface drift velocities exceeding 0.4 m.s^{-1}. The drift velocities were calculated from surface drifter observations between 31 December 1995 and 2 January 2007 with drogues at 15 m. Red dots indicate eastward and northward drift, while and blue dots indicate westward and southward drift. The sections across which transports were calculated from the model are indicated by the dashed black lines.

	MZC	SEMC	AC
Total number of drifters	13	32	22 (27)
Number of these in AC / AR	5 (5)	14 (18)	3 (6)
% of total	38 (38)	44 (56)	14 (22)

Table 6.2: Row 1: the total number of drifters observed between 31 December 1995 and 2 January 2007 in the respective sections for the MZC at 20°S, the SEMC at 45°E and the Agulhas Current at 32°S. Row 2: the number of the drifters observed in the MZC and SEMC sections that subsequently reached the Agulhas Current section, and the number of drifters that reached zonal section in the South Atlantic Ocean from the Agulhas Current section (column 3). Row 3: the corresponding percentage of drifters reaching the respective sections. The numbers in brackets are the result of the same analysis with an Agulhas Current section extended to 34°E, 34°S.

and Environmental Data Services at Fisheries & Oceans Canada (`www.meds-sdmm.dfo-mpo.gc.ca`), and data between 31 December 1995 and 2 January 2007 was analysed. Daily average drift velocities were calculated and speeds exceeding 0.4 m.s^{-1} were split into meridional (Figure 6.4a) and zonal (Figure 6.4b) components.

In order to quantify the number of drifters arriving at the Agulhas Current from the MZC and SEMC respectively, only drifters that pass through the MZC or the SEMC sections and subsequently reach the Agulhas Current are taken into account. Similarly, to quantify the number of drifters that crossed the Agulhas Current section and flowed into the South Atlantic Ocean, only the drifters that crossed the zonal section in the South Atlantic Ocean at 36°S were selected. The results are summarised in Table 6.2. The numbers in brackets represent the same statistics calculated for an Agulhas Current section extended to 34°E, 34°S.

In the MZC, the dominance of mesoscale eddies is evident by the fact that a relatively equal number of northward and southward drift observations persist throughout the channel (Figure 6.4a). Predominantly southward currents exceeding 0.4 m.s^{-1} are evident close to the Mozambican coast, while northward currents predominantly occur in the centre of the channel. This result is in agreement with the model simulation which indicates that the transport variability is dominated by eddies that tend to propagate southward along the Mozambican shelf edge.

South of Madagascar, the outflow from the southern extension of the EMC is predominantly westward (Figure 6.4b), with few eastward velocities evident, suggesting, that a mean westward flow dominates. The mean position of the westward flow from the SEMC toward the Agulhas Current at $\sim$ 27°S is also in good agreement with the model. Relatively few eddies are observed in the SEMC drifter data in agreement with the model results. Finally, evidence of anticyclonic eddies with eastward velocities near 31°S associated

with SEMC retroflection eddies and a return flow toward the South Indian Ocean does occur in agreement with Siedler et al. (2009).

In the Agulhas Current, southwestward drift velocities strongly dominate along the southern African coast extending from 27°S to 20°E, 38°S (Figures 6.4a and b). A few northward and eastward drift velocity observations are evident on the ocean side of the current core, indicating the periodic existence of eddies.

Despite the few number of drifters in the MZC, 38% of the drifters crossing the section in the MZC at 20°S are again observed in the Agulhas Current section at 32°S (Table 6.2), and no change in this percentage occurs by extending the length of the Agulhas Current section (Table 6.2). Comparatively, 44% of the drifters observed in the SEMC reach the Agulhas Current, and this percentage increases to 56% by extending the Agulhas Current section to 34°E, 34°S. It should be noted that significantly more drifters were observed in the SEMC between 31 December 1995 and 2 January 2007, which may effect the respective contributions. Nevertheless, the percentage re-occurrence of drifters in the Agulhas Current from the two Agulhas source regions are in rough agreement with the relative contribution estimates from the model transports (Section 6.3).

Further downstream, the retroflection loop is evident in the southward drift velocities between 16° and 20°E (Figure 6.4a) as well as the subsequent eastward flow toward the South Indian Ocean in the Agulhas return current at $\sim$ 40°S (Figure 6.4b). Westward drift toward the AR section is centered at approximately 39°S, in good agreement with the model simulation. In the retroflection region, between 14° and 18°E, an even distribution of northward and southward (eastward and westward) drift is indicative of the complex mesoscale variability that dominates the region. The northwestward meandering current, which in the analysis of the model simulation was suggested to play an important role in the overall leakage into the South Atlantic Ocean cannot be clearly identified. However, northwestward of 16°E, 36°S the surface drifters have predominantly northwestward tendencies, which is in agreement with the model simulation.

Of the drifters observed in the Agulhas Current at 32°S, 14% are observed drifting into the South Atlantic Ocean, crossing a zonal section in the South Atlantic at 36°S. This percentage is enhanced to 22% when the Agulhas Current section is extended to 34°E, 34°S.

Overall, these results validate the flow dynamics described by the model simulation for the different regions of the Agulhas Current system and supports the conclusions drawn from the model simulation in terms of the relative contribution of the mean and eddy flows toward the overall volume transport.

6.6 Correlation to vorticity

The contribution of the eddy volume flux to the overall volume transports throughout the greater Agulhas Current system has been analysed and quantified in Section 6.4 using the HYCOM model, and these results were assessed and validated using surface drifter observations in Section 6.5. In order to quantify the relationship of the weekly transport variability to eddy occurrences, weekly vorticity data from the four major transport sections in the model, estimated from the model current velocities at 10 m and, are analysed and correlated to the weekly model transports (Figure 6.5).

In the MZC, poleward propagating eddies tend to closely follow the continental shelf edge of the Mozambican coast. At 20°S high levels of vorticity associated with these poleward moving eddies are obtained between 37° and 40°E. In the SEMC, the mean vorticity for the section between 26° and 29.5°S was calculated, since this is the region where mesoscale variability predominantly occurs. In the Agulhas Current, only the mean vorticity further than 100 km offshore was estimated, to capture the large anticyclonic eddies propagating southwestward on the ocean side of the Agulhas Current . Finally for the AR, the mean vorticity was estimated from the section bounded by 36° and 42°S. This is where highest eddy kinetic energies are found and may indicate the dominant location for ring shedding into the South Atlantic Ocean.

The vorticity data in the MZC (Figure 6.5a) shows regular oscillations between positive and negative vorticity, suggesting the regular passage of eddies. The mean vorticity for the simulation period is positive suggesting that predominantly anticyclonic eddies occur, which is in agreement with previous model results (Backeberg et al., 2009). The negative vorticities evident in the channel are associated with cyclonic shear near the coast, which persists between the passage of subsequent eddies. The cross-correlation between the transports and vorticities for this zonal section in the MZC indicates that a weak positive correlation ($r = 0.203$) exists between strong poleward transports and positive vorticities at a 3 week lag. The correlation is statistically significant at the 95% confidence level[1], suggesting that strong poleward transports occur prior to an anticyclonic eddy (positive vorticity) crossing the 20°S latitude. Considering the composite current velocities for the MZC (Figure 6.3a), an anticyclonic eddy is located slightly to the north of the section. The lagged correlation is explained by the fact that intense anticyclonic eddies also induce equatorward (reduced poleward) currents with strong northward velocities to the east of the eddy centre. The maximum poleward transport across 20°S therefore occurs when the leading edge of the

[1]Unless otherwise indicated, all correlation coefficients discussed in this chapter are statistically significant at the 95% confidence level

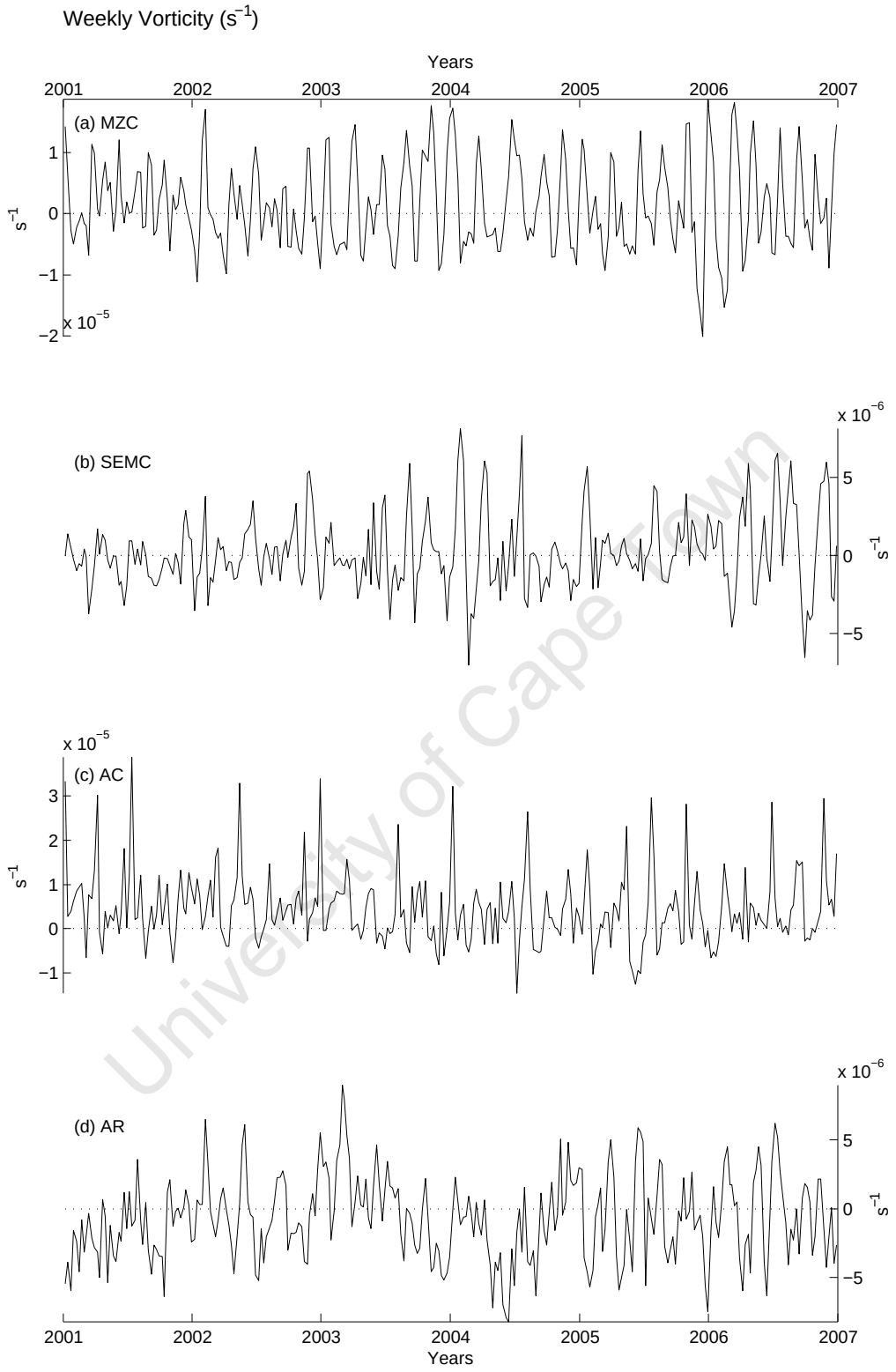

Figure 6.5: Weekly vorticities (s^{-1}) for the corresponding transport sections in (a) the Mozambique Channel at 20°S, (b) south of Madagascar at 45°E, (c) the Agulhas Current at 32°S, and (d) the Agulhas retroflection which represents the Agulhas leakage into the South Atlantic Ocean. The dotted line represents the zero line in each case.

poleward propagating anticyclonic eddy reaches the section.

South of Madagascar (Figure 6.5b), the strength of the vorticities are reduced by a factor of 2 in comparison to the MZC. Moreover, the vorticity variations are less regular than in the channel. These results suggest that the near surface expression of the mesoscale features south of Madagascar are smaller and less intense than in the MZC as also suggested by the dimensions compared in Table 6.1. The previous comparison of the models mesoscale variability to the eddy kinetic energy derived from satellite altimeter measurements furthermore confirms this (Backeberg et al., 2009). A negative correlation between westward transports and vorticities exists, $r = -0.268$. This correlation implies that strong westward transports occur during negative vorticity phases (preference for cyclonic shear), and conversely that weak westward transports are associated with positive vorticity phases (anticyclonic shear). As discussed in Section 6.4, weak westward transports are associated with a well-defined anticyclonic retroflection south of Madagascar that impose eastward return flow toward the Indian Ocean.

In the Agulhas Current the strongest periodically positive (anticyclonic) vorticities are found (Figure 6.5c). The frequency of these occurrences is approximately 5 times per year, which is in good agreement with the documented annual number of Natal Pulses (Lutjeharms and Roberts, 1988). Thus, Natal Pulses appear to often be formed in association with anticyclonic eddies. Anticyclonic eddies from the MZC have previously been observed to trigger Natal Pulses (Schouten et al., 2002). There is a relatively strong correlation of $r = 0.458$ between the transport and vorticity time series in the Agulhas Current. This correlation indicates that strong poleward transports often coincide with positive vorticity features associated with the passage of anticyclonic eddies, and is confirmed by the corresponding mean composite of the current velocities (Figure 6.3c). It should be noted that mesoscale anticyclonic eddies are not the only cause of strong poleward transports in the Agulhas Current core. As discussed previously, strong (weak) poleward transports are also sensitive to strong (weak) transport contributions from the MZC and SEMC.

The lagged cross-correlations of the vorticities near the Agulhas Current with those in the source regions of the MZC and the SEMC ($r_{MZC} = 0.134$, $r_{SEMC} = 0.155$) are weak but statistically significant at time lags corresponding to eddy propagation velocities of $8 - 9$ km.d^{-1}. Such eddy propagation velocities are typical for these latitutudes (Chelton et al., 2007), and eddies have previously been reported to propagate from the MZC and SEMC to the Agulhas Current (e.g. Schouten et al., 2002; Backeberg et al., 2008).

At the Agulhas retroflection, positive vorticity dominates, indicative of Agulhas ring shedding from the retroflection loop, occurring approximately $5 - 6$ times per year. This ring shedding frequency is in good

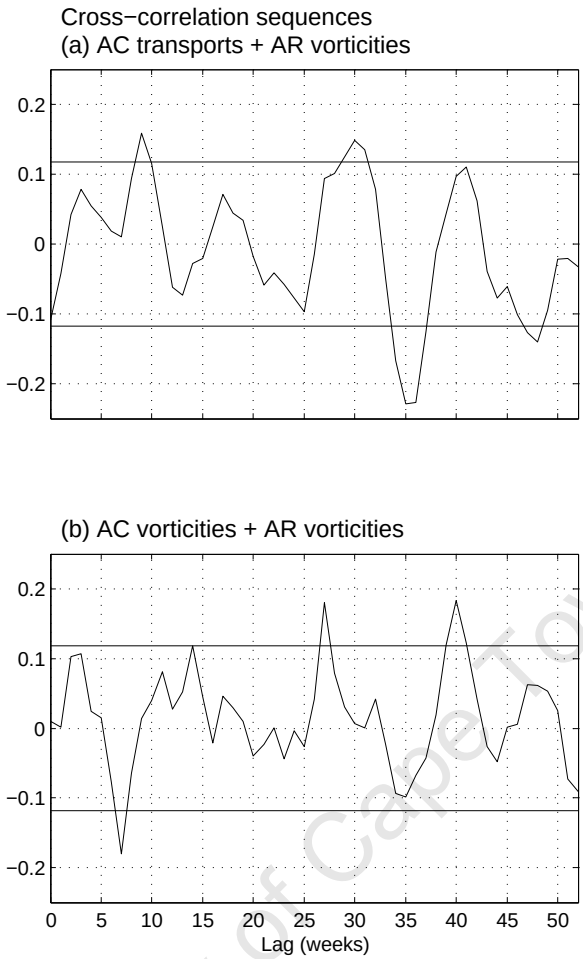

Figure 6.6: Cross-correlation sequences between (a) transports in the Agulhas Current and vorticities at the Agulhas retroflection, and (b) vorticities in the Agulhas Current and vorticities at the Agulhas retroflection.

agreement with the documented average number of Agulhas rings shed from the retroflection each year (Lutjeharms and van Ballegooyen, 1988). The cross-correlation to transports yields a positive correlation ($r = 0.191$) at a 4 week lag. Similarly to the MZC, the lag period indicates that strong westward (positive) transports into the South Atlantic Ocean occur prior to the passage of an anticyclonic eddy (positive vorticity), and is confirmed in the composite circulation map (Figure 6.3d) which shows an anticyclonic eddy located to the east of the section.

In order to relate Agulhas ring shedding to the transports and vorticity features occurring in the Agulhas Current, lagged correlations are calculated (Figure 6.6). The correlation between transports in the Agulhas Current and vorticities at the retroflection (Figure 6.6a) show positive statistically significant peaks at lags of 9 ($r = 0.159$) and 30 ($r = 0.149$) weeks, and a negative peak ($r = -0.229$) at a lag of 35 weeks.

The distance from the Agulhas Current section to the centre of the Agulhas retroflection section is approx-

imately 1650 km. The corresponding propagation velocity associated with this distance and the peak at 9 weeks (Figure 6.6a) is 26 km.d^{-1} (0.3 m.s^{-1}), which suggests that 9 weeks after a strong transport pulse in the Agulhas Current, a westward protrusion of the retroflection occurs, which is usually associated with the shedding of an Agulhas ring (Pichevin et al., 1999).

The second peak at 30 weeks in the transport correlation may be associated with the southwestward propagation of anticyclonic eddies from the Agulhas Current at 32°S to the retroflection. The downstream propagation of eddies is supported by the close agreement of the correlation between vorticities in the Agulhas Current and at the retroflection (Figure 6.6b), which show a positive correlation at a lag of 27 weeks ($r = 0.181$). These lag periods correspond to a feature propagation velocity of $8 - 9$ km.d^{-1} ($0.09 - 0.10$ m.s^{-1}), which agrees well with previous estimates of eddy propagation in the region (Backeberg et al., 2008) as well as the documented propagation velocity of Natal Pulses (Lutjeharms and Roberts, 1988). Hence, both transport pulses and anticyclonic eddies propagating into the Agulhas retroflection region appear to contribute toward the shedding of Agulhas rings, in agreement with previous findings (van Leeuwen et al., 2000; Pichevin et al., 1999).

The negative correlation at a lag of 35 weeks (Figure 6.6a) indicates that negative vorticities occur following the positive correlation at a lag of 30 weeks. Agulhas rings are known to form due to a zonal protrusion of the retroflection loop and the subsequent occlusion of an anticyclonic eddy (Pichevin et al., 1999). Following the occlusion of an Agulhas ring, negative vorticities might occur, which may explain this negative correlation.

Finally the positive correlation ($r = 0.183$) between the vorticities in the Agulhas Current and at the retroflection occuring at a lag of 40 weeks (Figure 6.6b), suggests another westward protrusion of the retroflection loop. This correlation coincides with a weak, and statistically insignificant, correlation ($r = 0.110$) between transports in the Agulhas Current and vorticities at the retroflection at a lag of 41 weeks (Figure 6.6a). The propagation velocity associated with this correlation is about 6 km.d^{-1} (0.07 m.s^{-1}), which is slower but still within the range of the previously documented eddy propagation velocities in the system (Backeberg et al., 2008).

Although mesoscale eddies are not the only source of transport variability in the greater Agulhas Current region, robust and consistent results from the vorticity analysis are obtained. Strong poleward transport pulses in the Agulhas Current are frequently associated with the passage of anticyclonic eddies on the currents ocean side, and lagged cross-correlations indicate that these originate from the source regions in

the Mozambique Channel and south of Madagascar. Further downstream, a westward protrusion of the retroflection loop followed by the possible shedding of an Agulhas ring seems to be related to the arrival of strong transport pulses and mesoscale eddies from the northern Agulhas Current region. This connection will be analysed in further detail in Section 6.7.

6.7 Downstream effect of strong transports in the Agulhas Current

To further investigate the westward protrusion of the retroflection and eventual ring shedding in relation to the upstream condition of the Agulhas Current, composite maps of current and vorticity fields from the model output at 10 m were produced and analysed (Figure 6.7). Weekly transports in the Agulhas Current at 32°S, exceeding the 95^{th} percentile were selected to estimate the composite of the mean circulation and associated vorticity fields in the Agulhas Current and the retroflection region, hereafter referred to as T_{+0} (Figure 6.7a). Following this, composite maps of the weeks following T_{+0} were calculated for T_{+9}, T_{+15}, T_{+23}, T_{+29}, and T_{+37} weeks (Figures 6.7b−f). These represent the composite mean circulation in the region 9, 15, 23, 29, and 37 weeks after the strong transports in the Agulhas Current at 32°S. The composite maps are based on an average of 9 events that occur over a 6 year period (Figure 6.2), which is likely not enough to obtain a statistically significant estimate of the mean circulation during high transport events. However, the composite maps provide an indication that maximum poleward transports in the Agulhas Current are (at least partially) associated with the occurrence of anticyclonic eddies on the ocean side of the current core.

At T_{+0} (Figure 6.7a) a strong anticyclonic eddy, with high positive vorticities, is associated with the strong poleward transports in the Agulhas Current core at 32°S. Another strong anticyclonic eddy is located near 30°E, 36°S northeast of the relatively shallow Agulhas Plateau (outlined by the 4000 m isobath), and at the northwestern edge of the plateau at 25°E, 37°S a further anticyclonic feature is evident. Some of the flow from the Agulhas Current appears to retroflect "early" in association with this latter feature, returning eastward. The core of the Agulhas Current, however, closely follows the 1000 m isobath southwestward until it reaches the southern tip of the Agulhas Bank at 21°E, 37°S, where it continues westward and splits into a northwestward flowing current, that approximately follows the 4000 m isobath into the South Atlantic, and the anticyclonic retroflection loop clearly centred at 18°E, 40°S.

The retroflection seems to be in the process of detaching from the Agulhas Current, forming a large Agulhas ring, however strong east-northeastward currents returning toward the South Indian Ocean remain evident.

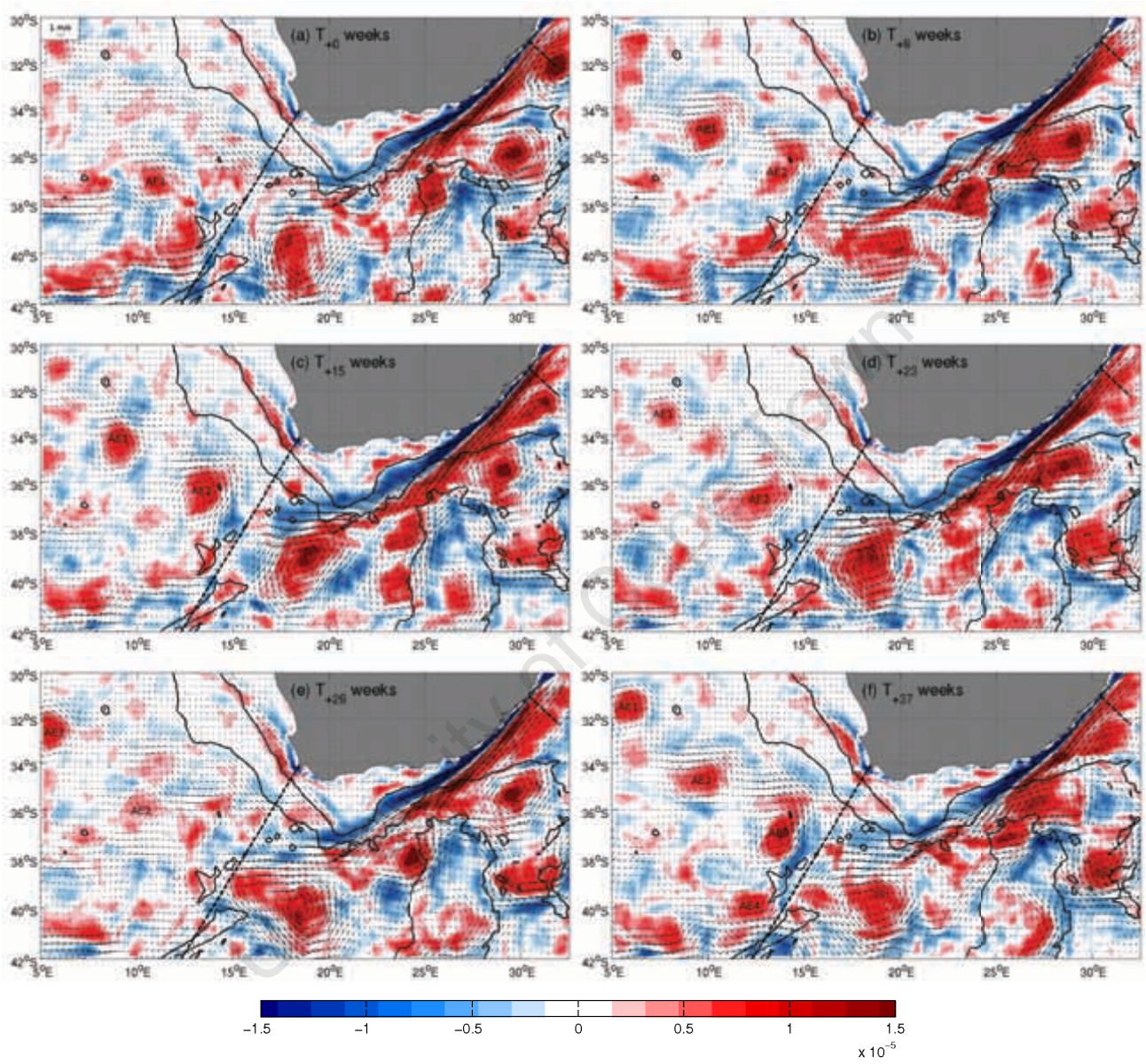

Figure 6.7: Composite maps of current velocities (m.s ^{1}) and vorticities (s ^{1}) at T_{+0} (a) when the Agulhas Current transports at 32°S exceed the 95^{th} percentile. Composite maps of weeks $T_{+9,+15,+23,+29,+37}$ following T_{+0} are provided as b f, respectively. The black dashed line in (a) indicates the section in the Agulhas Current across which transports from HYCOM were calculated, and the black dashed line in (b) and (e) is the section across which transports for the Agulhas retroflection were calculated. The 1000 and 4000 m isobaths of the model bathymetry (GEBCO) are also plotted.

Note that the retroflection loop lies to the east of shallow bathymetric features, namely the Agulhas Ridge (2000 m) and the Schmitt-Ott and Erica Sea-mounts (1300 m). At T_{+0} an anticyclonic eddy (hereafter referred to as AE_1) with positive vorticity is also found at 12°E, 37°S. Its horizontal diameter is approximately 250 km, and it extends to a depth of 700 m. Assuming a drift velocity of 4 km.d^{-1} (0.05 m.s^{-1}), the corresponding volume transport associated with AE_1 is approximately 8 Sv.

In the nine weeks following the strong transport pulse in the Agulhas Current core (Figure 6.7b, T_{+9}), the anticyclonic eddy which initially caused the transport pulse has propagated southwestward and subsequently become integrated in the Agulhas Current. The strong anticyclonic eddy, which was previously "trapped" northeast of the Agulhas Plateau has shifted west-northwestward to 28°E, 35°S and is gradually stretched into the narrow gap between the northern edge of the Agulhas Plateau and the South African continental shelf. It is unclear whether this west-northwestward shift and stretching of the "trapped" eddy is due to the merging of the upstream eddy with the current core, or if it is due to the "trapped" eddy's westward self-propagation, perhaps a combination of the two. However, the corresponding downstream propagation velocity of eddies from the Agulhas Current section at 32°S to 28°E, 35°S in nine weeks is 8 km.d^{-1} (0.09 m.s^{-1}), which is in good agreement with previous estimates (Backeberg et al., 2008), suggesting that the downstream propagating feature does play a role in the westward migration of the "trapped" eddy.

The anticyclonic feature at the northwestern edge of the Agulhas Plateau has shifted to 24°E, 38°S and intensified forming an anticyclonic eddy, which continues to cause some of the flow from the Agulhas Current to retroflect "early" and return east-northeastward.

The anticyclonic retroflection loop at T_{+9} has not been able to fully detach and move westwards away from the Agulhas Current. This is likely due to the blockage by the shallow Agulhas Ridge and the Schmitt-Ott and Erica Sea-mounts. Instead, at T_{+9} the retroflection loop has protruded slightly westward extending across the AR transport section. It has also moved slightly northward, avoiding the shallow Agulhas Ridge. The positive vorticity associated with this protrusion may be interpreted to explain the correlation at 9 weeks lag between Agulhas Current transports at 32°S and vorticities at the retroflection as discussed previously (Figure 6.6a). However, since it is difficult to adequately track the transport pulse from 32°S to the retroflection and explicitly attribute the westward protrusion to the transport pulse without the use of tracers, this assumption remains uncertain.

A second anticyclonic eddy (AE_2) at 14°E, 37°S has also formed at T_{+9}. Its diameter is up to 300 km

wide, and with a depth of 700 m, the corresponding volume transport reaches 10 Sv associated with a drift of 4 km.d^{-1} (0.05 m.s^{-1}). In the meantime AE_1 has drifted to 10°E, 35°S, a distance of about 290 km, which corresponds to an eddy drift velocity of $4 - 5$ km.d^{-1} ($0.05 - 0.06$ m.s^{-1}), in good agreement with Olson and Evans (1986).

At T_{+15} (Figure 6.7c), another anticyclonic eddy occurs on the ocean side of the Agulhas Current core at 31°E, 33°S, while the "trapped" eddy northeast of the Agulhas Plateau at 28°E, 35°S continues to persist. Westward of the Agulhas Plateau a northward elongated positive vorticity feature has formed between 37° and 41°S centered at about 24°E. Its origin is not fully understood, however, it may partly result from the upstream eddy being pushed through the narrow gap between the northern edge of the Agulhas Plateau and the continental shelf.

The positive vorticities associated with the Agulhas retroflection loop at 18°E, 37°S have intensified at T_{+15}, and a negative vorticity feature has intruded near 22°E, 40°S, initiating a stronger occlusion of the retroflection loop than previously noticed. The anticyclonic eddies AE_1 and AE_2 have respectively propagated 180 km and 100 km further into the South Atlantic, corresponding to eddy drift velocities of 4 and 3 km.d^{-1} (i.e. 0.05 and 0.03 m.s^{-1}). While no new eddies were shed in the weeks following T_{+9}, AE_2 in particular has intensified during the 6 week period up to T_{+15}.

In the weeks up to T_{+23}, the anticyclonic eddy near the Agulhas Current core at 31°E, 33°S at T_{+15}, has dissipated and merged with the current, while another anticyclonic eddy has propagated into the region offshore of the current core at 32°S. The "trapped" anticyclonic eddy northeast of the Agulhas Plateau again stretches toward the narrow gap between the plateau and the continental shelf. The reason for this periodic westward stretching and its relation to the integration of anticyclonic eddies upstream in the Agulhas Current remains unclear.

West of the Agulhas Plateau, another north-south elongated positive vorticity feature has replaced the one that was located there at T_{+15}. The latter has propagated westward and merged with the closed Agulhas retroflection loop causing it to intensify. In the eight weeks since T_{+15}, the occluded Agulhas retroflection loop has again not been able to leave the area due to the presence of the shallow bathymetric features to the west. However at this stage the retroflection loop has fully detached from the Agulhas return current, and its orbital velocities have intensified.

AE_1 has drifted 230 km northward at a speed of 4 km.d^{-1} (0.05 m.s^{-1}) and weakened, while AE_2 has remained more stationary, only drifting 70 km at a speed of 1 km.d^{-1} (0.01 m.s^{-1}) in eight weeks. The

reason for the relatively slow drift of AE_2 is unclear.

At T_{+29} (Figure 6.7e) the anticyclonic eddy previously near the Agulhas Current core at 32°S has again dissipated and merged with the current. The "trapped" anticyclonic eddy has shifted eastward to 29°E, 35°S, while another positive vorticity feature has replaced the feature previously observed to the west of the Agulhas Plateau, which has propagated westward and merged with the occluded retroflection loop in the 6 weeks following T_{+23}.

At this stage, the Agulhas retroflection again protrudes westward. The positive vorticities corresponding to this westward protrusion across the AR transport section are evident, which is consistent with the positive correlations to transports and vorticities in the Agulhas Current at 32°S discussed previously (Figure 6.6). Similarly to the westward protrusion of the retroflection at T_{+9}, the loop seems to avoid the Agulhas Ridge. The currents and vorticities associated with this protrusion are moreover stronger at T_{+29} than at T_{+9}. As with the westward protrusion of the retroflection loop at T_{+9}, it is not possible to explicitly attribute its westward migration to the arrival of a specific eddy from the upstream regions. The dynamics in the southern Agulhas Current are far to complex, and in order to explicitly track eddies in the region tracers (e.g. Garraffo et al., 2001a,b) should be used.

AE_1 has strengthened slightly and drifted 140 km to the west, which corresponds to a speed of 4 km.d^{-1} (0.05 m.s^{-1}). AE_2, on the other hand, has clearly weakened and gradually dispersed.

Finally at T_{+37} (Figure 6.7f), another anticyclonic eddy is located on the ocean side of the Agulhas Current core at approximately 31°E, 33°S, and the "trapped" eddy upstream of the Agulhas Plateau, is again in the process of stretching through the narrow gap between the northern edge of the plateau and the continental shelf. The strong positive vorticities associated with the Agulhas retroflection loop, have returned eastward following the westward protrusion at T_{+29}, although weaker positive vorticities persist to the east of the AR transport section. At T_{+39} these positive vorticities cross the AR transport section consistent with the positive correlation at a lag of 40 weeks (Figure 6.6). Note also the negative vorticities that occur to the west of the AR section, which is consistent with the negative correlation at a lag of 35 weeks (Figure 6.6a), associated with the occlusion of an anticyclonic eddy from the retroflection loop (Pichevin et al., 1999).

Finally since T_{+29}, AE_1 has moved 220 km northward to 6°E, 31°S, while AE_2 has drifted 140 km northwestward to 9°E, 35°S and intensified. The corresponding speeds of the two eddies are 4 km.d^{-1} and 2.5 km.d^{-1} (i.e. 0.05 and 0.03 m.s^{-1}) respectively. Following the westward protrusion of the retroflection

loop at T_{+29}, two more eddies (AE_3 and AE_4) have subsequently formed northwest and west of the Schmitt-Ott and Erica Sea-mounts at 14°E, 37°S (AE_3) and at 12°E, 40°S (AE_4). Their diameters are 200 and 330 km respectively and they extend to depths of 700 m. With a mean drift velocity of 4 km.d^{-1} (0.05 m.s^{-1}) the corresponding eddy volume flux is $8 - 10$ Sv.

While this composite analysis does not explain the mechanism of eddy formation at the retroflection, it seems reasonable to conclude that the eddy formation process in our model simulation is related to a westward protrusion of the retroflection loop. Additionally, the shallow bathymetric features, namely the Agulhas Ridge and the Schmitt-Ott and Erica Sea-mounts, also seem to play an important role. They force the retroflection loop to remain east of 15°E, even when it closes upon itself occluding a very large anticyclonic eddy, which would otherwise propagate westward. As a result of the interference from these relatively shallow bathymetric features, the westward propagating eddies drifting into the South Atlantic are somewhat smaller in diameter than the retroflection loop.

In total during the 37 weeks following strong transports in the Agulhas Current core, four eddies were shed from the retroflection. In contrast, the composite analysis of the characteristic circulation pattern for transports that were lower than the 5^{th} percentile at T_{+0} indicates that only two eddies were shed from the retroflection in 37 weeks following weak transports in the Agulhas Current core. This result is in agreement with the theory, that strong transports in the Agulhas Current core increase the eddy volume flux into the South Atlantic Ocean (Pichevin et al., 1999; Rouault et al., 2009). While this analyses do not explicitly attribute the shedding of Agulhas rings to the arrival of transport pulses or mesoscale eddies at the retroflection from the upstream regions, the correlation of Agulhas Current transports to westward protrusions of the retroflection at lag periods of 9 and 37 (and 40) weeks is reflected in the composite analysis. These results suggest that the strength of the Agulhas Current influences the number of eddies shed from the retroflection and hence the leakage into the South Atlantic Ocean. While the above discussion of the dynamics at the Agulhas retroflection mainly focuses on the evolution of anticyclonic eddies, a persistent northwestward current flowing into the South Atlantic Ocean exists with varying degrees of strength during the 37 weeks of the composite analysis. The contribution of this northwestward flowing current appears to play a comparative role in the overall volume transport into the South Atlantic Ocean in addition to the ring shedding.

6.8 Summary and conclusion

From a hind-cast simulation experiment with an eddy-resolving $^1/_{10}{}^{th}$ of a degree regional Hybrid Coordinate Ocean Model, the volume transports in the greater Agulhas Current system were analysed and their relation to mesoscale variability quantified.

Four regions were selected, namely the Mozambique Channel, the southern extension of the East Madagascar Current, the Agulhas Current and the leakage into the South Atlantic via the Agulhas retroflection. The respective mean transports extracted from the model for these sections are in good agreement with previously reported observations and findings. Moreover, a comparison of the general model derived flow dynamics to surface drifter observations yields good results and reinforces the model simulation.

It was found that the variations of the transports through the Mozambique Channel are predominantly related to the presence or absence of eddies, while south of Madagascar the overall westward transport variability is determined by the strength of the retroflection of the southern extension of the East Madagascar Current in addition to the contribution from eddies.

Moreover, the poleward flow through the Mozambique Channel and the westward volume flux south of Madagascar play important roles for the transport variations in the Agulhas Current. Highest poleward transports of 103 Sv in the model simulation of the Agulhas Current occur when the volume transport contribution from the respective source regions are at their maximum (MZC: 28 Sv + SEMC: 60 Sv), in combination with the contribution from southwestward propagating anticyclonic eddies on the ocean side of the Agulhas Current core (13 Sv). These anticyclonic eddies may originate from either the Mozambique Channel or from south of Madagascar, and constitute 22% (12%) of the mean (maximum) transport of the Agulhas Current .

Further downstream, the model simulation indicates that the maximum leakage into the South Atlantic Ocean reaches 38 Sv and is a combination of the mean westward transport (6 Sv), the eddy volume flux ($8 - 10$ Sv), a well defined northwestward current (15 Sv) and wind driven Ekman transports (5 Sv). The eddy volume flux in the retroflection region is therefore up to 160% of the mean, and during maximum leakage Agulhas rings may constitute 26% of the total westward volume transport into the South Atlantic Ocean.

Furthermore, a cross-correlation of the transports and vorticities in the Agulhas Current at 32°S with the vorticities at the Agulhas retroflection indicates statistically significant correlations at lags of 9 and

37 weeks. An analysis of the currents and vorticity fields following periods of strong transports in the Agulhas Current confirms that westward protrusions of the retroflection loop, which may be associated with the shedding of Agulhas rings, occur at these lag periods. Moreover, the results suggest that the number of eddies shed from the retroflection is sensitive to the strength of the Agulhas Current, with more eddies propagating into the South Atlantic following periods of strong transports in the Agulhas Current compared to periods of weak transports. The sensitivity of the eddy volume flux demonstrated in this study, is in agreement with the theory (Pichevin et al., 1999) as well as a recent study combining observations with a regional eddy-permitting model simulation of the region (Rouault et al., 2009).

In conclusion, this study quantifies the contribution of mesoscale eddies in the transport variations of the greater Agulhas Current system. It was shown that the strength of the Indo-Atlantic inter-ocean exchange, as well as the number of eddies shed from the retroflection is sensitive to the strength of the Agulhas Current. In turn, the Agulhas Current is influenced by the flow dynamics in the Mozambique Channel and south of Madagascar, suggesting a more direct link to the large-scale variability in the Indian Ocean. Due to the complexity of the currents in the retroflection region and the intense mesoscale eddies, it is challenging to undertake measurements of the circulation patterns and inter-ocean fluxes. Moreover, while along-track satellite altimetry data, of the Jason-type 10-day repeat cycle, are well-suited for monitoring variability at periods longer than $\sim$ 70 days, in the greater Agulhas Current system, these data do not capture the high frequency variability in the Agulhas Current before it separates from the continent (Byrne and McClean, 2008). Adequate quantitative understanding of the complicated dynamics in this region is consequently incomplete, which motivates for further development of realistic model simulations.

Chapter 7

Discussion and conclusion

7.1 Summary

This thesis consists of four major chapters in which the Hybrid Coordinate Ocean Model of the Agulhas Current is implemented and an advances numerical advection scheme is tested and thoroughly evaluated. Moreover, the model output is applied to advancing the understanding of the mesoscale dynamics and eddy evolving processes in the greater Agulhas Current region.

In Chapter 3, the Hybrid Coordinate Ocean Model was set up in a nested configuration for the greater Agulhas Current system and an 11 year simulation experiment was performed for January 1996 to December 2006 forcing conditions. The results demonstrate that HYCOM is able to represent the general circulation patterns and their characteristic spatial and temporal variability reasonably well. Some deficiencies are noted, which include a train of eddies extending from the Agulhas Plateau to the retroflection rather than a well-defined meandering current, and exaggerated spatial scales of Agulhas Rings that display a too narrow drift pathway into the ring shedding corridor in the Southeast Atlantic Ocean. A space-time analysis provided a quantitative means of validating the model fields, and in addition to confirming the model's capacity to adequately represent the spatial and temporal scales of the region, it was found that anticyclonic eddies occur in the Mozambique Channel approximately $5-6$ times per year. Both the model as well as sea level anomaly observations from satellite altimeter measurements indicate that these eddies drift southwards and merge with the offshore side of the northern Agulhas Current. Approximately 70% of the Mozambique Channel eddies track southwestward to the southern Agulhas Current, and ultimately nearly $2/3$ of these appear at the Agulhas retroflection where they contribute towards the mesoscale vari-

ability and ring shedding. Agulhas ring shedding events are found to occur at a frequency of 5 times per year, and in comparison the model indicates a ring shedding frequency of $3-4$ times per year. The Indo-Atlantic inter-ocean exchange occurs predominantly via the shedding of Agulhas rings. These results highlight the importance of accurately simulating the variability at the retroflection, together with the upstream processes, to which the ring shedding is sensitive.

While it was shown that HYCOM, provided an adequate representation of the general circulation and mesoscale variability of the greater Agulhas Current system when a second order momentum advection scheme was used, some inaccuracies were recognised in Chapter 3. Notably, a train of eddies extended from the Agulhas Plateau to the retroflection, instead of a well-defined current core. This deficiency has significant implications for the simulation of the Agulhas leakage into the South Atlantic Ocean.

With the goal of improving the model simulation, in Chapter 4 a 4^{th} order momentum advection scheme was implemented and a second simulation experiment was run, using the same horizontal and lateral boundary conditions as in first simulation. To objectively quantify the inter-comparison of the two simulation experiments, skewness and spatial variograms were applied, and using these statistical measures the simulation experiments were compared to satellite altimetry measurements. Although these statistical tools are very simple and classical, their use in oceanography is still rare. It was found that sea level skewness is an ideal tool for studying flows with meanders that become unstable and change into eddies. In an eddy field, it is able to distinguish between a preference for cyclonic or anticyclonic rotation, and the zero skewness identifies the mean position of meandering currents. The variogram analysis, provided a quantitative tool for comparing and validating the spatial scales of ocean features simulated in the two model simulations. Additionally, it was able to identify (unrealistic) periodic signals in the simulation of Mozambique Channel eddies. Using these statistical tools, it was shown that applying a higher order momentum advection scheme significantly improved the model simulation of the greater Agulhas Current regime. The most significant improvement noted is the change in the southern Agulhas Current, from a train of successive eddies, to a well-defined meandering current. Stronger poleward transports and a much improved vertical structure of the Agulhas Current near 32°S is evident. These improvements may contribute toward a better southwestward penetration of the temperature field, and implies a stronger leakage of warm, saline Indian Ocean water into the South Atlantic Ocean, vital for the Meridional Overturning Circulation. Chapter 4 concludes that HYCOM, using a 4^{th} order momentum advection scheme, is well suited for further studies of the mesoscale dynamics in the greater Agulhas Current region as well as the Indo-Atlantic inter-ocean exchange.

In Chapters 3 and 4, the HYCOM simulation of the greater Agulhas Current system is thoroughly evaluated and then improved by applying advances in numerical algorithms. In Chapter 5 the formation mechanism of Mozambique Channel Eddies is addressed. Output from the improved model simulation, using the 4^{th} order momentum advection scheme, is combined with geostrophic current observations derived from satellite altimeter measurements to investigate the eddy formation process in the Mozambique Channel and its connection to the South Equatorial Current north of Madagascar. Both the model and altimeter data indicate that positive vorticity features enter the Mozambique Channel, and that these are associated with transport fluctuations of the South Equatorial Current at both mesoscale and seasonal time-scales. The model simulation indicates that eddies form in the narrows of the channel approximately 20 weeks following a vorticity anomaly occurring north of Madagascar that is associated with a strong westward transport pulse in the South Equatorial Current. Through this mechanism, seasonal and interannual signals associated with large-scale changes in the gyre circulation of South Indian Ocean may enter the channel and modulate the eddy formation frequency. Previously, Mozambique Channel eddies have been implicated in generating disturbances in the Agulhas Current that affect the Indo-Atlantic inter-ocean exchange. A connection between Mozambique Channel eddies and the large-scale variability of the South Indian Ocean is significant, because it suggests that, ultimately, variability in the Agulhas system and the inter-ocean leakage is driven by changes in the gyre circulation of the Indian Ocean, which in turn may be related to interannual climate modes such as the Indian Ocean Dipole and the El Niño Southern Oscillation.

In the final chapter of this thesis (Chapter 6), the model output from the simulation using the 4^{th} order momentum advection scheme is used to investigate the mesoscale transport variability in the source regions of the Agulhas Current, the Agulhas Current core and in the retroflection region. It was found that the variations of the transport through the Mozambique Channel are predominantly related to the passage of mesoscale eddies, and south of Madagascar, the overall westward transports are dominated by the strength of the retroflection of the southern extension of the East Madagascar Current in addition to the contribution from eddies. The contribution from eddies in the Mozambique Channel, as well as variations in the mean westward flow south of Madagascar, play important roles in determining the overall poleward volume flux in the Agulhas Current at 32°S. Maximum poleward transports in the Agulhas Current are reached when the volume transport contribution from the respective source regions are at their maximum, in addition to the presence of anticyclonic eddies on the ocean side of the current core. Furthermore, these mesoscale eddies originate from either the Mozambique Channel or from south of Madagascar. The

resulting strong transports in the Agulhas Current at 32°S are subsequently shown to be correlated with westward protrusions of the Agulhas retroflection loop, and possible Agulhas ring shedding, at lag periods of 9 and 37 weeks. A composite analysis of the currents and vorticity fields following periods of strong transports in the Agulhas Current confirms that westward protrusions of the retroflection loop occur at these lag periods. Moreover, this analysis suggests that the number of eddies shed from the retroflection is sensitive to the strength of the Agulhas Current, with more eddies propagating into the South Atlantic following periods of strong transports in the Agulhas Current compared to periods of weak transports. Finally, the model simulation indicates that the maximum leakage of warm, saline water into the South Atlantic Ocean may reach up to 38 Sv, and the estimated contribution from Agulhas rings is significant, since at $8 - 10$ Sv each ring constitutes up to 26% of the overall westward transport. In conclusion, this study quantifies the contribution of mesoscale eddies in the transport variations of the greater Agulhas Current system, and shows that the strength of the Indo-Atlantic inter-ocean exchange, as well as the number of eddies shed from the retroflection, is sensitive to the strength of the Agulhas Current. In turn, the Agulhas Current transport is influenced by the flow dynamics in the Mozambique Channel and south of Madagascar, providing a link to large-scale variability in the Indian Ocean.

7.2 Major findings

The four major chapters presented in this thesis document the capability of HYCOM with a horizontal resolution of $1/10^{th}$ of a degree to simulate the greater Agulhas Current region. It is demonstrated that applying the model output in combination with remote sensing and *in-situ* observations advances the understanding of the mesoscale dynamics and eddy evolving processes in the region. The major findings of this work are both methodological and oceanographic in nature, since this work comprises a combination of ocean model development and validation together with oceanographic application.

Methodology

The application of a 4^{th} order momentum advection scheme was found to significantly improve the model simulation of the region. In particular, overall stronger poleward transports and a much improved vertical structure of the Agulhas Current near 32°S are evident. These improvements contribute toward a better representation of the southern Agulhas Current, as a well-defined meandering current, rather than a train

of successive eddies. These enhancements of the simulation are considered to be a vital part of the model's suitability for further studies of the Agulhas leakage.

The statistical measures used to quantify the above enhancements are simple and classical, yet their use in oceanographic applications and in particular model validation remain rare. It was found that these measures are useful techniques for model validation as well as providing new perspectives in terms of studying mesoscale variability in the ocean. The skewness analysis of sea surface height data was shown to be an ideal tool for studying flows with meanders that become unstable and change into eddies. Furthermore, in an eddy field, sea level skewness is able to distinguish between a preference for cyclonic or anticyclonic rotation. The variogram analysis is a simple and robust technique, which is able to quantify the variances and spatial scales of mesoscale features in the ocean.

Oceanographic application

Eddy formation in the Mozambique Channel was found to be related to the South Equatorial Current north of Madagascar. These cause positive vorticity anomalies to enter the channel which then contribute toward the formation of anticyclonic eddies in the narrows of the channel. This mechanism suggests that the formation of the eddies is connected to large-scale changes in the gyre circulation of the Indian Ocean, which can be related to interannual climate modes such as the Indian Ocean Dipole and the El Niño Southern Oscillation.

Mozambique Channel eddies are shown to occur $5-6$ times per year, and approximately 70% of the eddies drift southward to merge with the offshore edge of the northern Agulhas Current. Furthermore, maximum poleward transports in the Agulhas Current core occur during such mergers of anticyclonic eddies if the volume flux contribution from the Mozambique Channel and from south of Madagascar are at their respective maximum. Note that anticyclonic eddies may originate from either the Mozambique Channel or south of Madagascar.

Approximately $^2/_3$ of the eddies formed in the Mozambique Channel are shown to propagate into the Agulhas retroflection region where they contribute toward the overall mesoscale variability and ring shedding processes there. The shedding of Agulhas rings from the retroflection is thought to be the predominant mechanism through which the Indo-Atlantic inter-ocean exchange occurs. Analyses of the HYCOM simulation indicates that Agulhas rings contribute up to 26% toward the overall volume transport into the South Atlantic Ocean, when the Agulhas leakage is at its maximum. Finally, the Indo-Atlantic inter-ocean

exchange, and the shedding of Agulhas rings from the retroflection, is shown to be sensitive to the strength of the Agulhas Current, which in turn is influenced by the flow dynamics in the Mozambique Channel and south of Madagascar, providing a link to large-scale variability in the Indian Ocean.

7.3 Future work

Model development and improvements are advancing at an enormous rate. At the time of implementation in this thesis, version 2.1 of the HYCOM code was used. A newer version of HYCOM (v2.2) is now available, which incorporates all the latest enhancements from the community, which may provide an improved simulation of the region. The lateral boundary conditions provided by the basin-scale model of the Indian and Southern Ocean have a horizontal resolution of $30 - 40$ km in the greater Agulhas Current region. Currently, a $1/12^{th}$ of a degree global HYCOM is available (Hurlburt et al., 2008), which also includes data assimilation, and it may provide improved lateral boundary conditions for the regional model. Furthermore, in the model simulation presented in this thesis, river run-off from the African continent as well as tidal forcing were excluded. Both these factors may influence the model's representation of the Agulhas Current system and their inclusion needs to be tested, in particular for an operational system. Improved representation of river fluxes in the model has become available, in which river run-off from a hydrological model (TRIP; Oki and Sud, 1998) and ECMWF data are combined. Finally, advances in data assimilation techniques (e.g. Counillon and Bertino, 2008) and the consistent availability of data especially from satellite remote sensing platforms may significantly increase the realism of the model simulations of the region. Data assimilation techniques should be implemented, and are in fact a necessity for an operational system to provide useful information on the state of the ocean.

From the perspective of advancing the oceanographic understanding in the greater Agulhas Current region, the importance of mesoscale variability and a connection to the large-scale variability of the Indian Ocean has been documented here. The proposed formation mechanism of Mozambique Channel eddies needs to be analysed in detail with respect to the eddy physics. Further work may include investigating baroclinic, barotropic or mixed baroclinic-barotropic instabilities in idealised simulation experiments. To further quantify the interactions between the Agulhas Current and mesoscale eddies originating in the Mozambique Channel and south of Madagascar, simulated drifters should be implemented in the model. Furthermore the strength of the mesoscale signals throughout the greater Agulhas Current regime make it an attractive region in which to test and apply eddy tracking programs (e.g. Hodges, 1994; Chelton et al., 2007).

Such tools would also provide important contributions toward validating model simulations of mesoscale variability, and may provide more quantitative information on the contribution from eddies in particular for the Agulhas leakage.

The Indo-Atlantic inter-ocean exchange of warm and saline water south of Africa is considered to be an important component of the Atlantic meridional overturning circulation, which plays a key role in maintaining the thermohaline circulation of the ocean (Gordon et al., 1992). Furthermore, the associated ocean-atmosphere interactions may have significant impacts on regional and global climate (Reason, 2001; Peeters et al., 2004). High resolution models combined with satellite and *in-situ* measurement programmes will play an integral role towards realising a quantitative understanding of the importance of the Agulhas leakage for the thermohaline circulation and for climate.

Bibliography

Backeberg, B. C. (2006). Mesoscale variability study of the agulhas current from satellite radar altimetry and a high resolution model. Master's thesis, University of Bergen, Norway. Affiliation: Mohn-Sverdrup Center.

Backeberg, B. C., Bertino, L., and Johannessen, J. A. (2009). Evaluating two numerical advection schemes in HYCOM for eddy-resolving modelling of the Agulhas Current. *Ocean Sci.*, 5(2):173–190.

Backeberg, B. C., Johannessen, J. A., Bertino, L., and Reason, C. J. C. (2008). The greater Agulhas Current system: An integrated study of its mesoscale variability. *J. Op. Oceanogr.*, 1(1):29–44.

Backeberg, B. C. and Reason, C. J. C. (2010). A connection between the South Equatorial Current north of Madagascar and Mozambique Channel Eddies. *Geophys. Res. Lett.*, 37(L04604).

Barnier, B., Madec, M., Pendruff, T., Molines, J.-M., Treguier, A. M., Sommer, J. L., Beckmann, A., Biastoch, A., Bönning, C., Dengg, J., Derval, C., Durand, E., Gulev, S., Remy, E., Talandier, C., Theetten, S., Maltrud, M. E., McClean, J., and de Cuevas, B. A. (2006). Impact of partial steps and momentum advection schemes in a global ocean circulation model at eddy permitting resolution. *Ocean Dyn.*, 56(5-6):543–567.

Bentsen, M., Evensen, G., Drange, H., and Jenkins, A. D. (1999). Coordinate transformation on a sphere using conformal mapping. *Mon. Wea. Rev.*, 127:2733–2740.

Biastoch, A., Böning, C. W., and Lutjeharms, J. R. E. (2008a). Agulhas leakage dynamics affects decadal variability in Atlantic overturning circulation. *Nature*, 456:489–492.

Biastoch, A. and Krauss, W. (1999). The role of mesoscale eddies in the source regions of the Agulhas Current. *J. Phys. Oceanogr.*, 29:2303–2317.

Biastoch, A., Lutjeharms, J. R. E., Böning, C. W., and Scheinert, M. (2008b). Mesoscale perturbations control inter-ocean exchange south of Africa. *Geophys. Res. Lett.*, 35(L20602).

Biastoch, A., Reason, C. J. C., Lutjeharms, J. R. E., and Boebel, O. (1999). The importance of the Mozambique Channel for the seasonality of the Agulhas Current. *Geophys. Res. Lett.*, 26:3321–3324.

Bleck, R. (2002). An oceanic general circulation model framed in hybrid isopycnic-Cartesian coordinates. *Ocean Modell.*, 37:55–88.

Bleck, R. (2006). *Ocean Weather Forecasting*, chapter 4: On the use of hybrid vertical coordinates in ocean circulation modeling., pages 109–126. Springer, Netherlands.

Bleck, R. and Smith, L. (1990). A wind-driven isopycnic coordinate model of the North Atlantic and Equatorial Atlantic Ocean. 1: Model development and supporting experiments. *J. Geophys. Res.*, 95:3273–3285.

Boebel, O., Lutjeharms, J. R. E., Schmid, C., Zenk, W., Rossby, T., and Barron, C. (2003a). The Cape Couldron: a regime of turbulent inter-ocean exchange. *Deep Sea Res. II*, 50:57–86.

Boebel, O., Rossby, T., Lutjeharms, J. R. E., Zenk, W., and Barron, C. (2003b). Path and variability of the Agulhas Return Current. *Deep Sea Res. II*, 50:35–56.

Bracewell, R. (1999). *The Fourier Transform and Its Application.* New York: McGraw-Hill.

Browning, G. L. and Kreiss, H. O. (1982). Initialization of the shallow water equations with open boundaries by the bounded derivative method. *Tellus*, 34:334–351.

Browning, G. L. and Kreiss, H. O. (1986). Scaling and computation of smooth atmospheric motions. *Tellus*, Ser. A 38:295–313.

Bryden, H. L., Bacon, S., Beal, L. M., et al. (1995). RRS Discovery cruise 214, 26 Feb-09 Mar 1995: Agulhas Current Experiment. Cruise Report 249. *Institute of Oceanographic Sciences, Wormley*, page 85 pp.

Bryden, H. L., Beal, L. M., and Duncan, L. M. (2005). Structure and Transport of the Agulhas Current and Its Temporal Variability. *J. Oceanogr.*, 61:479–492.

Byrne, D. A., Gordon, A. L., and Haxby, W. F. (1995). Agulhas eddies: A synoptic view using GEOSAT ERM data. *J. Phys. Oceanogr.*, 25:902–917.

Byrne, D. A. and McClean, J. L. (2008). Sea level anomaly signals in the Agulhas Current region. *Geophys. Res. Lett.*, 35(L13601).

Chelton, D. B., Schlax, M. G., Samelson, R. M., and de Szoeke, R. A. (2007). Global observations of large oceanic eddies. *Geophys. Res. Lett.*, 34(L15606).

Counillon, F. and Bertino, L. (2008). Ensemble Optimal Interpolation: multivariate properties in the Gulf of Mexico. *Tellus*, 61:296–308.

Davies, H. C. (1983). Limitations of some common lateral boundary schemes used in NWP models. *Mon. Wea. Rev.*, 111:1002–1012.

de Ruijter, W. P. M., Biastoch, A., Drijfhout, S. S., Lutjeharms, J. R. E., Matano, R. P., Pichevin, T., van Leeuwen, P. J., and Weijer, W. (1999a). Indian-Atlantic interocean exchange: Dynamics, estimation and impact. *J. Geophys. Res.*, 104(C9):20885–20910.

de Ruijter, W. P. M., Ridderinkhof, H., Lutjeharms, J. R. E., Schouten, M. W., and Veth, C. (2002). Observations of the flow in the Mozambique Channel. *Geophys. Res. Lett.*, 29(10):1502–1504.

de Ruijter, W. P. M., van Aken, H. M., Beier, E. J., Lutjeharms, J. R. E., Matano, R. P., and Schouten, M. W. (2004). Eddies and dipoles around South Madagascar: formation, pathways and large-scale impact. *Deep Sea Res.*, 51:383–400.

de Ruijter, W. P. M., van Leeuwen, P. J., and Lutjeharms, J. R. E. (1999b). Generation and Evolution of Natal Pulses: Solitary Meanders in the Agulhas Current. *J. Phys. Oceanogr.*, 29:3043–3055.

Ducet, N., Le Traon, P.-Y., and Reverdin, G. (2000). Global high-resolution mapping of ocean circulation from TOPEX/Poseidon and ERS-1 and -2. *J. Geophys. Res.*, 105:19477–19498.

Duncombe-Rae, C. M. (1991). Agulhas retroflection rings in the south atlantic ocean: An overview. *S. Afr. J. Mar. Sci.*, 11:327–344.

Duncombe-Rae, C. M., Garzoli, S. L., and Gordon, A. L. (1996). The eddy field of the southeast Atlantic Ocean: a statistical census from the Benguela sources and transports project. *J. Geophys. Res.*, 101:11949–11964.

Farrow, D. E. and Stevens, D. P. (1995). A new tracer advection scheme for bryan and cox type ocean general circulation models. *J. Phys. Oceanogr.*, 25:1731–1741.

Fu, L.-L. (2006). Pathways of eddies in the South Atlantic Ocean revealed from satellite altimeter observations. *Geophys. Res. Lett.*, 33(L14610).

Garraffo, Z., Griffa, A., Mariano, A. J., and Chassignet, E. P. (2001a). Lagrangian data in a high resolution numerical simulation of the North Atlantic. II: On the pseudo-Eulerian averaging of Lagrangian data. *J. Mar. Sys.*, 29:177–200.

Garraffo, Z., Mariano, A. J., Griffa, A., Veneziani, C., and Chassignet, E. P. (2001b). Lagrangian data in a high resolution numerical simulation of the North Atlantic. I: Comparison with in-situ float data. *J. Mar. Sys.*, 29:157–176.

Gneiting, T., Sasvári, Z., and Schlather, M. (2001). Analogies and correspondences between variograms and covariance functions. *Adv. Appl. Prob.*, 33:617–630.

Goni, G. J., Garzoli, S. L., Roubicek, A. J., Olson, D. B., and Brown, O. B. (1997). Agulhas ring dynamics from TOPEX/POSEIDON satellite altimeter data. *J. Mar. Sys.*, 55:861–883.

Gordon, A. L. (1985). Indian-Atlantic transfer of thermocline water at the Agulhas Retroflection. *Science*, 227:1030–1033.

Gordon, A. L., Weiss, R. F., Smethie Jr., W. M., and Warner, M. J. (1992). Thermocline and intermediate water communication between the South Atlantic and Indian Oceans. *J. Geophys. Res.*, 97(C5):7223–7240.

Gründlingh, M. L. (1983). On the course of the Agulhas Current. *S. Afr. Geograph. J.*, 65:49–57.

Hermes, J. C., Reason, C. J. C., and Lutjeharms, J. R. E. (2007). Modeling the Variability of the Greater Agulhas Current System. *J. Clim.*, 20:3131–3146.

Heywood, K. J. and Somayajulu, Y. K. (1997). Eddy activity in the South Indian Ocean from ERS-1 altimetry. In *Third ERS Symp. on Space in the Service of Our Environment*, volume ESA SP-414, pages 1479–1483. European Space Agency.

Hodges, K. (1994). A General Method for Tracking Analysis and its Application to Meterological Data. *Mon. Wea. Rev.*, 122:2573–2586.

Holland, W. R., Chow, J., and Bryan, F. (1998). Application of a third-order upwind scheme in the NCAR ocean model. *J. Clim.*, 11:1487–1493.

Hurlburt, H. E., Chassignet, E. P., Cummings, J. A., Kara, A. B., Metzger, E. J., Shriver, J. F., Smedstad, O. M., Wallcraft, A. J., and Barron, C. N. (2008). Eddy-resolving global ocean prediction. In Hecht, M. and Hasumi, H., editors, *Ocean Modeling in an Eddying Regime*, volume 177 of *Geophys. Monograph Ser.*, pages 353–381. American Geophysical Union, Washington, DC.

Jakobsen, P. K., Ribergaard, M. H., Quadfasel, D. R., Schmith, T., and Hughes, C. W. (2003). Near-surface circulation in the northern North Atlantic as inferred from Lagrangian drifters: Variability from the mesoscale to interannual. *J. Geophys. Res.*, 108(C8):3251.

Jerlov, N. G. (1976). *Marine Optics*. Elsevier, New York.

Kara, A. B., Rochford, P. A., and Hurlburt, H. E. (2000). Efficient and accurate bulk parameterizations of air-sea fluxes for use in general circulation models. *J. Atmos. Ocean Tech.*, 17:1421–1438.

Large, W. G., McWilliams, J. C., and Doney, S. C. (1994). Oceanic vertical mixing: A review and a model with a nonlocal boundary layer parameterization. *Rev. Geophys.*, 32:363–403.

Le Traon, P.-Y. (2002). *Ocean Forecasting*, chapter Satellite oceanography for ocean forecasting, pages 19–36. Springer, New York.

Legates, D. and Willmott, C. (1990). Mean seasonal and spatial variability in gauge-corrected, global precipitation. *J. Clim.*, 10:111–127.

Leonard, B. (1979). A stable and accurate convective modelling procedure based on quadratic upstream interpolation. *Comp. Methods Appl. Mech. Eng.*, 19:59–98.

Lisæter, K. A., Rosanova, J., and Evensen, G. (2003). Assimilation of ice concentration in a couple ice-ocean model, using the ensemble kalman filter. *Ocean Dyn.*, 52:368–388.

Lutjeharms, J. R. E. (1981). Features of the southern Agulhas Current circulation from satellite remote sensing. *S. Afr. J. Sci.*, 77:231–236.

Lutjeharms, J. R. E. (1985). Location of frontal systems between Africa and Antarctica: some preliminary results. *Deep Sea Res.*, 32(12):1499–1509.

Lutjeharms, J. R. E. (2006). *The Agulhas Current*. Springer-Praxis Books.

Lutjeharms, J. R. E. and Ansorge, I. J. (2001). The Agulhas Return Current. *J. Mar. Sys.*, 30(1-2):115–138.

Lutjeharms, J. R. E. and Roberts, H. R. (1988). The Natal Pulse: An extreme transient on the Agulhas Current. *J. Geophys. Res.*, 93:631–645.

Lutjeharms, J. R. E. and Valentine, H. R. (1984). Southern Ocean thermal fronts south of Africa. *Deep Sea Res.*, 31(12):1461–1475.

Lutjeharms, J. R. E. and van Ballegooyen, R. C. (1988). The retroflection of the Agulhas Current. *J. Phys. Oceanogr.*, 18:1570–1583.

Lutjeharms, J. R. E. and Webb, D. J. (1995). Modelling the Agulhas Current system with FRAM (Fine Resolution Antarctic Model). *Deep Sea Res.*, 42(4):523–551.

Lutjeharms, J. R. E., Wedepohl, P. M., and Meeuwis, J. M. (2000). On the surface drift of the East Madagascar and the Mozambique Currents. *S. Afr. J. Sci.*, 96:141–147.

Matano, R. P. and Beier, E. J. (2003). A kinematic analysis of the Indian / Atlantic interocean exchange. *Deep Sea Res. II*, 50:229–249.

Matano, R. P., Beier, E. J., Strub, P. T., and Tokmakian, R. (2002). Large-scale forcing of the Agulhas variability: The seasonal cycle. *J. Phys. Oceanogr.*, 32:1228–1241.

Matano, R. P., Simionato, C. G., and Strub, P. T. (1999). Modeling the wind driven variability of the South Indian Ocean. *J. Phys. Oceanogr.*, 29:217–230.

Morel, Y., Darr, D., and Tailandier, C. (2006). The stability of coastal upwelling and downwelling currents. *J. Phys. Oceanogr.*, 36:875–896.

Oki, T. and Sud, Y. C. (1998). Design of Total Runoff Integrating Pathways (TRIP) - A global river channel network. *Earth Interactions*, 2:1–37.

Olson, D. B. and Evans, R. H. (1986). Rings of the Agulhas Current. *Deep Sea Res.*, 33:27–42.

Palastanga, V., van Leeuwen, P. J., and de Ruijter, W. P. M. (2006). A link between low-frequency mesoscale eddy variability around Madagascar and the large-scale Indian Ocean variability. *J. Geophys. Res.*, 111(C09029).

Peeters, F. J. C., Acheson, R., Brummer, G. A., de Ruijter, W. P. M., Schneider, R. R., Ganssen, G. M., Ufkes, E., and Kroon, D. (2004). Vigorous exchange between the Indian and Atlantic oceans at the end of the past five glacial periods. *Nature*, 430:661–665.

Penven, P., Chang, N., and Shillington, F. A. (2006a). Modelling the Agulhas Current using SAfE (Southern Africa Experiment). *Geophys. Res. Abstr.*, 8(Abstract 04225).

Penven, P., Lutjeharms, J. R. E., and Florenchie, P. (2006b). Madagascar: A pacemaker for the agulhas current system? *Geophys. Res. Lett.*, 33:L17609.

Pichevin, T., Nof, D., and Lutjeharms, J. R. E. (1999). Why are there Agulhas Rings. *J. Phys. Oceanogr.*, 29(4):693–707.

Pond, S. and Pickard, G. L. (1983). *Introductory Dynamical Oceanography.* Elsevier Butterworth-Heinemann, 2nd edition.

Quadfasel, D. R. and Swallow, J. C. (1986). Evidence for 50-day period planetary waves in the South Equatorial Current of the Indian Ocean. *Deep Sea Res.*, 33:1307–1312.

Quartly, G. D. and Srokosz, M. A. (2004). Eddies in the southern Mozambique Channel. *Deep Sea Res. II*, 51(1-3):69–83.

Reason, C. J. C. (2001). Evidence for the Influence of the Agulhas Current on Regional Atmospheric Circulation Patterns. *J. Clim.*, 14:2769–2778.

Reynolds, R. W. (1988). A real-time global sea surface temperature analysis. *J. Clim.*, 1:75–86.

Reynolds, R. W. and Marsico, D. C. (1994). An improved real-time global sea surface temperature analysis. *J. Clim.*, 7:929–948.

Reynolds, R. W., Rayner, N. A., Smith, T. M., Stokes, D. C., and Wang, W. (2002). An improved in situ and satellite sst analysis for climate. *J. Clim.*, 15:1609–1625.

Richardson, P. L. (2007). Agulhas leakage into the Atlantic estimated with subsurface floats and surface drifters. *Deep Sea Res.*, 54:1361–1389.

Richardson, P. L. and Garzoli, S. L. (2003). Characteristics of intermediate water flow in the Benguela current as measured with RAFOS floats. *Deep Sea Res. II*, 50:87–118.

Ridderinkhof, H. and de Ruijter, W. P. M. (2003). Moored current observations in the Mozambique Channel. *Deep Sea Res. II*, 50:1933–1955.

Rio, M.-H. and Hernandez, F. (2004). A mean dynamic topography computed over the world ocean from altimetry, in situ measurements, and a geoid model. *J. Geophys. Res.*, 109(C12032).

Rio, M.-H., Schaeffer, P., Lemoine, J.-M., and Hernandez, F. (2005). Estimation of the ocean mean dynamic topography through the combination of altimetric data, in-situ measurements and grace geoid. In *From global to regional studies, Proceedings of the GOCINA international workshop*.

Rouault, M. and Lutjeharms, J. R. E. (2003). Estimation of sea-surface temperature around southern Africa from satellite-derived microwave observations. *S. Afr. J. Sci.*, 99:489–494.

Rouault, M., Penven, P., and Pohl, B. (2009). Warming in the Agulhas Current system since the 1980's. *Geophys. Res. Lett.*, 36(L12602).

Sætre, R. and da Silva, A. J. (1984). The circulation of the Mozambique Channel. *Deep Sea Res.*, 31:485–508.

Sanderson, B. G. (1998). Order and resolution for computational ocean dynamics. *J. Phys. Oceanogr.*, 28:1271–1286.

Schott, F. A., Fieux, M., Kindle, J., Swallow, J. C., and Zantopp, R. (1988). The boundary currents east and north of Madagascar: 2. Direct measurements and model comparison. *J. Geophys. Res.*, 93(C5):4963–4974.

Schouten, M. W., de Ruijter, W. P. M., and van Leeuwen, P. J. (2002). Upstream control of Agulhas Ring shedding. *J. Geophys. Res.*, 107(C8):3109–3120.

Schouten, M. W., de Ruijter, W. P. M., van Leeuwen, P. J., and Ridderinkhof, H. (2003). Eddies and variability in the Mozambique Channel. *Deep Sea Res. II*, 50:1987–2003.

Siedler, G., Rouault, M., Biastoch, A., Backeberg, B. C., Reason, C. J. C., and Lutjeharms, J. R. E. (2009). Modes of the southern extension of the East Madagascar Current. *J. Geophys. Res.*, 114(C01005).

Siedler, G., Rouault, M., and Lutjeharms, J. R. E. (2006). Structure and origin of the subtropical South Indian Ocean Countercurrent. *Geophys. Res. Lett.*, 33.

Slutz, R., Hiscox, S. L. J., Woodruff, S., Jenne, R., Joseph, D., Steurer, P., and Elms, J. (1985). Comprehensive ocean-atmosphere dataset; Release 1. Tech. Rep. NTIS PB86-105723, NOAA Environmental Research Laboratories, Climate Research Program, Boulder, CO.

Smagorinsky, J. (1963). General circulation experiments with the primitive equations: I. the basic experiment. *Mon. Wea. Rev.*, 91:99–164.

Stramma, L. and Lutjeharms, J. R. E. (1997). The flow field of the subtropical gyre in the South Indian Ocean. *J. Geophys. Res.*, 99:14053–14070.

Swallow, J. C., Fieux, M., and Schott, F. A. (1988). The boundary currents east and north of Madagascar: 1. Geostrophic currents and transports. *J. Geophys. Res.*, 93(C5):4951–4962.

Teague, W. J., Carron, M., and Hogan, P. J. (1990). A comparison between the Generalized Digital Environmental Model and Levitus climatologies. *J. Geophys. Res.*, 95(C5):7167–7183.

Thompson, K. R. and Demirov, E. (2006). Skewness of sea level variability of the world's oceans. *J. Geophys. Res.*, 111(C05005).

Treguier, A. M., Boebel, O., Barnier, B., and Madec, G. (2003). Agulhas eddy fluxes in a 1/6° Atlantic model. *Deep Sea Res. II*, 50:251–280.

Troccoli, A. and Kållberg, P. W. (2004). Precipitation correction in the ERA-40 reanalysis. Technical Report 13, ERA-40 Project Report Series.

Uppala, S. M., Kållberg, P. W., Simmons, A. J., Andrae, U., Da Costa Bechtold, V., Fiorino, M., Gibson, J. K., Haseler, J., Hernandez, A., Kelly, G. A., Li, X., Onogi, K., Saarinen, S., Sokka, N., Allan, R. P., Andersson, E., Arpe, K., Balmaseda, M. A., Beljaars, A. C. M., Van De Berg, L., Bidlot, J., Bormann, N., Caires, S., Chevallier, F., Dethof, A., Dragosavac, M., Fisher, M., Fuentes, M., Hagemann, S., Hólm, E., Hoskins, B. J., Isaksen, L., Janssen, P. A. E. M., Jenne, R., McNally, A. P., Mahfouf, J.-F., Morcrette, J.-J., Rayner, N. A., Saunders, R. W., Simon, P., Sterl, A., Trenberth, K. E., Untch, A., Vasiljevic, D., Viterbo, P., and Woollen, J. (2005). The era-40 re-analysis. *Q.J.R. Meteorol. Soc.*, 131(612):2961–3012.

van Leeuwen, P. J., de Ruijter, W. P. M., and Lutjeharms, J. R. E. (2000). Natal Pulses and the formation of Agulhas Rings. *J. Geophys. Res.*, 105:6425–6436.

van Sebille, E., Biastoch, A., van Leeuwen, P. J., and de Ruijter, W. P. M. (2009). A weaker Agulhas Current leads to more Agulhas leakage. *Geophys. Res. Lett.*, 36(L03601).

Wackernagel, H. (1998). *Multivariate geostatistics: An Introduction with Applications*. Springer-Verlag Telos, 2nd rev edition.

Webb, D. J., Cuevas, B. A., and Richmond, C. (1998). Improved advection schemes for ocean models. *J. Atmos. Ocean Tech.*, 15:1171–1187.

Winther, N. G. and Evensen, G. (2006). A hybrid coordinate ocean model for shelf sea simulation. *Ocean Modell.*, 13:221–237.

Winther, N. G., Morel, Y., and Evensen, G. (2007). Efficiency of high order numerical schemes for momentum advection. *J. Mar. Sys.*, 67:31–46.